University of Iowa

Iowa Research Online

Spring 2016

Mechanisms of resistance to fluid shear stress in malignant cells

Benjamin Lee Krog
University of Iowa

Recommended Citation
Krog, Benjamin Lee. "Mechanisms of resistance to fluid shear stress in malignant cells." MS (Master of Science) thesis, University of Iowa, 2016.
https://doi.org/10.17077/etd.d741ter4

MECHANISMS OF RESISTANCE TO FLUID SHEAR STRESS IN MALIGNANT
CELLS

by

Benjamin Lee Krog

A thesis submitted in partial fulfillment
of the requirements for the Master of Science
degree in Biomedical Engineering in the
Graduate College of
The University of Iowa

May 2016

Thesis Supervisors: Associate Professor Michael D. Henry
                        Associate Professor Sarah C. Vigmostad

Graduate College
The University of Iowa
Iowa City, Iowa

CERTIFICATE OF APPROVAL

_____

MASTER'S THESIS

_____

This is to certify that the Master's thesis of

Benjamin Lee Krog

has been approved by the Examining Committee for
the thesis requirement for the Master of Science degree
in Biomedical Engineering at the May 2016 graduation.

Thesis Committee: _____

                     Michael D. Henry, Thesis Supervisor

                     _____

                     Sarah C. Vigmostad

                     _____

                     James A. Ankrum

To my parents.

ACKNOWLEDGEMENTS

ABSTRACT

Cancer cells traveling to distant tissues during metastasis must survive passing through the circulation. However, the influence of this fluid microenvironment on these cells is poorly understood. It was previously viewed that exposure to the hemodynamic shear forces within circulation was inhospitable to cancer cells, causing the cells to be destroyed. Recent evidence indicates that transformed cells are markedly more resistant to fluid shear stress when compared to non-transformed epithelial cells. Furthermore, these cells selectively adapt following exposure to fluid shear stresses and become more resistant to subsequent exposures to shear stress. The mechanisms behind this difference in phenotype and induced resistance are investigated. The elastic modulus, a measure of stiffness, may play a role in resistance and is shown to be altered upon exposure to fluid shear forces. Additionally, plasma membrane repair is a critical process in the resistance phenotype as cells sustain damage but are able to maintain viability. Cytoskeletal dynamics are also shown to play a role in resistance to fluid shear forces.

PUBLIC ABSTRACT

During metastasis, cancer cells traverse the circulation to travel to a distant part of the body and set up a secondary, metastatic tumor site, often with lethal consequences. Yet, cancer cell behavior within this microcirculatory environment is poorly understood. It was previously believed that this intermediate step was inefficient and metastatic cells were sensitive to fluid shear forces. However, our group found that these malignant cancer cells are significantly more resistant to fluid shear stresses compared to normal, non-transformed cells. Additionally, these cells displayed an induced resistance to these stresses. Upon repeated exposure to brief pulses of high levels of fluid shear, cells became more resistant in subsequent exposures. The mechanisms behind this cell biology are investigated. Plasma membrane repair is a critical process in the resistance phenotype as cells sustain damage but are able to maintain viability. Cell structural dynamics and mechanical properties, such as stiffness, are shown to be influenced by exposure to fluid shear stresses.

TABLE OF CONTENTS

B. Development of a microfluidic device

LIST OF TABLES

Table

LIST OF FIGURES

x

CHAPTER 1 INTRODUCTION

Metastasis

Metastasis is the spread of cancer from a primary tumor site to distant tissues and this process is often associated with a poor prognosis. It is the leading cause of cancer mortality, contributing up to 90% of human cancer deaths. Metastasis consists of several steps including local tissue invasion, entry into the vasculature, transport to a distant part of the body, extravasation from the circulation, and colonization of surrounding tissues.

Despite significant progress in many areas of cancer research, the influence of the circulation on tumor cell biology remains largely unanswered. The environment that these malignant cells are exposed to is radically different than the primary tumor site. Previously, it was thought that compared to benign, non-transformed cells, malignant cells were susceptible to the circulatory environment and that this was a relatively inefficient stage of metastatic dissemination. This was believed due to a number of factors including the immune response, anoikis (programmed cell death induced by cell detachment), deformation within the microvasculature, and hemodynamic shear forces. However, studies found circulating tumor cells in blood samples taken from patient's arm, suggesting that perhaps malignant cells survive passage through the circulation in greater numbers than thought (Ashworth 1869). Here, we focus on the influence of hemodynamic shear forces on tumor cell biology and the mechanisms effecting tumor cell survivability in this circulatory environment.

1

Within the circulation, this dynamic and stressful atmosphere is radically different than the primary tumor environment. They are exposed to a range of mechanical stresses that depend on the fluid properties of blood. Vessel diameter changes dramatically depending on location, with capillaries as narrow as 5 μm, to the aorta with a diameter of 3 cm. In addition, flow rates vary considerably as fluid dynamics changes between the low and high resistance macro- and micro-vasculature, respectively.

Cells that are suspended in blood or lymph will experience fluid shear stress (FSS), a type of mechanical stress, which depends on several characteristics of the fluid. Increases in flow rate and viscosity and decreases in vessel diameter result in elevated levels of FSS. FSS is important for many biological functions. For example, endothelial cells, located at the wall of blood vessels and thus experiencing the maximum FSS, undergo shape changes and microfilament remodeling, aligning with the direction of the flow (Dewey, Bussolari *et al.* 1981). Dysfunction of these mechanisms, possibly due to changes in FSS, may result in the development of vascular diseases such as atherosclerosis. Additionally, red blood cells can be destroyed with high levels of shear in certain environmental (eg. mechanical heart valves) or pathological conditions (Dasi, Simon *et al.* 2009; Leverett, Hellums *et al.* 1972). A long standing view was that survival of metastatic cancer cells was poor during this stage of metastatic dissemination, despite little research done, possibly due to the difficulty of tracking and accounting for these small fractions of cells *in vivo* where it is estimated that there is only one circulating tumor cell (CTC) per billion blood cells in advanced cancer patients (Yu, Stott *et al.*

2

2011). Thus, it was thought that transport in the circulation was a rate-limiting step of metastatic disease progression. While studies have shown FSS-induced death of malignant cells, for example exposing cells to FSS through the use of a viscometer, exposure time was up to one hour (Brooks 1984). The time of exposure to elevated levels of FSS in circulation is estimated to be significantly less than this time frame, on the order of milliseconds to seconds.

Particles that are suspended in flowing blood are exposed to a FSS value that is dependent on the radial position of the cell within the vessel. At the wall of the vessel, cells experience the maximum value of fluid shear stress whereas at the axis of the vessel, the minimum FSS level is experienced. FSS varies considerably in different locations of the circulation. The magnitude of FSS can change by up to five orders of magnitude between small diameter capillary beds and the left ventricle or aorta. This has important implications in the magnitude of stresses malignant cells encounter during metastasis.

<u>A model to investigate effects of fluid shear stress</u>

Summary

A simple model was developed in our group to expose malignant cells to FSS to investigate their cell biology (Barnes, Jones *et al.* 2012). Cells are expelled through a needle and are exposed to high levels of fluid shear stress. The level of exposure is dependent on system and fluid parameters, such as flow rate and needle diameter. Cells

within the needle are exposed to a parabolic velocity profile and thus fluid shear stress is dependent on the radial position of the particle.

Materials and methods

Cells

All cell lines are cultured according to protocols given by suppliers. Cancer cell lines were obtained from ATCC. Primary prostatic and mammary epithelial cells were acquired from Clontech and cultured in appropriate medium. PrEC LH, LHSR, and LHMK cells were acquired from Dr. William Hahn (Dana Farber Cancer Institute). These cell lines are cultured as recommended (Berger, Febbo *et al.* 2004). Some cell lines are transfected with an integrating retrovirus encoding the firefly luciferase gene using procedures previously described (Drake, Gabriel *et al.* 2005).

Flow characteristics

Fluid shear stress (FSS, τ), is a stress, or force per unit area, that is coplanar with a cross section. It is the result of adjacent layers of fluid with viscosity μ moving at different velocities, a result of the no-slip condition, which states that fluid velocity is zero at the wall boundary. The maximum FSS, experienced at the wall of the vessel, is determined using Poiseuille's equation,

4

$$\tau_{max} = \frac{4Q\mu}{\pi R^3},\tag{1}$$

where τ is the maximum wall shear stress in dyn/cm^2, Q is the flow rate in m^3/s passing through the needle, μ is the dynamic viscosity of the media (dyn*s/cm^2), and R is the radius of the needle. In standard assays at room temperature, the medium viscosity is treated as water, a Newtonian fluid, and assumed to be 0.01 dyn*s/cm^2. The needle used is a 30G ½" needle with an internal radius of $7.94 * 10^{-3}$ cm. The cell volume fraction of the suspension passing through the needle is <0.2%, obeying Poiseuille flow. As is evidenced by the equation, the magnitude of FSS is inversely proportional to R^3. Thus, FSS is incredibly sensitive to changes in radius. This results in the large range in FSS throughout the circulation which can vary by up to five orders of magnitude.

The magnitude of the fluid shear stress depends on the radial position of the particle experiencing the stress. At the wall of the vessel, cells experience the maximum value of fluid shear stress whereas at the axis of the vessel, the minimum FSS level is felt.

Other conditions of the flow that are investigated can be found in Appendix A. This includes assessment of laminar versus turbulent flow, velocity and fluid shear stress profiles within the region of exposure, and average times of exposure in addition to other parameters. The influence of these parameters on cell behavior and survival, such as threshold fluid shear stress magnitudes, is discussed in further detail as well.

The development and preliminary testing of this fluid shear stress model are published (Barnes, Jones *et al.* 2012). Samples are collected at approximately 75-80% confluency with either 0.05% or 0.25% trypsin, depending on the cell line. Cells are then resuspended in appropriate serum containing medium to neutralize trypsin. Samples are centrifuged at room temperature for 5 minutes at 150g. Pellets are resuspended to $5 * 10^5$ cells/mL and transferred to 14 mL polypropylene round-bottom tubes (BD Falcon #352059) cut down to the 6 mL line. Cells are then drawn into a 5 mL syringe (BD Biosciences #309603) without a needle attached. The suspension is gently expelled back into the 6 mL collection tube. A non-exposed, naïve sample is collected and treated as a 100% viability control. The suspension is again drawn into the syringe and a 30G ½" needle (BD Biosciences #305106) is attached, unless otherwise noted. The syringe containing the cell suspension is placed onto a syringe pump (Harvard Apparatus PHD-2000 Infuse/Withdraw). Settings for the syringe pump are set to match syringe diameter and desired flow rate. During expulsion, the collection tube is placed at a 45° angle at the tip of the needle to collect sample. Intermediate duplicate 100 µL aliquots are taken and placed in a 96-well black plate (Costar #3915) to assess viability upon completion of assay. The process is repeated until ten passages are completed. All assays are done at room temperature. Collected samples are then measured to assess viability.

Bioluminescence imaging (BLI) and CellTiter-Blue assays are used to determine cell viability. Viability measured by flow cytometry is discussed in Chapter 2. For bioluminescence imaging, 100 µL of D-luciferin (Promega) is added to the 100 µL aliquots of cells expressing firefly luciferase to a final concentration of 150 µg/mL D-luciferin. Cells are incubated for 5 minutes at room temperature and imaged for 5 minutes using an AMI-1000 (Spectral Instruments). Measurements are collected using AMIView (Spectral Instruments). The photon fluxes of the duplicate aliquots for each passage are averaged and divided by the 100% naïve, unexposed control sample to give percent viability.

CellTiter-Blue assays are used to confirm viability determined by bioluminescence imaging. Duplicate 100 µL aliquots are taken at respective passage and pipetted into a 90-well black plate. 20 µL of CellTiter-Blue reagent is added to the samples. Plates are shaken for 10 seconds and incubated for 2 hours in the dark at 37°C. Fluorescence is recorded at 590 nm using a BioTek Synergy HT plate reader. Average background fluorescence values of the culture medium are subtracted from experimental wells. Naïve, unexposed samples are treated as 100% viability controls.

Fragmentation of non-viable cells and debris

To investigate the fate of cells that are intact but non-viable, cells are treated for thirty minutes in complete cell culture medium containing 10 µm ionomycin (Sigma

7

Aldrich). Cells are counted with Trypan blue before and after treatment and aliquots are taken to assess viability with BLI. Following treatment, cell suspensions are exposed to one passage of the FSS assay at 250 µL/sec. Samples are taken for BLI and Trypan blue counts. BLI is measured as previously described.

Statistics

Repeated measures ANOVA with Bonferroni's multiple comparisons tests are used to compare viability of multiple cell lines over several passages. Paired 2-tailed t-tests are done to analyze the end point analysis of two cell lines or flow rates. To compare endpoint survival of three or more cell lines, one-way ANOVA is used.

Results

Using the FSS model described above, the viability of a human prostate carcinoma cell line, PC-3, is tested and is consistent with previous results obtained in the lab for the flow rate of 250 µL/sec with 10 passages of exposure (**Figure 1.1A**). The maximum FSS is $6.36 * 10^3$ dyn/cm^2. The PC-3 cell line displays a biphasic response to FSS when exposed to repeated passages of FSS. Loss of viability is higher in the initial one to two passages compared later passages. BLI is used to assess the viability of samples. When PC-3 cells are tested in parallel with PrEC LH, an immortalized, non-transformed prostate epithelial cell line using the same experimental protocol, cell death is much more significant in the PrEC LH line (**Figure 1.1B**). PrEC LH lose

approximately 25% more viability, resulting in a surviving fraction of less than half that of the PC-3 cells. In addition, PrEC LH cells have a similar biphasic curve, with a sharper change in viability loss after passage one. Average loss per passage is similar between the two cell lines after the initial passage.

PC-3 cells are treated with 10 µM ionomycin for 30 minutes at 37°C. Viability and cell integrity are assessed before and after treatment and after one passage of high FSS (**Figure 1.2A**). The majority of cells become trypan blue positive after treatment, indicating loss of viability. However, the cells remain intact, as shown by inspection using a hemocytometer. Upon exposure to high shear, nearly all cells are fragmented (**Figure 1.2B**).

Control experiments are done previously to ensure independence of loss of viability from cell density, cell culture confluency, method used to measure cell viability, debris material released into the medium, technique used to dissociate cells, time held in suspension (to address anoikis), temperature, cell cycle distribution, and cell size (Barnes, Jones *et al.* 2012). None of these variables appear to influence viability. Additional controls are performed to account for experimental technique variations, such as distance collection tube is held from needle tip and angle of collection tube with respect to needle. Viability is independent of these factors when testing reasonable variations in experimental technique that might be present between runs and users.

9

Discussion

While malignant cancer cells are undergoing metastasis, they must survive passage through the circulation and withstand an enormous range of fluid shear stresses that are present throughout the circulation. Within the lymphatics and venous system, FSS is approximately 0.1-1 dyn/cm^2. The microcirculation consists of small diameter vessels with low flow blood and arterials contain medium diameter vessels at higher flow rates. These structures have levels of FSS between 0.1-100 dyn/cm^2. During the cardiac cycle, blood flow within the heart and aorta can become turbulent, resulting in high physiological FSS in the range of 1,000-3,000 dyn/cm^2. Additionally, arterial bifurcations and sudden expansions may lead to similar magnitudes of high FSS. For perspective, hemolysis of red blood cells has been recorded with brief, millisecond pulses at 5,000 dyn/cm^2 (Leverett, Hellums *et al.* 1972; Keshaviah 1970).

FSS plays a significant role in cellular biology. Within the circulation, endothelial cells respond and adapt to FSS. In disease states, these responses can be altered. When cancer cells are able to escape from a primary tumor site and metastasize to a distant part of the body, they often must traverse the circulation. Little is known about how this microcirculatory environment influences the behavior of circulating tumor cells.

Thus, a simple model was developed in our group to expose malignant cells to FSS to investigate their cell biology (Barnes, Jones *et al.* 2012). In this model, cells are suspended in medium and expelled through a small diameter needle using a syringe pump, collected, and assessed for viability. When malignant prostate carcinoma cells are exposed to high/supra-physiologic levels of brief FSS, they display remarkable resistance

10

when passaged multiple times, especially compared to benign, non-transformed epithelial cells of similar origin. The end viability of the prostate carcinoma line, PC-3, is roughly 50% whereas PrEC LH is 20%, demonstrating increased resistance to FSS in the malignant line. Furthermore, both malignant and non-transformed display a biphasic response to shear. In the initial passage of shear stress, viability loss is approximately four-fold greater than the remaining nine passages for PC-3 cells and sixteen-fold greater loss for PrEC LH cells. This response is shown to not be the result of enrichment of a subset of the population of cells tested that are inherently resistant (Barnes, Jones *et al.* 2012). Therefore, this biphasic curve suggests a fluid shear stress-induced resistance to fluid shear stress. The mechanism behind this induced resistance is unknown and is investigated.

The clinical relevance of furthering our understanding of this elevated and induced resistance is important in the subject of circulating tumor cells. One area of research and diagnostics is the isolation of circulating tumor cells (CTCs) from patient samples for characterization and testing. CTC isolation is currently hindered by the vast amount of unwanted cells that are collected from blood samples. While technology in this area is rapidly advancing, many problems still arise. For example, in the case of isolation of malignant cells of epithelial origin, oftentimes antibodies with anti-epithelial-cell-adhesion-molecule (EpCAM) are used (Nagrath, Sequiest *et al.* 2007). However, other cells of epithelial origin may still contaminate the filtered sample.

11
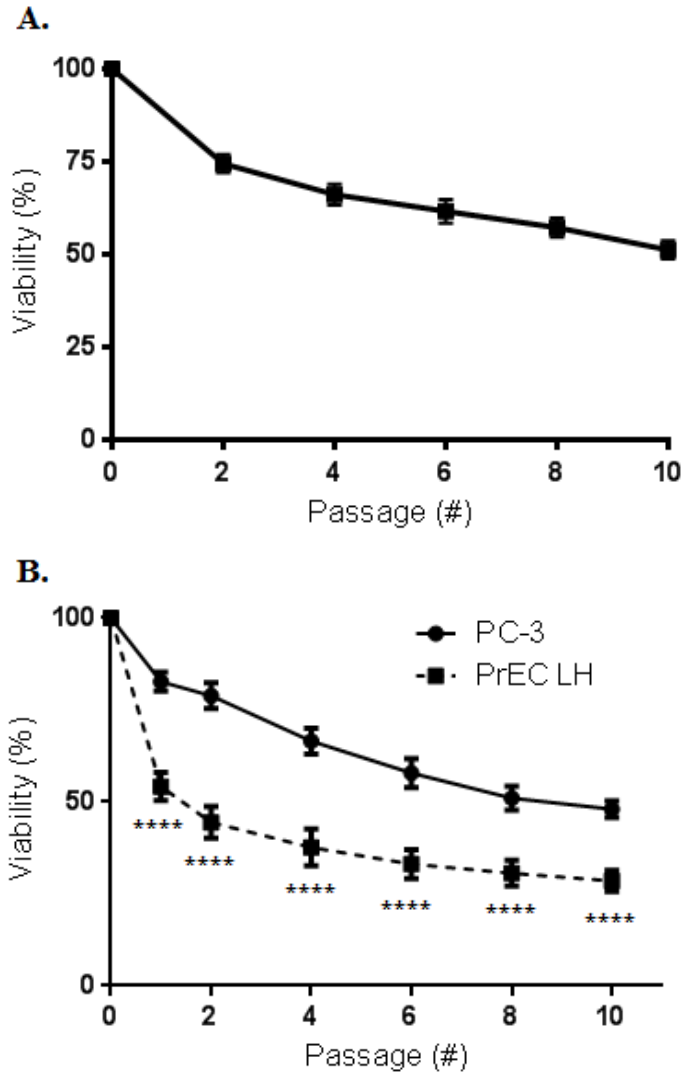
Figure 1.1: Fluid shear stress results in biphasic loss of viability.
Suspensions of PC-3 cells are exposed to the fluid shear stress at a flow rate of 250
μL/sec for 10 passages. The cell concentration is $5 * 10^5$ cells/mL. Viability is shown as
percent compared to a naïve, non-exposed control sample. **A)** Viability over repeated
passages of PC-3 cells. **B)** Comparison of viability over ten passages between PC-3 and
PrEC LH. (****, p<0.0001).

12
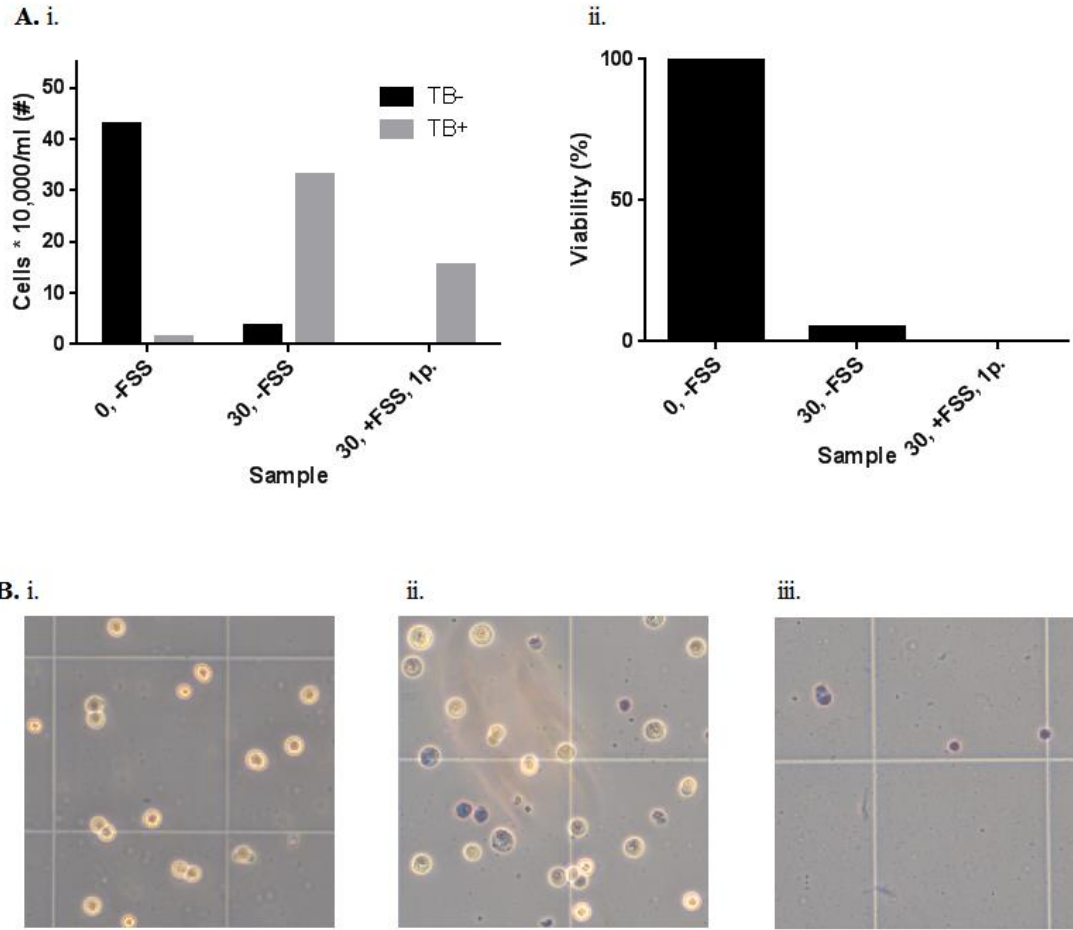
Figure 1.2: Non-viable cells are rapidly destroyed with high fluid shear stress.
A) *i.* Trypan blue positive and negative cells are counted to assess intact cell concentrations. *ii.* BLI is run in parallel to confirm loss of viability. **B)** *i.* Non-exposed, untreated cells. *ii.* Non-exposed, treated cells. *iii.* Fluid shear stress-exposed, treated cells.

In addition to CTCs, this phenotype can be employed to selectively destroy non-transformed FSS-sensitive cells that contaminate patient biopsy samples, either from solid tumors or fluids besides blood (eg. pleural effusions, urine). Sensitivity of certain genetic testing done on these samples is often reduced by contaminating, normal cells which contribute to the background noise of these samples. The FSS assay can take advantage of the phenotypic differences in malignant versus benign cells and selectively destroy sensitive, benign cells. This would allow enrichment of the tumor cells of interest for increased sensitivity of genetic testing.

Finally, increased understanding of tumor cell biology within the circulation during metastatic dissemination may lead to development of therapeutic solutions that reduce metastatic potential. Therapeutic intervention in early stages of cancer progression could target mechanistic pathways that result in this elevated resistance and biphasic response to FSS to sensitize tumor cells to FSS and thus lower the metastatic potential.

<u>Cellular responses to mechanical stimuli</u>

Cellular signaling pathways and mechanical properties are studied to elucidate the mechanisms behind the FSS resistance phenotype in malignant cells. This includes mechanisms of repair of plasma membrane injury via patching of lysosomes, plasma membrane and cytoskeletal stiffening, and actin cytoskeletal regulation pathways activated in response to fluid shear stress.

Membrane repair

14

Cells in diverse environments often experience plasma membrane injury. From muscle cell membranes being torn during strain to shear stress tearing membranes in endothelial cells when blood flow is disrupted, virtually all cells have some capacity to repair membrane injury. One mechanism of membrane repair is fusion of lysosomes to sites of injury to patch the hole and restore membrane integrity. This repair process is studied in both malignant tumor cells and benign, wild-type cells. Differential repair in the two cell types is evident. First, evidence of repair is studied with uptake of the membrane impermeable dye propidium iodide as cells are exposed to high levels of fluid shear stress. Next, fusion of lysosomes is confirmed by an increase of lysosomal protein expression on the surfaces of the cells. Finally, inhibition of different steps in the lysosomal fusion pathway resulted in reduced membrane repair ability, demonstrating it's significance in the FSS resistance phenotype.

Cytoskeletal and membrane dynamics

Biomechanical properties of cells influence cell mechanics, adhesion, migration, and division. In disease states, these properties can be altered, especially in the case of transformation. By changing their cell deformability, cancer cells can increase their ability to metastasize to distant tissues. In response to mechanical forces such as fluid shear stress, cells often reorganize their cytoskeletal structures to adapt to the stressful environment. A potential source of increased resistance in malignant cells is more efficient adaptation to FSS environments. The elastic modulus, a measure of a cells

15

deformability, is measured in malignant and benign cells that are either FSS-naïve or FSS-exposed. Alterations and differences in stiffness in both cell lines are observed. Inhibition of Rho-associated kinase, important in the regulation of actin filaments, is shown to play a role in the stiffness of malignant cells.

<div align="center">Actin cytoskeletal dynamics</div>

Membrane and cytoskeletal dynamics allow cells to sense and transduce signals in order to respond and adapt to mechanical forces. Disease states such as cancer have been extensively shown to have altered signal transduction and elevated expression of many regulators of the cytoskeleton. The importance of various regulators of cytoskeletal organization in the FSS resistance phenotype is explored in malignant carcinoma cells.

CHAPTER 2 MECHANISMS OF MEMBRANE REPAIR

Summary

When exposed to a mechanically stressful environment, the plasma membrane can sustain injury. Rapid repair of these injuries is critical to maintain cell viability. These repair mechanisms have been shown to require calcium to induce repair. If these mechanisms fail or the damage is too severe, cell death result can results in seconds. Significant numbers of cells exposed to fluid shear stress (FSS) sustain membrane damage from mild to severe. Thus, a crucial aspect of cell resistance to FSS, at least in initial passages of shear, is ability to efficiently and rapidly repair membrane damage.

The FSS assay is paired with flow cytometry to investigate membrane repair of cells exposed to brief high levels of FSS. Cell uptake of propidium iodide (PI) when exposed to the assay indicates membrane damage. Stains are performed afterwards to assess cell viability. Uptake of PI while maintaining viability indicated loss of plasma membrane integrity followed by successful repair to preserve viability. PC-3 and PrEC LH cells, in addition to other cell lines, are studied. While similar surviving fractions of cells displayed repair in both cell lines, the percentage of cells that repair out of all cells exposed is significantly less for PrEC LH cells. Additionally, calcium dropout experiments are performed and show dependence of repair on the presence of extracellular calcium.

<u>Introduction</u>

Whenever cells are subjected to a mechanically active or stressful environment, the integrity of the plasma membrane is often compromised. Rapid repair of these injuries is crucial to maintain cell viability. The plasma membrane prevents the loss of vital intracellular elements and maintains the essential electrochemical gradients necessary for normal cell activity. Failure to repair membrane disruptions can result in rapid cell death.

Cells in diverse environments experience stresses on their membranes. In milk-secreting epithelial cells, intracellular products and plasma membrane fragments are released into the lumen, causing membrane injury (Aumüller, Wilhelm *et al.* 1999). During periods of intense muscle use, muscle membranes may be ruptured and must be repaired (Tidball 2011). In a similar vein, cardiomyocytes may experience membrane disruption due to either normal physiological settings or pathophysiological stresses (Wang, Xie *et al.* 2010). As cardiomyocytes have very limited proliferative ability, repair of these cells is of paramount importance, as death can lead to myocardial fibrosis and eventual heart failure.

Furthermore, cells experience membrane damage due to fluid shear stresses. The endothelium can experience injury during flow disturbances, such as constriction of arterioles, which must be repaired (Gertz, Urestsky *et al.* 1981). Plasma membrane repair has been shown to be mediated by calcium-regulated fusion of lysosomes in several cell lines, including fibroblasts, endothelial cells, and epithelial cells (Reddy, Caler *et al.* 2001; McNeil & Kirchhausen 2005). When cells experience loss of membrane integrity, an influx of calcium occurs. This triggers localized cytoskeletal remodeling to facilitate

the transport of lysosomes to the plasma membrane. These vesicles form an aggregate and patch the membrane to restore normal cellular functions.

To investigate the FSS resistance phenotype that malignant PC-3 cells display, the presence of membrane repair is shown and mechanisms of membrane repair are studied. Repair in benign, sensitive PrEC LH cells is compared to these cancer cells. A stark contrast between efficiency of repair is seen between these two cell lines, in both the fractions of cells that are able to repair membrane damage and also in the mechanisms eliciting membrane repair. Membrane repair is examined by looking at viable cell uptake of membrane impermeable fluorescent dyes as well as extracellular membrane surface expression of LAMP-1 (lysosomal associated membrane protein). Upon fusion of lysosomes to the membrane to patch holes, LAMP-1 is displayed. Increases in signal intensity of this protein via flow cytometry detection indicate membrane injury repair via lysosomal exocytosis mechanisms. Different steps of this membrane repair processes are disrupted, such as calcium uptake and signaling molecules, and studied.

Materials and methods

Evidence of repair

Standard FSS assay and preparation: Cells are centrifuged after releasing from cell culture plates for 5 minutes at 300g. The pellet is resuspended to $5 * 10^5$ cells/mL in MEM. A control aliquot is taken. 10 µL Propidium iodide (PI) per 500 µL solution is added to the cell suspension. The standard FSS assay is performed with 500 µL samples

19

aliquoted at passages 0, 1, 2, 5, and 10 for flow cytometry analysis into 1.5 ml tubes in addition to standard aliquots every other passage for assessment of viability with BLI. All flow cytometry aliquots are placed on ice. 1 mL FACS buffer (1x PBS, 0.5% BSA, 0.1 NaN$_3$) at 4°C is added to samples to wash. They are centrifuged for 5 minutes at 200g at 4°C, the pellets are collected, and are resuspended in 1 mL FACS buffer. Cells are centrifuged again for 5 minutes at 200g at 4°C, the pellets are collected, and resuspended in 400 µL FACS buffer containing 16 µg/mL Hoechst 33258 (Thermo Fisher). Samples are kept on ice until run in the flow cytometer.

Processing and analysis: A BD LSR II Flow Cytometer is used to process samples. Cells are gated based on size and granularity. Live versus dead cells are discriminated using Hoechst intensity. Hoechst positive cells, as determined by control samples, are dead and gated out of analysis of PI uptake. A minimum of 10,000 viable cell events are recorded for each experiment. PI, added prior to exposure, is used as an indicator of membrane repair. The threshold for PI-/PI+ distinction is determined by the non-exposed control that does not contain PI. Geometric means (GM) of PI uptake are calculated for each sample. The GM of each sample is normalized to the FSS-naïve control that does not contain PI. BLI is measured according to the protocol described in Chapter 1.

Cells that are initially PI- and take up PI to become PI+ but remain Hoechst- are cells that sustained damage but remained viable. Cells that become PI+/Hoechst+ are damaged and non-viable. PI-/Hoechst- cells are viable and have not sustained sufficient damage to result in loss of membrane integrity for PI uptake to occur. For examples of dye uptake, refer to **Figure 2.1A**.

20

Counting bead standardization

Counting bead FSS assay and preparation: Preparation of samples for flow cytometry is the same as above. However, during the final resuspension, 2 μm fluorescent beads (#H3569, Thermo Fisher) are added at a dilution of 1:20.

Processing and analysis: During processing, counting beads are used as stopping gate events. Once a pre-determined number of beads are counted, recording is stopped. This number is used for all samples in a given assay. All other post-processing is the same as the previous experimental protocol. To determine percent viability for respective passages based on counting beads, the number of viable cells, as determined by Hoechst exclusion, is divided by the number of viable non-exposed cells.

Mechanism of repair

LAMP-1 FSS assay and preparation: An ionomycin positive control is aliquoted before exposure to FSS. This sample is centrifuged for 5 minutes at 200g at 4°C and resuspended in complete cell culture medium containing 10 μM ionomycin (#I0634 Sigma-Aldrich) for 10 minutes. The sample is centrifuged for 5 minutes at 200g at 4°C. The pellet is resuspended in 1 mL FACS buffer and kept on ice until all samples are collected. An additional isotype control is sampled to account for non-specific anti-body binding. An additional wash is added to the standard protocol discussed above. 1 mL

21

FACS buffer is added to all flow cytometry aliquots and samples are centrifuged for 5 minutes at 4°C at 200g. The supernatant is discarded and cells are resuspended in 300 µL FACS buffer containing a primary antibody staining for LAMP-1 (Developmental Hybridoma Studies Bank, Iowa City, Iowa) at 2 µg/mL. For the isotype control, 2 µg/mL anti-mouse IgG isotype control (Thermo Fisher) is added. Cells are incubated for 1 hour at 4°C. 1 mL FACS buffer is added to samples and centrifuged for 5 minutes at 200g at 4°C. Cells are resuspended in 300 µL FACS buffer containing the secondary antibody 2 µg/mL FITC (#F7250 Sigma-Aldrich). Cells are incubated for 1 hour at 4°C. 1 mL FACS buffer is added to samples and centrifuged for 5 minutes at 200g at 4°C. Cells are resuspended in 400 µL FACS buffer with 16 µg/mL Hoechst 33258.

During membrane repair, fusion of intracellular vesicles takes place to patch holes. Lysosomes contain LAMP-1 in the lumen of the vesicle. Thus, during membrane fusion, LAMP-1 will be expressed on the extracellular surface of the cell.

For calcium dropout experiments, cells are resuspended in calcium-free D-PBS (Gibco). To some suspensions, calcium chloride is added to a final concentration of 1.17 mM to match calcium content of culture medium. In calcium-free suspensions, EGTA is added to a final concentration of 10 µM.

Processing and analysis: Processing and analysis is done as described above. In addition, sample geometric means of the fluorescent intensities of LAMP-1 are examined in the

22

surviving, viable fraction of cells. Later passages are normalized to the unexposed, naïve control.

Synaptotagmin VII knockdown

PC-3 cells can be distinguished based on E-cadherin expression and sorted accordingly using flow cytometry. PC-3E cells are a subpopulation of PC-3 cells considered E-cadherin positive. In contrast, TEM-418 cells are the subpopulation that are E-cadherin negative. Stable knockdown of Syntaptotagmin VII (SYT7) is performed in the TEM-418 cell line and is achieved by lentiviral shRNA constructs targeting SYT7. Three lentiviral plasmids containing these pZIP-SYT7 constructs were obtained from Transmics (Trasomics). Documentation is followed for generation of lentiviral particles. Briefly, GP-293 cells are seeded in Dulbecco's Modified Eagle Medium (DMEM) in 6 well plates. These cells are transfected with 1 µg lentiviral plasmids with 0.1 µg of pVSV-G envelope plasmid and 0.9 µg packaging plasmid (pCMV-dR8.74psPAX2) with 4 µL OminiFect reagents. Cells are incubated, media is changed after 24 hours, and then 24 hours following seeded into 6 well plates. Virus-containing supernatant is collected, centrifuged at 1,300g for 5 minutes, then filtered through 0.45 µm low protein binding syringe filters. Viral supernatant is added to TEM4-18 cells with 8 µg/mL polybrene. Cells are incubated for 8 hours, media is changed, and cells are incubated for 24 hours. Selection steps are done for 72 hours with puromycin. Knockdown is validated by qRT-PCR. SYT7 knockdown cells are run in parallel with a control, scramble syringe.

23

<u>Results</u>

A schematic of the flow cytometry staining procedure is shown in **Figure 2.1A** for clarity on significance of different combinations of dye uptake. Typical flow cytometry dot plots and the gating procedure are shown in **Figure 2.1B**. Typical plots are displayed. Cells are gated based on size, granularity, and Hoechst intensity. Intact particle populations shift during exposure to repeated passages of FSS (**Figure 2.2A**). An initial, small population of dead, intact cells is present in naïve control samples, as indicated by elevated Hoechst intensity. This population shifts to become significantly PI+ upon a single pulse of FSS. The live, Hoechst- population can be seen to increase in PI intensity, with significant fractions of cells becoming PI+. Finally, the number of counted intact cell events is reduced by passage ten of exposure. This is due to loss of viability and standardization of processing time with counting beads. The histograms of the PI intensity of cells at various passages are shown in **Figure 2.2B** with the relative geometric means (RGM) quantified per passage for PC-3 (3.409) and PrEC lines (PrEC LH: 3.546, PrEC LHSR: 4.732, PrEC LHMK: 2.654) and in **Figure 2.2C** for passage 10 for several other lines (PWR-1E: 19.222, RWPE-1: 14.201, 22Rv1: 3.200). The relative fluorescent intensity of PI is fairly similar across all cell lines tested, with the exception of transformed, but non-malignant cells (PWR-1E and RWPE-1). The percent fraction of viable, PI- cells decreases in both PC-3 and PrEC LH cells as they are exposed, with increases in percentages of PI+ viable cells.

However, without the use of counting beads, accounting of completely destroyed cells is difficult. **Figure 2.3A** displays percent fractions of various populations of

differentially stained cells compared to the original, naïve control fraction. With

exposure, the number of destroyed cells increases with similar trends seen in PI+

populations. The fraction of cells that repair and stay viable of all cells processed is

significantly greater for PC-3 (35%) cells compared to PrEC LH cells (4%) (**Figure

2.3B**).

Evidence of fusion of lysosomes, as measured by the relative geometric mean of

LAMP-1 on the extracellular surface of cells, is present in PC-3 (1.386 vs. control 1.000)

cells but absent in PrEC LH cells (0.975 vs. control 1.000) (**Figure 2.4A**). The ionomycin

positive control is similar in the two cell lines, RGM is 1.303 in PC-3 and 1.319 in PrEC

LH (**Figure 2.4B**). Additional cell lines are tested for RGM of LAMP-1 intensity upon

exposure to FSS (RGMs, PrEC LH: 0.970, PrEC LHSR: 0.870, PrEC LHMK: 0.923)

(**Figure 2.4C**). BLI viability curves to confirm consistent assay behavior are shown in

Figure 2.4D. Note that PrEC LH and PrEC LHSR have slightly higher viabilities than

previously seen (refer to Barnes, Jones *et al.* 2012 for expected viability trends).

Finally, calcium dropout experiments are performed to test dependence of repair

on calcium. PI uptake trends differ between calcium-free and calcium-containing cell

suspensions (**Figure 2.5A**). Rapid uptake of PI is seen in viable cells in calcium-free D-

PBS, with a significant fraction of cells becoming PI+ in the initial two passages.

Quantification of PI uptake is shown in **Figure 2.5B**. While a slight increase in LAMP-1

intensity is apparent in nominally calcium-free D-PBS with EGTA, it flattens out after

passage the initial passages and is markedly reduced (RGM: 1.116) compared to calcium-

containing suspensions (**Figure 2.5C**). Calcium-containing D-PBS resulted in similar

25

LAMP-1 shifts (RGM: 1.397). Viability curves are shown in **Figure 2.5D** to confirm reduced viability in calcium dropout samples.

Knockdown of Synaptotagmin VII in GS689.Li cells altered the resistance phenotype compared to control, scramble cells (**Figure 2.6**).TEM4-18 cells with SYT7 knockdown are more sensitive to FSS compared to control cells. The percent knockdown for all cell lines is ~60%. Viability after ten passages of FSS at 250 μL/sec is 24.50%, 35.26%, and 27.15% in SYT7 knockdowns #1, #2, and #3, respectively. Note that only one sample is run for SYT7 knockdown #2. Scramble control viability run in parallel is 35.28%.

26
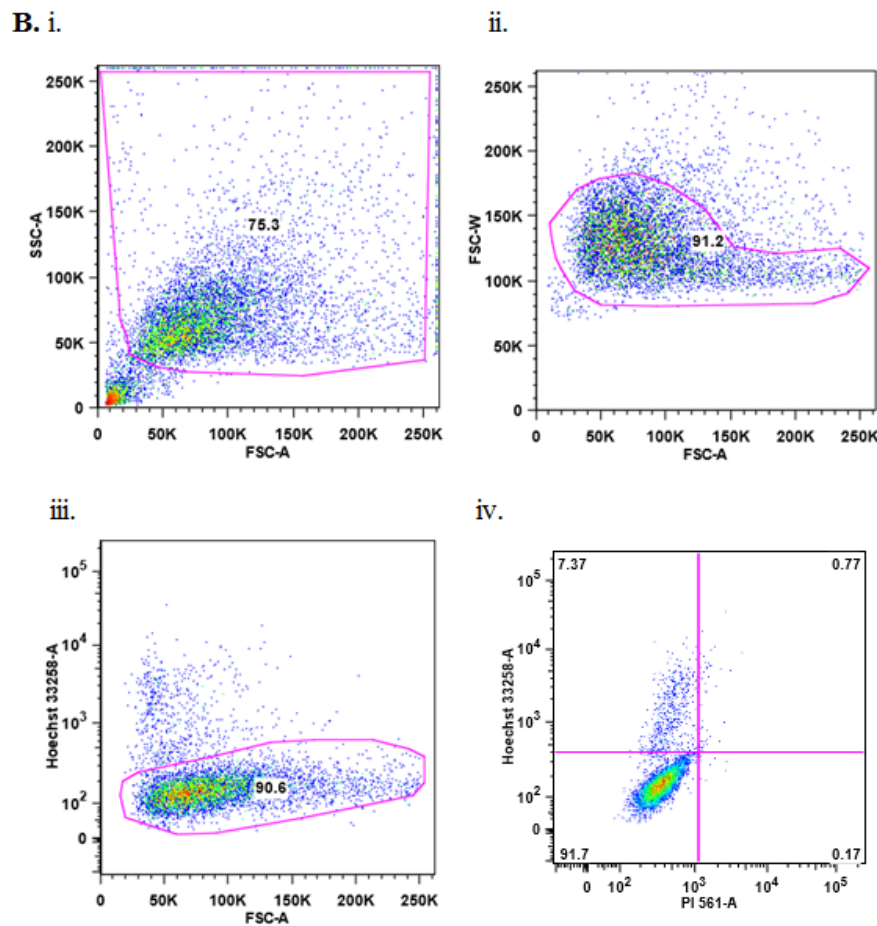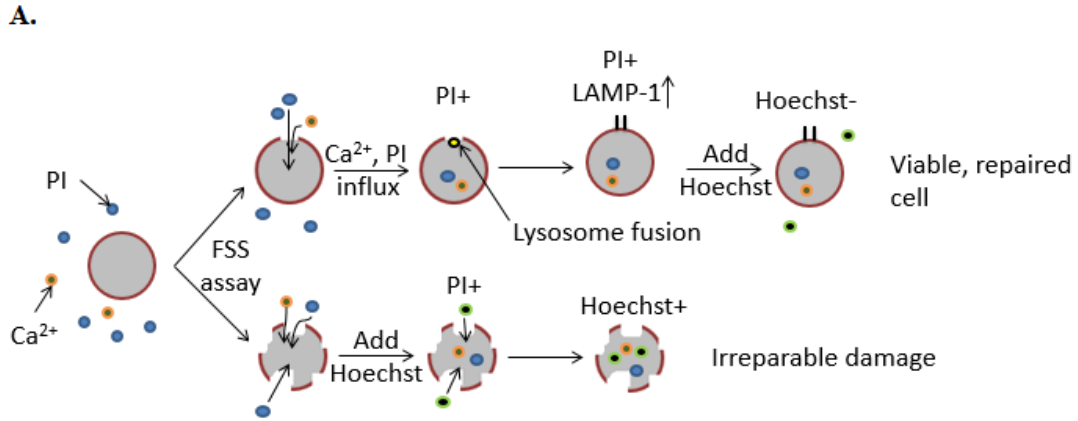
Figure 2.1: Experimental schematic and gating procedure for membrane repair.
A) Upon exposure to FSS, cells are damaged and take up PI and calcium. If repair is successful, some cells will repair injury via fusion of lysosomes and display LAMP-1 on the extracellular surface. Viable cells then exclude addition of Hoechst live/dead cell indicator. **B)** *i-iii*. Gating procedure based on cell size, granularity, and Hoechst intensity. *iv*. Quadrant used to determine PI+/- and Hoechst+/- using control sample.
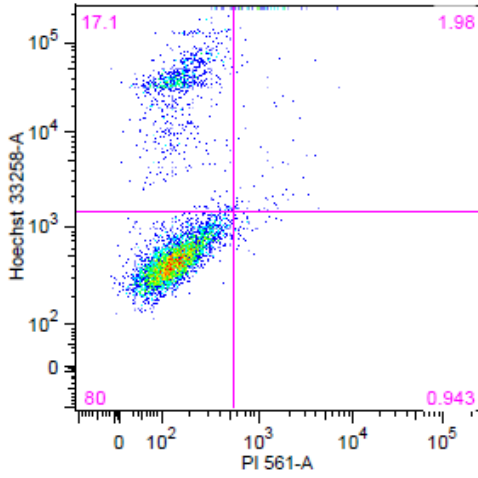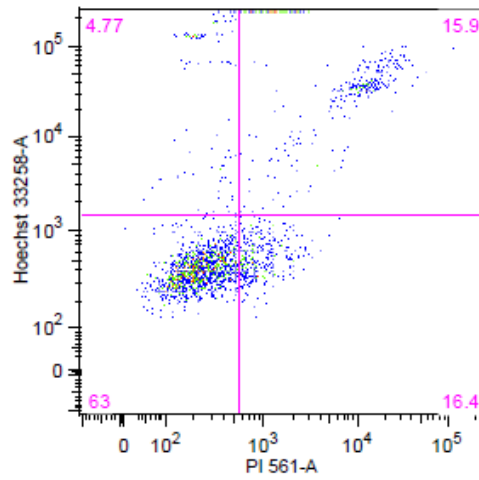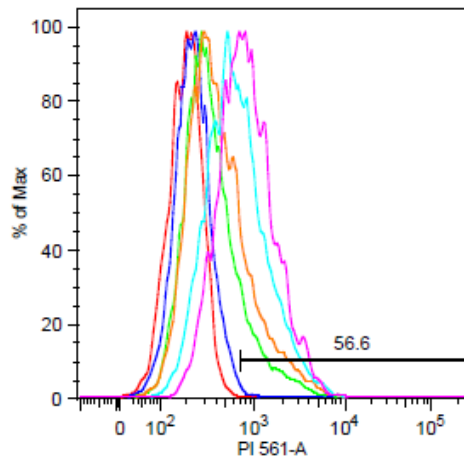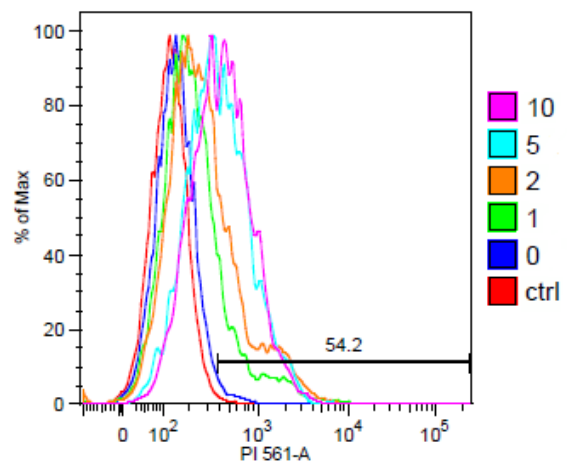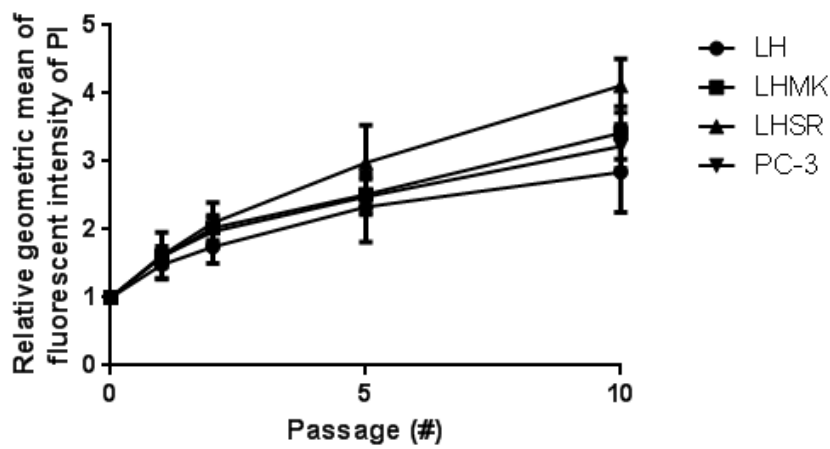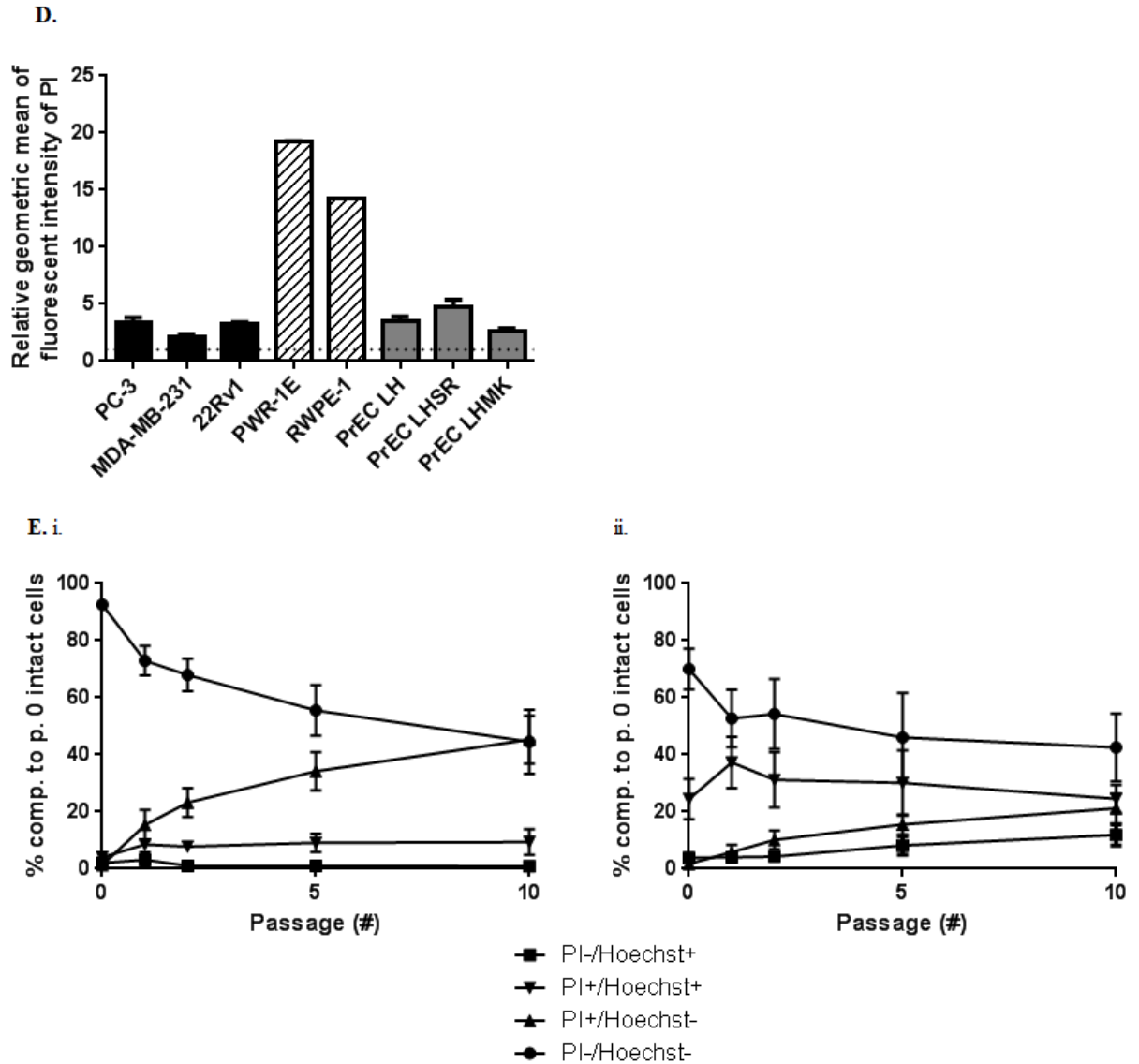
Figure 2.2: Evidence of repair by viable cell uptake of PI.
A) Quadrant of PrEC LH cells with PI and Hoechst fluorescent intensity displaying unrepaired and repaired live cells and dead cells: *i.* passage 0, *ii.* passage 10. **B)** PI intensity of PC-3 (*i.*) and PrEC LH (*ii.*) cells for sampled passages. **C)** Geometric means of live, intact cell lines upon exposure to ten passages of FSS. **D)** Passage 10 geometric means of all cell lines tested. Black: malignant cancer cells; diagonal slashes: transformed cells; gray: PrEC lines. **E)** Percent of stained fraction of PC-3 (*i.*) and PrEC LH (*ii.*) cells compared naïve control.

A. i.
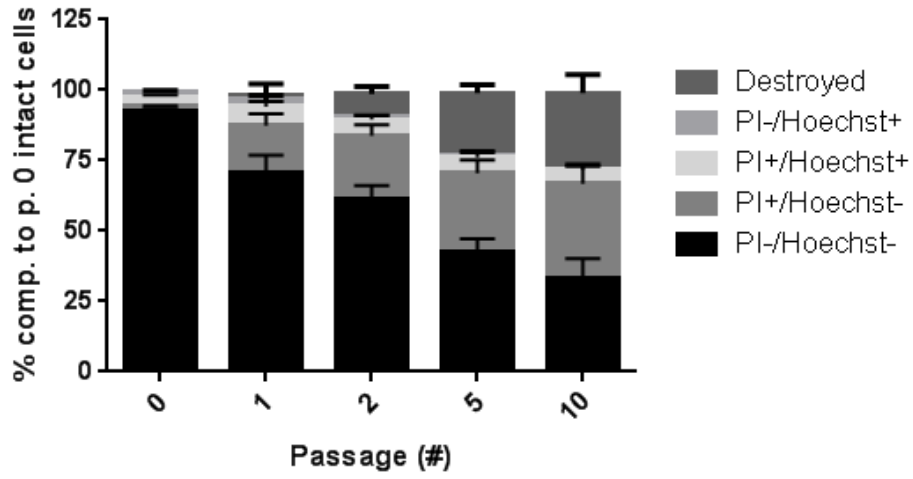
ii.
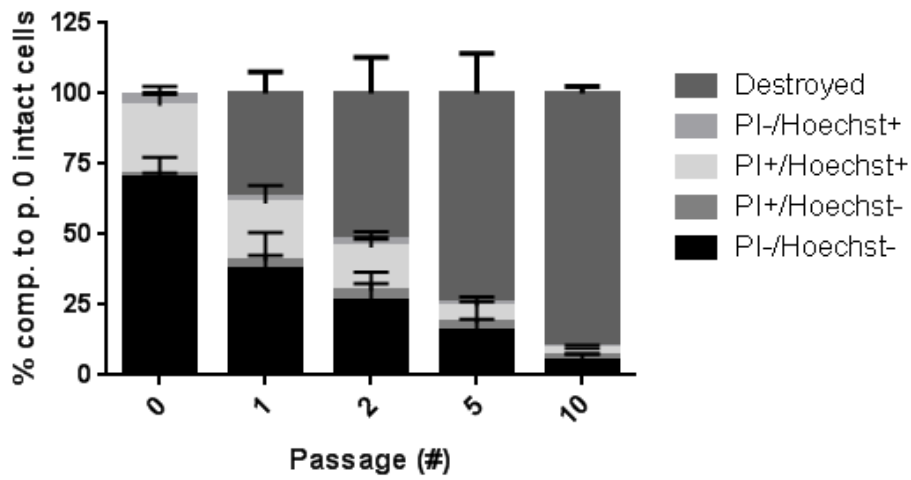
B.
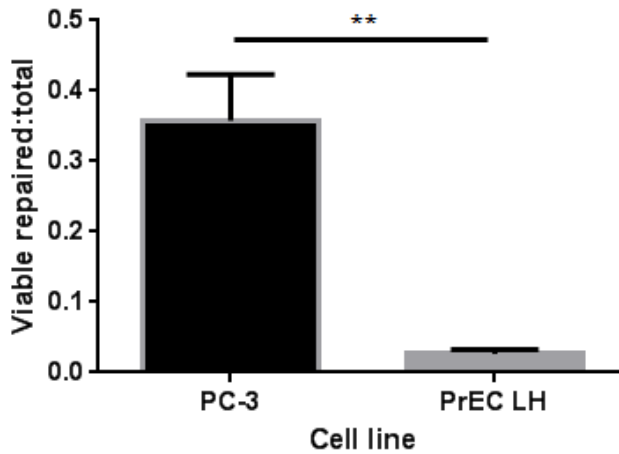
Figure 2.3: Standardization of samples for viable PI uptake.
Flow cytometry runs standardized to naïve control with counting beads to account for cell fragmentation. Destroyed cells are those of which have been completely destroyed by fluid shear stress. **A)** *i.* PC-3 cells. *ii.* PrEC LH cells. **B)** Fraction of cells exposed that are viable and have repaired in both PC-3 and PrEC LH cells (**p<0.01).

A.

B.

C.
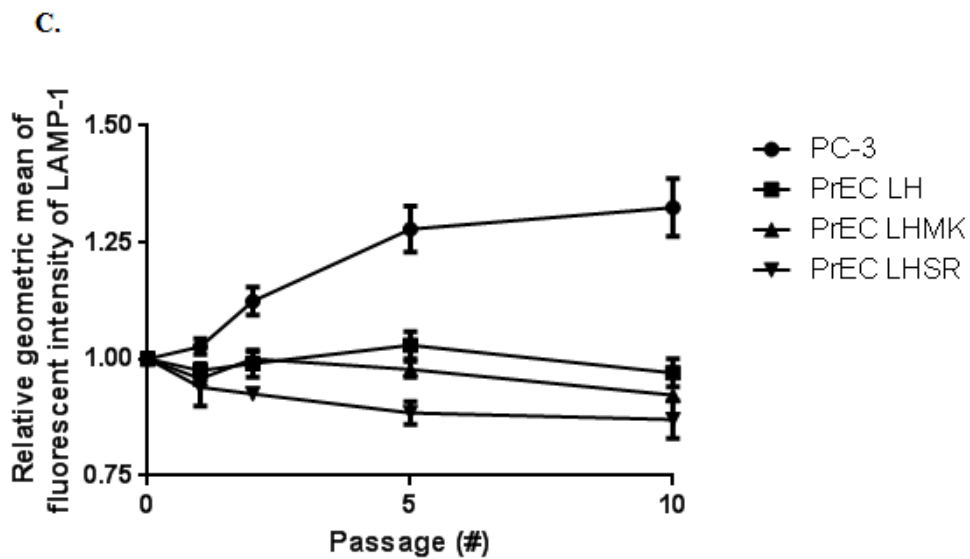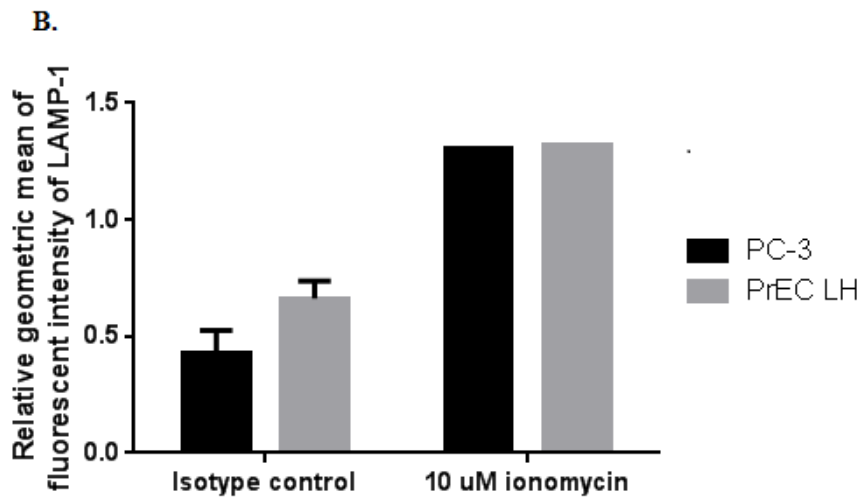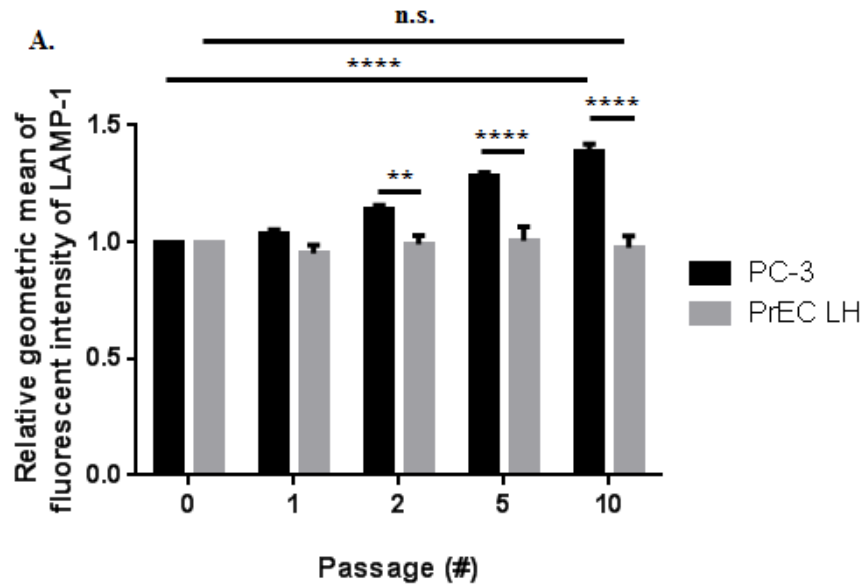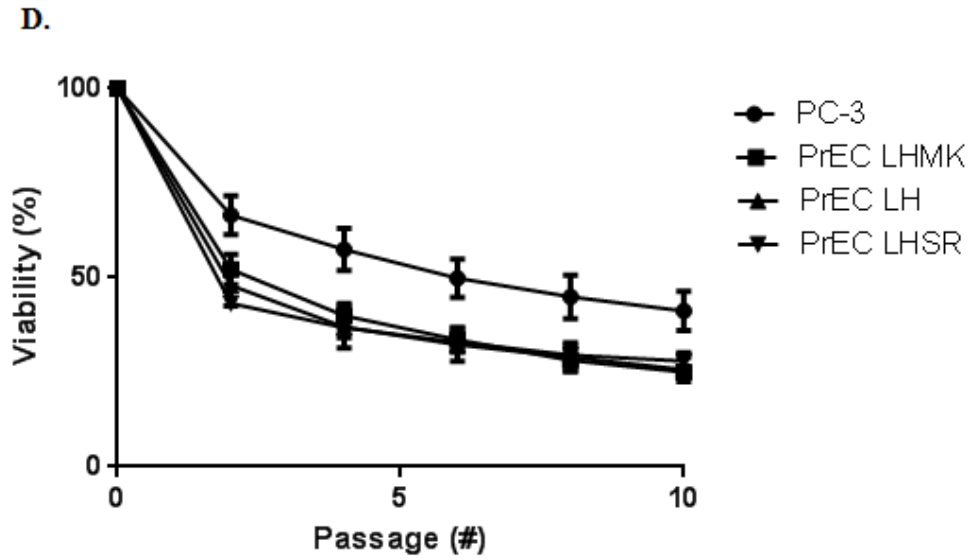
Figure 2.4: Fusion of lysosomes to plasma membrane for injury repair.
A) Relative geometric mean of LAMP-1 on the extracellular surface on the plasma
membrane in PC-3 and PrEC LH cells. **B)** Controls samples for non-specific binding of
antibodies and positive control for lysosome fusion. **C)** LAMP-1 expression for all PrEC
lines tested and PC-3 cells. **D)** Corresponding viabilities for LAMP-1 flow cytometry
experiments measured by BLI.

33
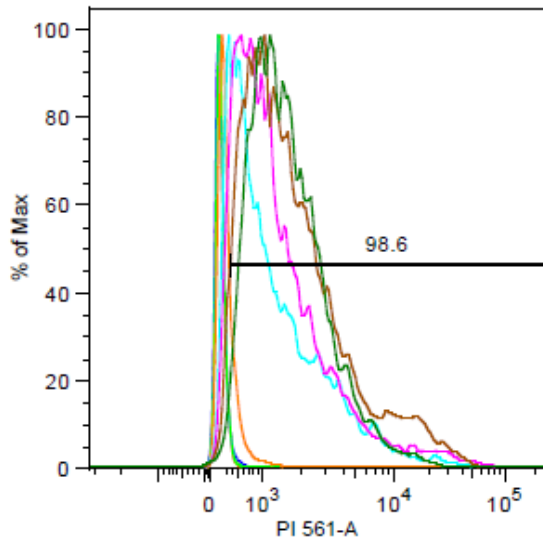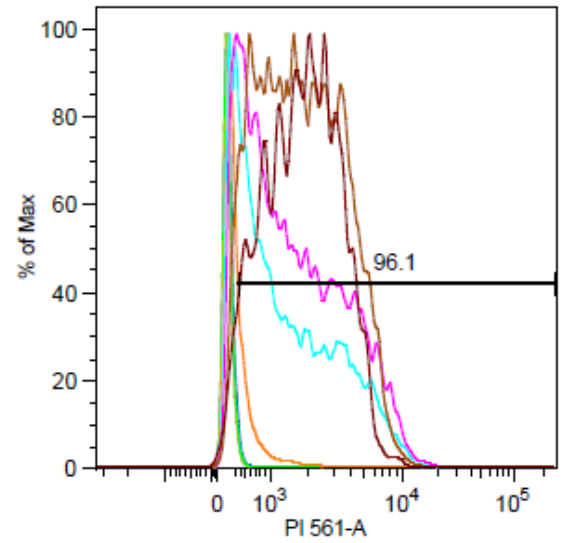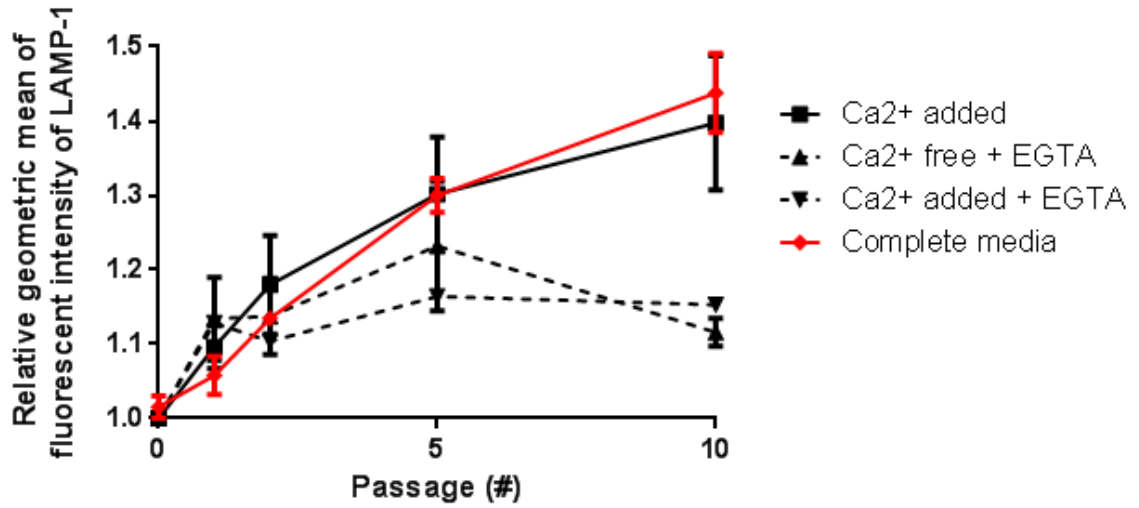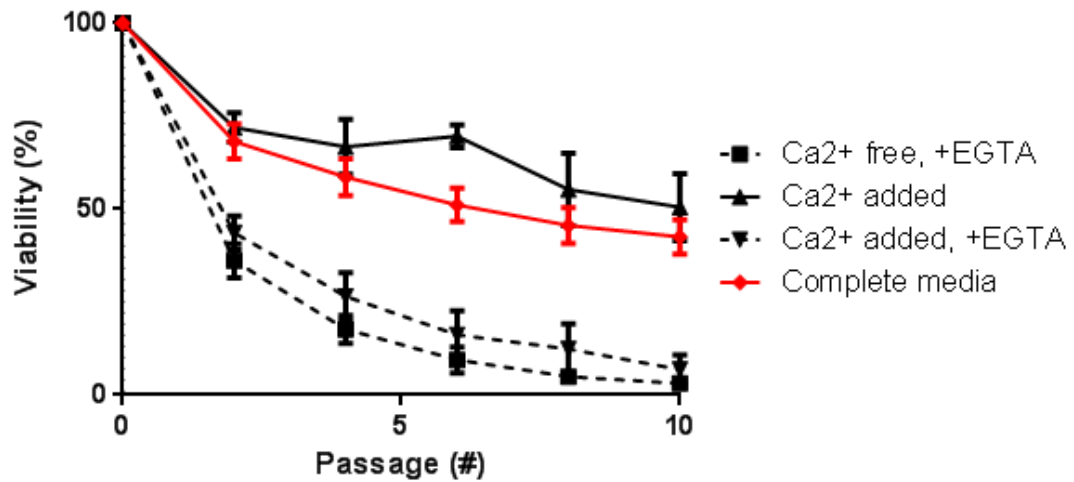
Figure 2.5: Membrane repair via lysosomes is calcium dependent.
A) Histograms of PC-3 cells demonstrating significant PI uptake. *i.* D-PBS medium
containing 1.17 mM $CaCl_2$. *ii.* Calcium-free D-PBS. **B)** Evidence of lysosomal fusion in
calcium-free and calcium-containing medium. Removal of calcium diminishes lysosomal
fusion. **C)** Viability of PC-3 cells measured by bioluminescence imaging. Calcium-free
or EGTA-containing medium results in significant loss of viability.
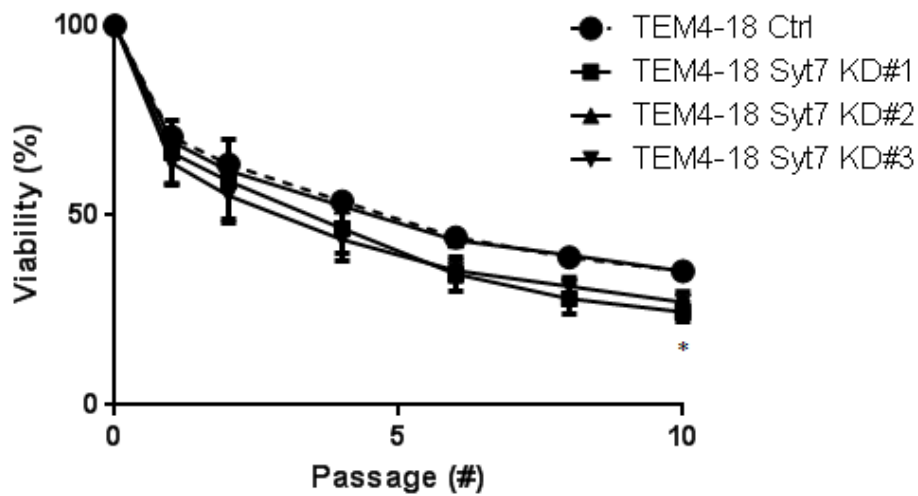
Figure 2.6: Synaptotagmin VII is required for efficient membrane repair.
Knockdown of Synaptotagmin VII (SYT7) in TEM4-18 cells done by lentiviral shRNA
constructs. The percent knockdown of all three SYT7 KD lines is ~60% as measured by
qRT-PCR. Cells are exposed to the standard fluid shear stress assay at 250 μL/sec (*,
p<0.05, Ctrl & SYT7 KD#1, Ctrl & SYT7 KD#3).

Discussion

Loss of membrane integrity is a frequent occurrence in many cells throughout the body. Cells have at their disposal numerous mechanisms and pathways to patch and repair their membranes, otherwise cell death will result. A common membrane damage response within cells is aggregation and fusion of intracellular vesicles. By fusing these vesicles to regions of membrane injury, a plug can be formed to restore normal cellular processes. One such vesicle is lysosomes, which have been implicated extensively in this membrane repair process.

First, evidence of membrane repair is shown by viable cell uptake of PI that is in the cell suspension medium during FSS exposure. Damage of the membrane resulting in holes allow PI to flood into the cell and bind to DNA, resulting in increased fluorescent intensity when measured by flow cytometry. Cells that manage to repair will remain viable and exclude Hoechst that is added after the FSS assay is completed. Thus, Hoechst negative, PI positive cells are cells that have repaired and maintained viability. Both PC-3 and PrEC LH cells demonstrate significant uptake of PI in viable populations. This PI intensity increased further as cells are exposed to repeated passages of FSS. These cell lines experienced similar relative changes in the geometric mean of PI. Additionally, PrEC LHSR and PrEC LHMK had comparable changes. This suggests that all of these cell lines can repair to some capacity. PI uptake is initially greater in the first couple passages. Uptake then is reduced in FSS-experienced cells, indicating that fewer cells are being damaged in these passages, consistent with the biphasic viability curves. This suggests that repair is more important in the FSS resistance phenotype in the initial, naïve

37

exposures. Furthermore, the population shifts, as evidenced by the histogram of each passage investigated, indicate similar PI uptake trends. Cells that are damaged more extensively should fluoresce greater with PI compared to cells that sustain only slight damage with small uptake of PI. The population shifts as a whole with a slight right-hand tail in both cell lines, indicating a small fraction of viable cells take up large amounts of PI, but overall, large percentages of cells are being damaged to some degree. These shifts, however, are only looking at the viable cell fraction of all events recorded.

One has to account for the absolute number of repaired cells to original control cells. When this is done by standardizing sample processing time, it is immediately apparent that PC-3 cells are much more efficient at membrane repair with over 30% of PC-3 cells exposed becoming PI+ after ten passages. On the other hand, less than 5% of PrEC LH cells exposed to FSS repair successfully, with a significant fraction of cells completely fragmented. Thus, while the percent fraction of viable cells that have repaired is similar between PrEC LH and PC-3 cells, the percentage out of all PC-3 cells exposed to FSS that repair is about eight-fold higher compared to PrEC LH cells. Further studies will be needed to elucidate the reasons behind this differential repair capacity between these malignant and benign cell lines. It is possible that the kinetics of membrane repair via fusion of lysosomes is not rapid enough in PrEC LH cells. Fewer cells are thus able to repair. Alternatively, an inherent property of PrEC LH cells may pre-dispose PrEC LH cells to more severe membrane damage that cannot be repaired. This may be due to a mechanical property, such as the stiffness of the membrane and cytoskeletal structures. Alternatively, it could be due to reduce or insufficient actin cytoskeleton dynamics.

PC-3 and PrEC LH cells displayed significantly different trends in LAMP-1 expression on the extracellular surface of the membrane as they are exposed to FSS. PC-3 cells exhibited approximately a 1.4 fold increase in LAMP-1 intensity, indicating plasma membrane repair via fusion of lysosomes. On the other hand, PrEC LH cells displayed no change in LAMP-1 expression after ten passages, indicating absence of membrane fusion of lysosomes to repair membrane damage sustained when exposed to FSS. Thus, if membrane repair is present in these cells, it is through a different mechanism. Despite no increase in LAMP-1, PrEC LH and PC-3 cells had similar increases in expression when treated with ionomycin. Treatment with ionomycin, an ionophore, catalyzes ion transport across membranes without extensive structural damage. PrEC LH may then have some capacity to fuse lysosomes to their plasma membrane, as ionomycin allows transport of calcium into the cell, triggering fusion. However, with large areas of membrane and cytoskeletal damage, PrEC LH cells lack sufficient ability to repair this more extensive, widespread injury. In addition, both exocytosis and endocytosis has been shown to be required to repair injury caused by pore-forming proteins, providing further evidence that repair of these two types of injury may be quite different (Idone, Tam *et al.* 2008). Finally, ionomycin may provide evidence of the maximum capacity of lysosome fusion in loss of membrane integrity and thus the maximum fluorescent intensity change of LAMP-1. Ionomycin will cause widespread lysosome fusion to remove these ionophores and which likely exhausts the membrane binding reserve of lysosomes. The increase in LAMP-1 fluorescence is comparable between passage ten in PC-3 cells and the ionomycin treated cells.

The repair process is calcium dependent. Initially, calcium dropout experiments were performed in D-PBS without addition of EGTA but lysosomal fusion is evident and similar increases in LAMP-1 were seen in calcium-free and calcium-added experiments. A hypothesis for this behavior is release of calcium from intracellular stores, such as the endoplasmic reticulum, to trigger lysosomal fusion to cellular membranes. Agonists that mobilize calcium from these intracellular stores have been shown to trigger lysosomal exocytosis, albeit at a lower level (Rodriquez, Webster *et al.* 1997). This intracellular calcium release may be due to internal organelle injury or signaling cascades that result in release of calcium, which triggers the membrane fusion pathway. Cell viability is further reduced in the presence of medium containing EGTA with no calcium, compared to calcium free medium with no EGTA. When the plasma membrane is compromised, EGTA can enter the cell. EGTA may chelate the intracellular calcium that is released either through signaling or damage to vesicles. This intracellular release may trigger lysosome fusion. Additionally, increases in LAMP-1 expression on the cellular membranes are diminished in cells exposed to the FSS assay in calcium free, EGTA containing medium. The fold increase is less than half that seen in calcium-containing medium. Consequently, fusion of lysosomes to repair membrane injury is a calcium-dependent process. However, removal of calcium from cell suspensions can alter other calcium-dependent cellular processes, such as mechanotransduction, which may alter FSS resistance.

Additionally, knockdown of Synaptotagmin VII (SYT7), a calcium-dependent sensor important in initial stages of membrane repair, sensitizes resistant malignant cells to FSS. Several cell lines with SYT7 knockdowns demonstrated a consistent ~10%

increase in loss of viability compared to control cells. In the three knockdown lines tested, SYT7 is reduced by approximately 60% compared to control scramble cells. Also, the increased viability loss is primarily seen in the initial first passage of FSS-exposure. SYT7 knockdown results in ~10% greater viability loss in the first passage while the later passages remain largely unaffected. This data suggests repair is more important in the naïve resistance response to FSS and is less of an influence in FSS-experienced cells.

Repair of membrane injury is a critical aspect of the resistance phenotype that PC-3 cells exhibit. With impaired membrane repair ability, PC-3 cells display increased sensitivity to FSS. Thus, FSS resistance evident in malignant PC-3 cells may be a result, at least in part, of increased membrane repair efficacy and warrants further investigation.

CHAPTER 3 MEMBRANE AND CYTOSKELETAL STIFFENING

Summary

Cells must be able to respond to dynamic and stressful environments. When in suspension, the stiffness of the cellular membrane and cytoskeleton can play a significant role in how forces and stresses are absorbed and transduced. Particles that are too stiff may be too brittle and break apart when subjected to fluid shear stress whereas particles that are too deformable may be torn apart.

Thus, using micropipette aspiration (MPA), the stiffness of two cell lines is studied under various conditions. In this technique, cells are partially aspirated into a small diameter micropipette and these projections are measured. Based on the pressure within the pipette and the length of this projection, the elastic modulus, a measure of stiffness, is calculated. Non-exposed prostate carcinoma cells, PC-3, had a smaller elastic modulus when compared to non-transformed prostate epithelial cells, PrEC LH. However, PC-3 cells displayed a significant increase in membrane stiffness when exposed to the fluid shear stress (FSS) assay. Alternatively, the PrEC LH cells did not experience a change in their elastic modulus. The preliminary results of this study have been previously published (Chivukula, Krog *et al.* 2015).

Micropipette aspiration

The micropipette aspiration consists of an inverted microscope, a micropipette and micromanipulator, and a water column connected to the pipette. A camera is connected to the microscope. Briefly, the water column is initially level with the height of the microscope stage. A suspension of cells is added to a microscope slide, the pipette is positioned close the cell, and the water column is lowered incrementally. A portion of the cell is aspirated into the pipette and projection lengths are measured at various stage heights. A schematic of the setup is shown in **Figure 3.1**. Cells are cultured and processed as previously described.

Pipette preparation and calibration: Borosilicate capillaries (TW150-3, World Precision Instruments Incorporated) with a diameter of 1 mm are heated and pulled using a micropipette puller (P-97, Sutter Instruments) to a fine, tapering end. Pulled pipettes are cut using a micro-forge (MF-900, Narishige Group). A pre-cut is made with a diameter smaller than desired to remove unwanted material. All pipettes are cut to a diameter of approximately 7-8 µm. Pipettes with jagged or curved tips are discarded. The prepared micropipette is filled with a microfilling needle (MicroFil) containing 1x PBS and examined for bubbles. A 1 cm section of Tygon tubing is glued onto the unmodified end of the micropipette to connect it to a T-valve and placed on the micromanipulator arm. Tubing is connected from the T-valve to the water column. A droplet of 1x PBS

43
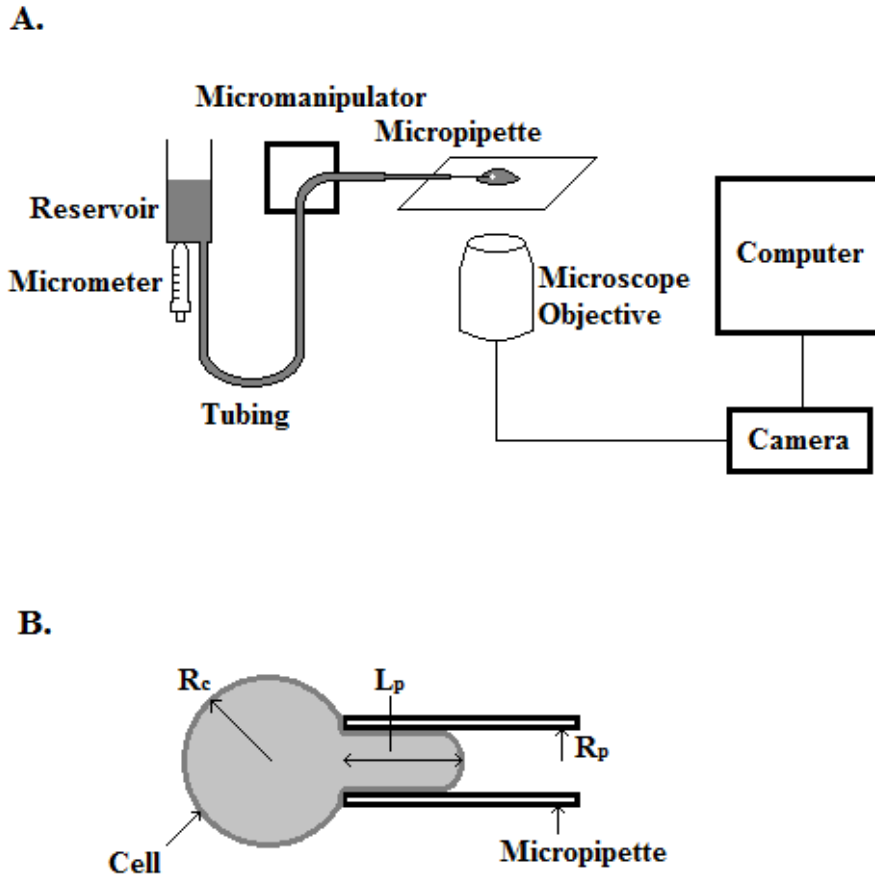
Figure 3.1: Micropipette aspiration setup.
A) The micropipette aspiration setup consists of a water reservoir, with the height controlled by a micrometer, connected to a micropipette. The micropipette is positioned with a micromanipulator near cells under an inverted microscope connected to a computer monitor with imaging capability. **B)** As the water column is lowered, cells with radii R_c are partially aspirated into a pipette with radius R_p. The length of the cell projection, L_p, at a pressure ΔP is related to the stiffness of the membrane and underlying cytoskeleton.

containing $1x10^5$ 2 µm microspheres/mL is placed on a microscope slide. The micropipette is manipulated towards beads to determine hydrostatic pressure of the pipette. Based on aspiration or expulsion of microspheres, the water column height is adjusted such that there is no movement of spheres when near the tip of the micropipette. This is considered 0 mm H_2O.

Aspiration of cells: Cells collected from culture plates or the FSS assay are diluted to approximately $1 * 10^4$ cells/mL. A droplet of cells, either unexposed or exposed, is placed on a microscope slide and positioned on the stage of an inverted microscope (TE-300, Nikon Corporation). The micropipette is positioned close to a cell and the water column is lowered a specific distance, typically 4 mm. The cell is partially aspirated into the pipette. The tip is raised slightly up to ensure the cell is not in contact with the slide. When the projection equilibrates, usually after one minute, an image is taken with a Stingray camera (Allied Vision Technologies GmbH). The stage is lowered again and this process is repeated three more times for a total of four images.

Treated cells are incubated with either the Rho-kinase inhibitor, Y-27632 (iROCK), at 10 µM for 20 hours or Cytochalasin D at 20 µM for 20 hours at 37°C in complete culture medium. A control, untreated sample is run in parallel with treated cells to confirm increased loss of viability in treated cells.

Analysis: Projections of cells that are aspirated into the pipette are measured using ImageJ software. Conversion of pixels to micrometers is done by using a micrometer slide with ten micrometer divisions. Change in pressure is determined using $\Delta P = \rho g h$,

45

where ΔP is the change in pressure in Pa, ρ is the density, assumed to be water at 20°C, g is the gravitational constant of 9.81 m/s^2, and h is the height the stage is lowered. The general equation for the elastic modulus is:

$$E = \frac{stress}{strain} \tag{2}$$

where E is the elastic modulus in Pa. Stress is simply a force per unit area and strain is the change in length of a material divided by original length. A material that is stiffer will have a smaller change in length under an applied load or stress. Thus, the material will have a larger elastic modulus. The elastic modulus in micropipette experiments is determined by the equation (Theret, Levesque *et al.* 1988):

$$\Delta P = \frac{2\pi}{3} E \frac{L_p}{R_p} \Phi, \tag{1}$$

where ΔP is the change in pressure in Pa, E is the elastic modulus in Pa, L_p is the length of the cell projection within the micropipette in μm, R_p is the radius of the micropipette in μm, and Φ is a term that depends the thickness of the pipette wall and the radius of the pipette, often assumed to be approximately 2.1.

Statistical analysis

An unpaired, two-tailed Student's t-test is performed between cell lines. Ordinary one-way ANOVA with Holm-Sidak's multiple comparisons adjustment is performed to test significance between types of exposure in PC-3 and PrEC LH cells.

PC-3 versus PrEC LH

Control cells are released from culture plates and measured. Exposed PC-3 and PrEC LH cells are passed through the standard FSS assay. Typical images obtained at various water reservoir heights are shown in **Figure 3.2A** with the corresponding slopes, which are proportional to the elastic modulus, graphed in **Figure 3.2B**. The elastic moduli of PC-3 and PrEC LH cells that are either naïve control or FSS-exposed are shown in **Figure 3.3A**. PC-3 cells are exposed either at a low flow rate of 20 µL/sec or the high flow rate of 250 µL/sec whereas PrEC LH cells are only examined at the standard 250 µL/sec rate. The mean elastic modulus for PC-3 cells before FSS exposure, 19.81 Pa, is over two-fold lower than the PrEC LH cells, 45.91 Pa. When exposed to similar magnitudes of FSS, PC-3 cells increased their elastic modulus to 35.38 Pa while PrEC LH cells did not significantly change (41.08 Pa). However, despite stiffening in response to FSS, exposed PC-3 cells are still less stiff than exposed PrEC LH cells. Additionally, PC-3 cells exposed to the lower flow rate increased their elastic modulus to 29.25, a lesser extent when compared to PC-3 cells exposed to the high flow rate.

The effects of multiple passages of shear stress is examined by measuring PC-3 cells exposed to only one passage of the FSS assay and comparing to the standard ten passages of shear (**Figure 3.3B**). At one passage of 250 µL/sec, the elastic modulus of PC-3 cells increased significantly to 27.49 Pa. The elastic modulus increase in the initial passage is approximately half that seen after ten passages of shear.

47

D.
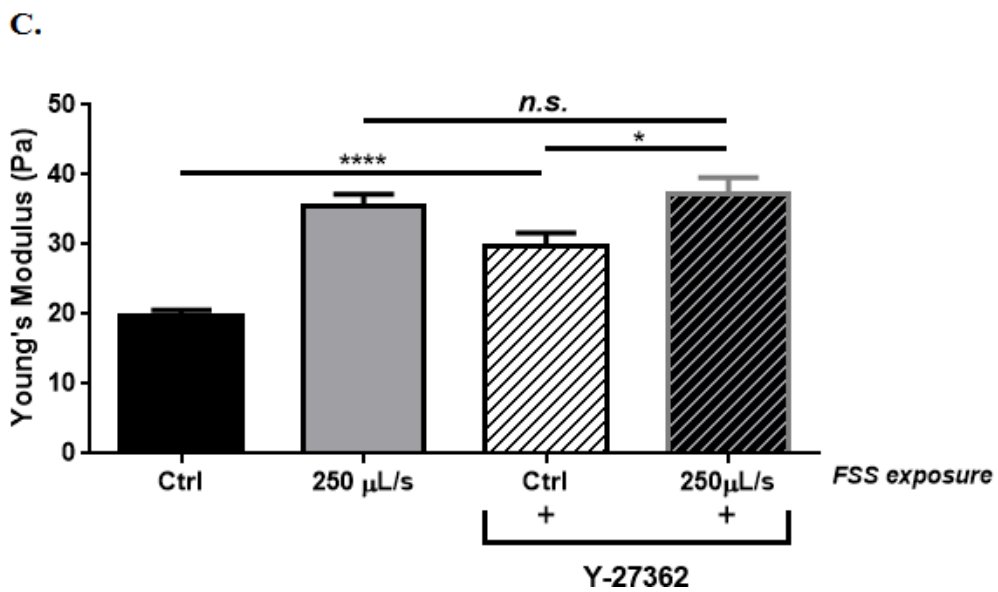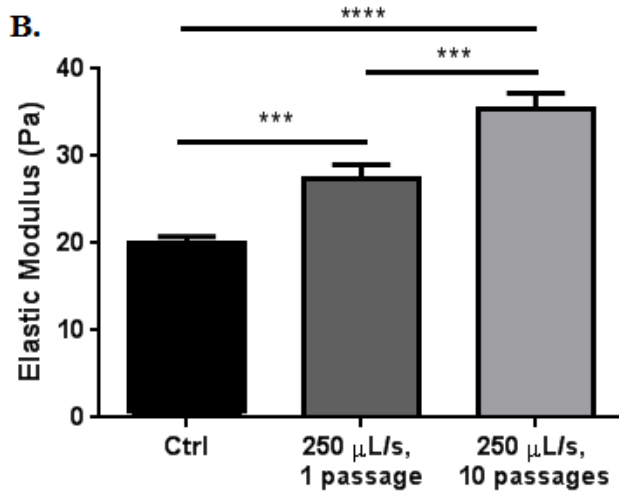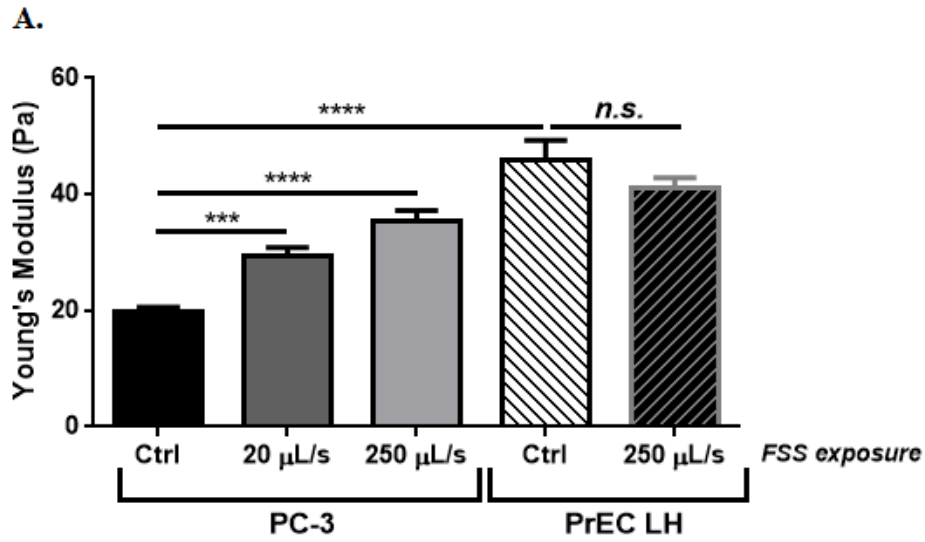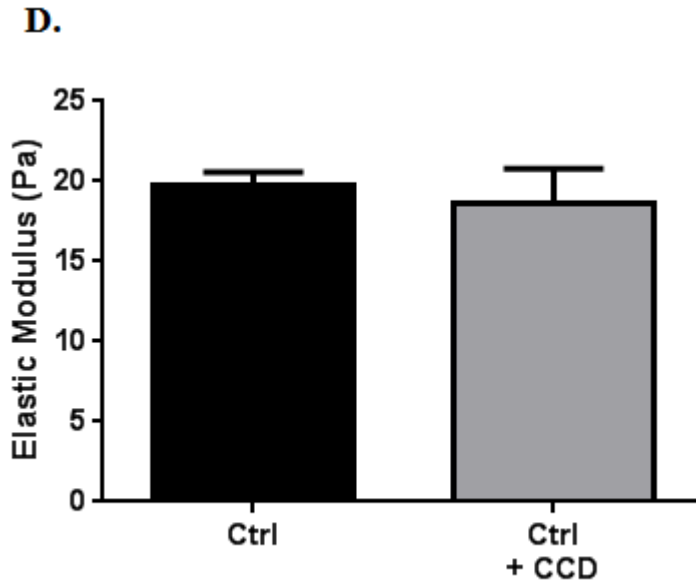
Figure 3.2: Elastic moduli of naïve and fluid shear stress-exposed PC-3 and PrEC LH cells.
A) PC-3 and PrEC LH non-fluid shear stress-exposed controls and fluid shear stress-exposed cell's elastic moduli are measured using micropipette aspiration. **B)** PC-3 elastic moduli both after one and ten passages of fluid shear stress are compared to naïve control cells. **C)** Y-27632 treated or untreated PC-3 cells before and after fluid shear stress. **D)** Treatment with Cytochalasin D compared to untreated controls. (*, $p<0.05$; ***, $p<0.001$; ****, $p<0.0001$).

A) Typical aspiration lengths of a PC-3 at various pipette pressures. **B)** Determination of the elastic modulus. Slope of $\frac{L_p}{R_p}$ and suction pressure is proportional to the elastic modulus of the plasma membrane.
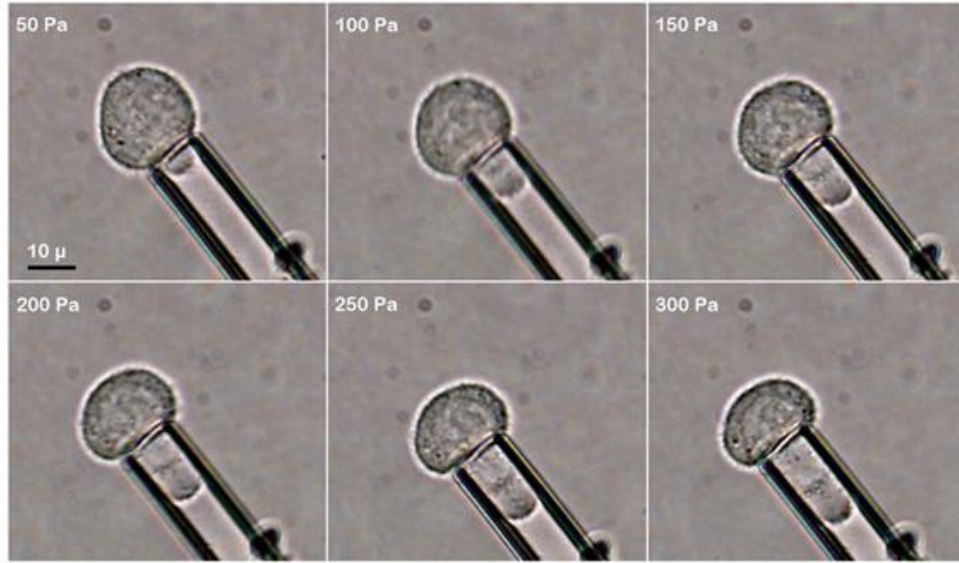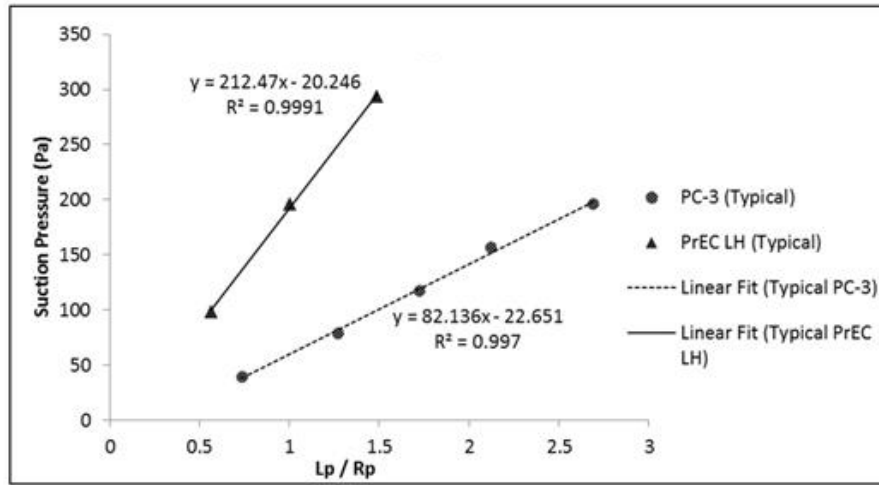
Figure 3.3: Aspiration of cells and determination of elastic modulus

Drug treatments

PC-3 cells are also treated with either Y-27632 (**Figure 3.3C**), a Rho-kinase inhibitor, or Cytochalasin D (CCD) (**Figure 3.3D**), an inhibitor of actin polymerization. Inhibition by Y-27632 led to an elastic modulus of 29.80 Pa in unexposed cells while treated cells exposed to the standard FSS assay had a similar modulus, 37.16 Pa, to non-treated exposed cells. Thus, the percent increase in stiffness upon FSS exposure in Rho-kinase inhibited cells is less than non-treated exposed cell. Control, naïve cells treated with CCD did not change their elastic modulus (18.62 Pa) significantly compared to untreated naïve cells.

Gaussian fit

Histograms of the elastic modulus for naïve PC-3 cells and PC-3 cells exposed to 20 and 250 µL/sec are shown in Figure 3.4A and non-exposed and FSS-exposed PrEC LH cells in Figure 3.4C. Gaussian distributions are fit to these PC-3 elastic modulus frequency diagrams to assess the normality of the distribution (Figure 3.4B). In non-exposed cells, the fit is high ($R^2 = 0.95$), but then reduces when exposed to 20 µL/sec ($R^2 = 0.87$) and is a poor fit at 250 µL/sec ($R^2 = 0.68$). Naïve PrEC LH had a poor fit with an $R^2 = 0.74$ whereas FSS-exposed PrEC LH had a good fit with an $R^2 = 0.94$ (Figure 3.4D).

51

A.

B.
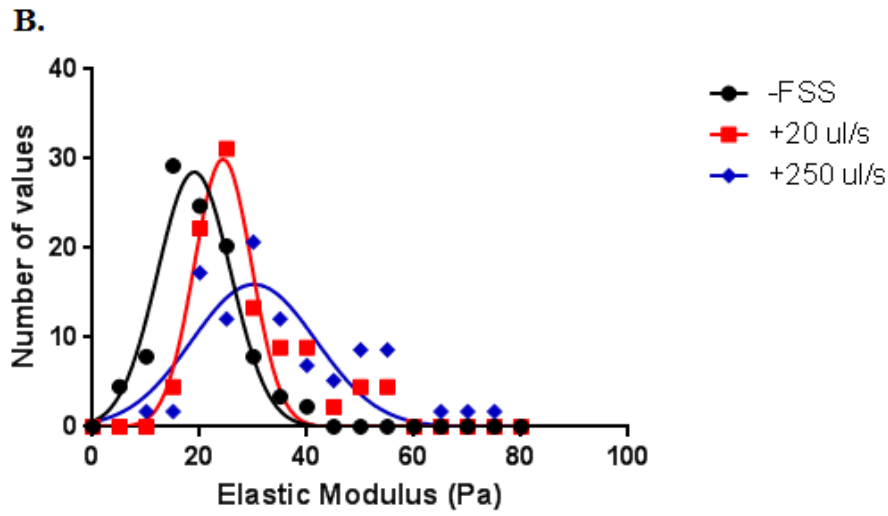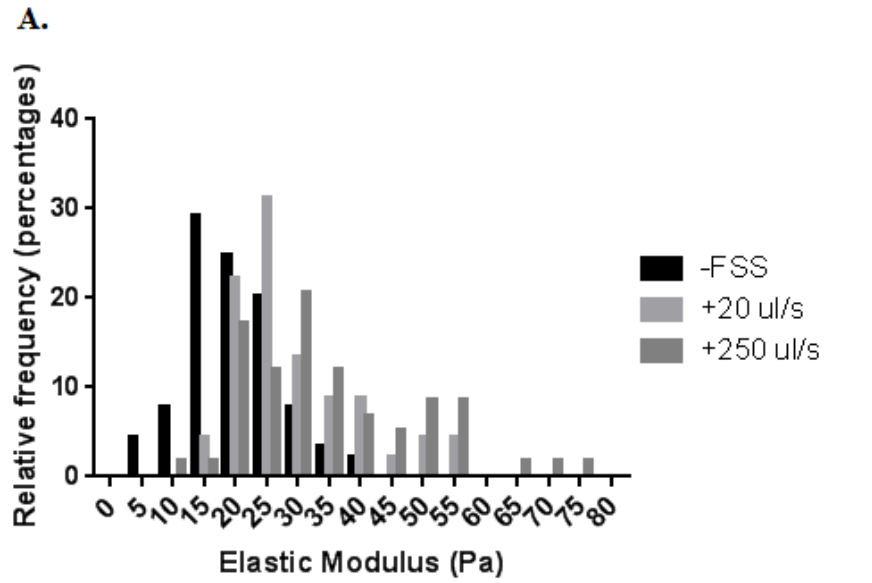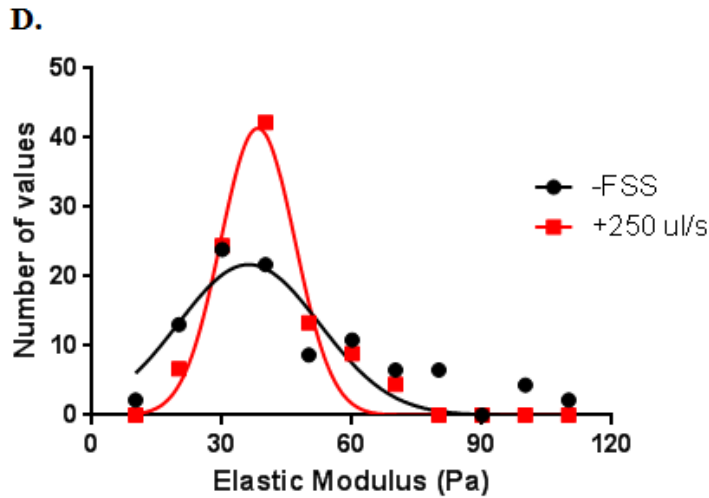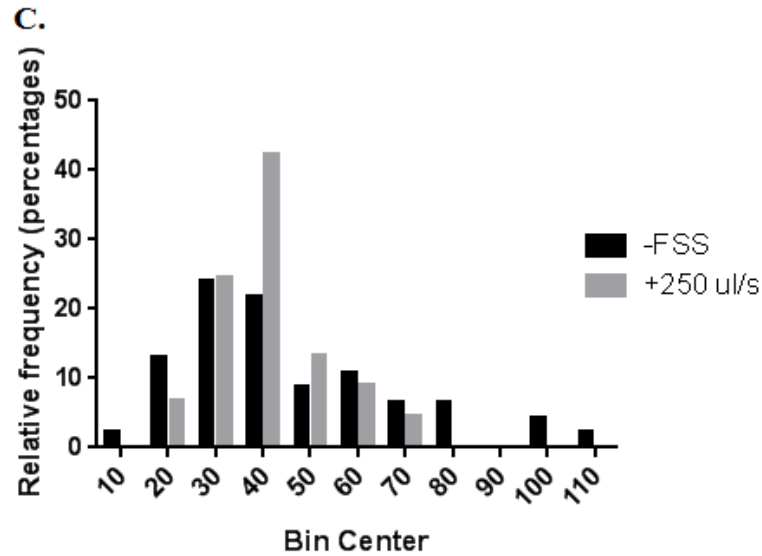
Figure 3.4: Frequency and normality distributions of elastic moduli.
A) Relative frequency (percentage) of elastic modulus in non-exposed and fluid shear stress-exposed (20 and 250 µL/sec) PC-3 cells. **B)** A Gaussian distribution curve is calculated for each experimental case in PC-3 cells. **C)** Relative frequency (percentage of elastic modulus in non-exposed and fluid shear stress-exposed (250 µL/sec) PrEC LH cells. **D)** A Gaussian distribution for PrEC LH cells.

The deformability of cells is a paramount property in their survivability and function in various environments. For example, white blood cell extravasation requires that these cells be able to squeeze through the small gaps between endothelial cells. Furthermore, red blood cell deformation while traversing capillary beds has been a longstanding topic with significant interest and is often used as a model system due to the lack of a nucleus. In the context of human disease progression, changes in mechanical properties can influence cell behavior (Suresh 2007). Studying the process of mechanical force transduction into biological responses and how cell biology can elicit responses to these forces can provide important insights of how cells are able to withstand these stressful environments and carry out their tasks.

There are numerous biophysical techniques to measure certain mechanical properties of cells. When looking at these properties, atomic force microscopy (AFM), magnetic beads, substrate stretching, optical tweezers, and others can be used. A simple, inexpensive method to measure membrane stiffness is micropipette aspiration. Using micropipette aspiration, one can extend a portion of a cell into a pipette to measure the mechanical stiffness of the cell membrane and underlying cytoskeleton. To model cellular deformation, certain assumptions must be made to simplify the complexity of a cell's inner structures and contents. The cell is treated as a solid if it does not flow into the pipette when the aspiration length (L_p) exceeds the radius of the pipette (R_p). Thus, the aspiration length increases linearly with increases in suction pressure. Conversely,

cells behaving as a liquid drop will freely flow into the micropipette when L_P exceeds R_p (Hochmuth 2000). The cells measured are all treated as solid particles.

Differences in mechanical properties between the prostate carcinoma cells and wild-type prostate epithelial cells provide clues to the mechanism behind the PC-3 cells resistance phenotype to fluid shear stress. The elastic modulus, a measure of material stiffness, of the membrane is measured using micropipette aspiration. Several significant findings came out of this study.

Firstly, consistent with previous findings, the stiffness of malignant cells is less than wild-type, benign cells, both of similar origin. PrEC LH cells are approximately 2.5 times stiffer than the PC-3 cells. Several studies have reported this biophysical property and it appears to be conserved across many malignant cancer cell lines (Lekka, Laidler *et al.* 2005; Ward, Li *et al.* 1990). Several reasons for this result have been discussed. Malignant cells are less stiff due to different cytoskeleton organization, such as reduced F-actin or damage to microtubule and microfilaments (Sato & Suzuki 1976; Guck, Schinkinger *et al.* 2005). The stages of metastatic dissemination that require malignant cells to navigate through connective tissues, undergo intravasation into the circulation, and undergo extravasation from blood vessels, akin to leukocytes undergoing diapedesis, necessitate a measure of deformability to pass through these tight interfaces. Malignant cells that are too stiff to effectively perform any of these steps likely have reduced metastatic potential. Nonetheless, some measure of rigidity is expected to be needed during passage through the circulation where high fluid shear stresses are present. Particles that are too deformable are likely to be pulled apart under high shear rates. Thus, it is possible that PrEC LH cells are initially too stiff for efficient force absorption

55

or deflection and are sensitive to fluid shear stress. PC-3 cells, which are less stiff, may be able to mitigate damage by avoiding high regions of FSS which are closer to the wall. Ample evidence has been shown that deformable particles exhibit drift towards the axis of flow compared to stiff particles (Di Carlo 2009; Segre & Silberberg 1962; Hur, Henderson-MacLennan *et al.* 2011). PC-3 cells that use this fluid mechanics principle may reduce their level of exposure by moving towards low shear regions near the axis of flow. PrEC LH cells may be too stiff and experience higher magnitudes of FSS, causing the stiffer particles to be destroyed and selectively enriching the less stiff PrEC LH cells. This may explain the slight decrease in the elastic modulus seen after FSS exposure.

Secondly, PC-3 cells exhibited a substantial increase in their elastic modulus when exposed to high levels of brief fluid shear stress. Furthermore, when PC-3 cells are exposed to a substantially lower flow rate with a maximum fluid shear stress greater than an order of magnitude smaller, their elastic modulus increased significantly. This finding suggests several explanations: 1) PC-3 cells are able to sense the mechanical force and adapt by increasing the stiffness of the membrane/cytoskeleton to optimize force transduction, or 2) when exposed to FSS, cells sustain damage, repair, and an increase in stiffness is witnessed as a by-product of these events, or 3) cells that are less stiff are selectively destroyed. PC-3 cells may be able to respond to FSS by stiffening their membrane via cytoskeletal changes through mechanosensitive channels. Finally, the cellular machinery that is required to mend and repair membrane and cytoskeletal damage upon exposure to FSS may alter the stiffness of the cell. Cytoskeletal dynamics, especially actin, has been implicated in streamlining fusion of intracellular vesicles to fuse to the membrane to repair damage. These processes may change the elastic modulus

56

of the membrane, at least locally, and explain the increase in stiffness measured. This is consistent with trends in cortical F-actin expression that is localized to specific areas of the plasma membrane (Chapter 4). However, the increase in the elastic modulus seen at the lower flow rate is substantial when considering the number of cells destroyed or damaged in this mild exposure. A mechanotransduction response that results in stiffening at low flow rates would be suggestive of a low-shear priming effect. However, as shown in Chapter 4, priming at low flow rates does not appear to significantly affect viability at high shear exposures.

The elastic modulus distribution shifts and gains a right-handed tail, with the tail becoming more evident with higher magnitudes of exposure. This is demonstrated by reduced fit of a Gaussian distribution on the data, with the control being a good fit while exposure at 250 μL/sec is a poor fit, with an R^2 of 0.68. This suggests that only a fraction of cells stiffen significantly, possibly supporting the hypothesis that only cells that repair appreciable damage become stiffer. Many cells may experience only minor or no damage with a corresponding mild change in stiffness. Alternatively, it suggests that less stiff cells are more sensitive to FSS and are destroyed, with slightly stiffer cells becoming enriched. The data obtained for individual cells does not suggest that there is differential destruction of originally more pliable cells. Close examination of the histogram reveals no cells stiffer than 40 Pa in naïve populations. With a 250 μL/sec exposure, approximately 30% of cells measured have elastic moduli greater than 40 Pa. Only ~50% of PC-3 cells are destroyed during the FSS assay. Clearly, an enrichment of this magnitude is not possible with the viability loss and increase in elastic modulus.

57

Alternatively, PrEC LH did not change their elastic modulus when exposed to the FSS assay. While there does appear to be a consistent slight decrease when exposed, possibly suggesting that these cells are too stiff and thus more sensitive, the finding is not statistically significant ($p = 0.0865$). As shown in Chapter 2, PrEC LH cells did not demonstrate efficient, lysosome-dependent membrane repair and did not display any lysosomal fusion activity. This finding may support the idea that the increase in elastic moduli PC-3 cells exhibit is a result of the membrane repair processes. However, the surviving fraction of PrEC LH cells did display evidence of repair via PI uptake. Different repair mechanisms between PC-3 and PrEC LH cells may be affecting the elastic moduli differently. However, PrEC LH cells that are both too deformable and too stiff appear to be destroyed, as is evidenced with frequency diagrams, and the population spread becomes considerably smaller after exposure. This suggests that PrEC LH cells that are significantly more stiff or deformable than the population mean may be more susceptible to FSS. Thus, membrane stiffness may be important to FSS resistance.

PC-3 cells elastic moduli also exhibited a dependence on the number of passages of shear stress. The elastic modulus increased significantly when exposed to a single passage of high FSS. Interestingly, the modulus of PC-3 cells exposed to a single passage of high shear is very similar to PC-3 cells exposed to ten passages of low shear. Another thing to note is that the increase is not consistent with a constant increase in the elastic modulus from passage to passage. Instead, analogous to the response of viability to FSS, the elastic modulus appears to be biphasic in nature, with a significant increase in the initial, naïve passage of FSS while less substantial increases in the remaining passages. Again, this may be consistent with the theory that membrane repair is influencing the

58

stiffness as most membrane repair appears to occur in the initial passages. Alternatively, rapid mechanotransduction may lead to a change in the elastic modulus and stiffening of the membrane and cytoskeleton elements.

Finally, the effects of inhibition of actin cytoskeletal dynamics on membrane stiffening upon FSS exposure are explored. PC-3 cells are treated with either Y-27632 or CCD, both inhibitors of cytoskeletal dynamics. Previous studies in our lab (Barnes, Jones *et al.* 2012) found that inhibition of Rho-associated kinase with Y-27632 led to increased sensitivity to FSS in PC-3 cells. Unexpectedly, an increase in the naïve control cell elastic modulus is measured when treated with the Rho-kinase inhibitor Y-27632. After exposure, treated cells displayed a similar elastic modulus compared to untreated PC-3 cells. Increased activity of other cellular structures, such as microtubules, may be trying to compensate for the inhibition of actin polymerization. Thus, inhibition of only ROCK may not be sufficient to reduce actin cytoskeletal reorganization after exposure to FSS. Membrane stiffening in naïve cells may also reduce the efficiency of other repair processes or force transduction pathways that play a role in resistance to FSS.

Treatment with Cytochalasin D increases loss of viability in PC-3 cells exposed to the FSS assay but does not significantly alter the elastid modulus of naïve cells. While treated cells exposed to FSS have not been tested, it is possible that inhibition of actin polymerization does not change their elastic modulus significantly. However, when exposed to FSS, these treated cells may lack the actin dynamics required to alter their elastic modulus and become stiffer. This could be important in determining whether the elastic modulus increases resistance to FSS or is simply a by-product of other cellular processes.

CHAPTER 4 REQUIREMENT OF ACTIN CYTOSKELETAL DYNAMICS

Summary

Forces that cells sense and transmit play a critical role in cell structure and function. Actin cytoskeletal dynamics have been implicated extensively in cell responses to mechanical stimuli in a variety of physiological settings, especially with regard to fluid shear stress (FSS). Impairment of many of these pathways that influence actin cytoskeletal dynamics reduces the cells ability to adapt to fluid shear stress and subsequently results in reduced resistance to FSS in cells. Rho GTPases, serine effector kinases, and actin-binding domains are examined. Inhibition of these pathways all resulted in increased sensitivity to fluid shear stress in malignant prostate carcinoma cells. Furthermore, cortical F-actin is shown to increase in malignant cells upon exposure to FSS.

Materials and methods

Cells are cultured as described in Chapter 1. All cells are collected at approximately 70-80% confluency and run according to the standard FSS protocol. Prior to FSS exposure, drugs are added for recommended times and doses based on literature.

RhoA knockdown: GS689.Li cells are grown according to supplier documentation. Cells are transfected with firefly luciferase. Using shRNA technology, the expression of Rho A/Rho C in GS689Li cells is silenced using either lentiviral (Rho C/PLKO.1) or

retroviral (Rho A/pSiren) particles. Non-targeting control cells (SCR) are also established using the above vectors. The cells are selected with proper antibiotics and are evaluated for silencing efficiency by immunoblotting and Rho pull-down assay. All knockdowns are approximately 60% successful.

Inhibition of MLCK: To inhibit myosin light-chain kinase, 20 μM ML-7 (#I2764, Sigma Aldrich) is added to complete PC-3 DMEM/F12 medium and incubated at 37°C for one hour. Cells are released from culture plates following standard protocol and exposed according to the technique outlined in Chapter 1. The cells are exposed to the assay without ML-7 present in the medium. ML-7 stock is suspended in DMSO. Thus, a control syringe is run in parallel with DMSO present in the medium to match the concentration in treated cells.

Inhibition of myosin II: Blebbistatin (#B0560, Sigma Aldrich), an inhibitor of myosin II, is added to culture medium at 100 μM and cells are treated at 37°C for 3 hours. The media is aspirated after incubation and cells are released as described above. The drug is not present in the medium while cells are exposed. A control syringe with cells suspended in DMSO-containing DMEM/F12 complete medium is run in parallel with treated cells.

Inhibition of Abl kinase: 10 μM Imatinib (Gleevec), an inhibitor of Abl kinase, is added to complete cell culture medium and incubated at 37°C for 10 minutes. Culture medium is collected and cells are released with trypsin. Cells are resuspended in 10 μM Imatinib-

containing medium and run through the standard FSS assay. Controls cells in medium containing DMSO is run in parallel with treated cells.

Cortical F-actin measurements: Rapid fixation of cortical F-actin is required. Protocol followed is previously described (Egger, Burda *et al.* 2001). In brief, a fixation mixture is prepared using two parts 2x phosphate buffer, pH 7.4; one part 75% glycerol in water; and one part 20% formaldehyde, prepared from paraformaldehyde. To fix cells, 1 mL fixation mixture, kept on ice, is added immediately to a 200 µL sample from the FSS assay. Samples are fixed for ten minutes at 4°C, centrifuged for 5 minutes at 100g, and resuspended in 1 mL FACS buffer. 3.3 µg/mL methanol FITC-phalloidin stock solution is prepared and stored at -20°C in the dark. When needed, stock is diluted in 9 parts distilled water to 1 part stock. Samples are centrifuged again and then resuspended in 350 µL of FITC-phalloidin solution. They are incubated in the dark on ice for 30 minutes. Samples are centrifuged and resuspended in 400 µL of 16 µL/mL Hoechst 33258 FACS buffer. The flow cytometry processing and analysis steps discussed in Chapter 2 are used for flow cytometry, with the exception that Phalloidin is measured as opposed to LAMP-1.

Priming FSS assay: Calcium has extensively been shown to play a role in mechanotransduction pathways. PC-3 cells are exposed to an initial FSS assay at a flow rate of 35 µL/sec and sampled every other passage for ten passages. PC-3 cells are then exposed to the standard FSS assay using protocol detailed in Chapter 1 at 250 µL/sec for ten passages. In calcium dropout experiments, calcium-free cells are exposed to an initial

10 passages of FSS at 20 µL/sec in nominally calcium-free D-PBS. They are centrifuged for 5 minutes at 200g and resuspended in 1.16 mM calcium-containing D-PBS. A control sample is held in suspension in 1.16 mM calcium-containing D-PBS during the priming run and then run in parallel with the primed cells.

Results

Cells are treated with various inhibitors of actin cytoskeletal dynamics. RhoA and RhoC knockdown GS689.Li cells are exposed to the FSS assay at 250 µL/sec (**Figure 4.1A**). RhoC knockdown cells display similar loss of viability to scramble control cells with end viability 20.89% and 24.16%, respectively, whereas RhoA knockdown cells are significantly more sensitive to FSS compared to control cells with 13.95% viability after the FSS assay. Confirmation of successful knockdown is done by western blotting. Inhibition of myosin light chain kinase (MLCK) with ML-7 in PC-3 cells shows that MLCK is an important protein involved in resistance to FSS (**Figure 4.1B**).End viability of ML-7 treated cells is 35.67% while DMSO treated controls are 54.67% viable. On a similar note, inhibition of myosin II by blebbistatin, downstream of MLCK, also reduces PC-3 resistance to FSS (end viability 42.77%) compared to DMSO controls (end viability 59.75%) (**Figure 4.1C**). Finally, Abl kinase inhibition with STI-571 displays no significant change in loss of viability compared to untreated control cells (**Figure 4.1D**). Control viability after the FSS assay is 43.50% while STI-571 treated cells are 47.50% viable.

63

Actin is shown to be important in FSS-resistance. To examine actin dynamics, cortical F-actin is measured upon FSS-exposure. As measured by flow cytometry, a significant increase in the relative geometric mean of F-actin to 1.23 is seen after the initial passage of the FSS assay (**Figure 4.2A**). However, F-actin expression diminishes after ten passages of FSS and is not significantly different than naïve control cells after ten passages (relative geometric mean = 1.065). A similar trend is observed by rapid fixation and staining of PC-3 cells and examination with fluorescent microscopy (**Figure 4.2B**). An initial increase is seen in F-actin that decreases to basal control levels by the end of the FSS assay. Localized staining of cortical F-actin is observed after exposure to high levels of FSS in fluorescent microscopy (**Figure 4.2C**).

PC-3 cells are primed at a lower flow rate of 35 μL/sec before being exposed to the standard FSS assay at 250 μL/sec with a control, unprimed syringe (**Figure 4.3A**). PI fluorescent intensity is measured in samples collected at various passages (**Figure 4.3B**). Minimal loss of viability is experienced in the priming passages. Initially, primed cells display higher viability than control cells during the high shear exposure. However, viability at ten passages is not different. PC-3 cells are primed in either the presence or absence of calcium (**Figure 4.3C**). Both samples are then exposed to high shear. No significant differences are seen between samples in both priming and high FSS exposures.

64

D.
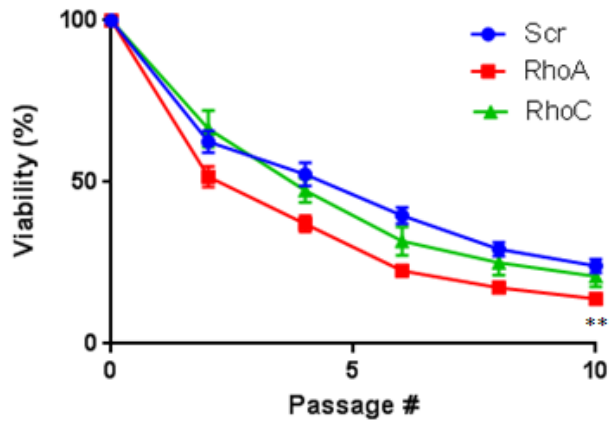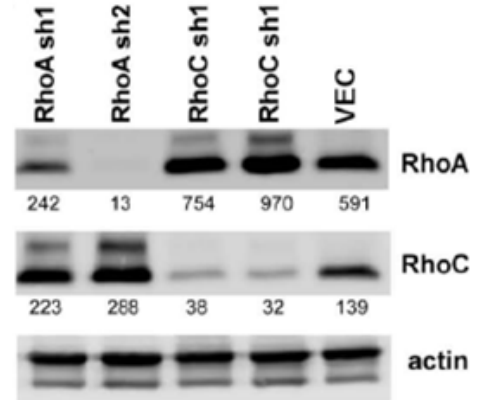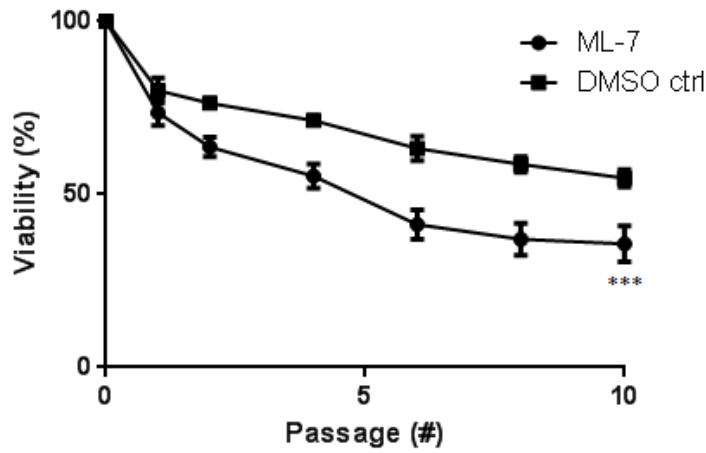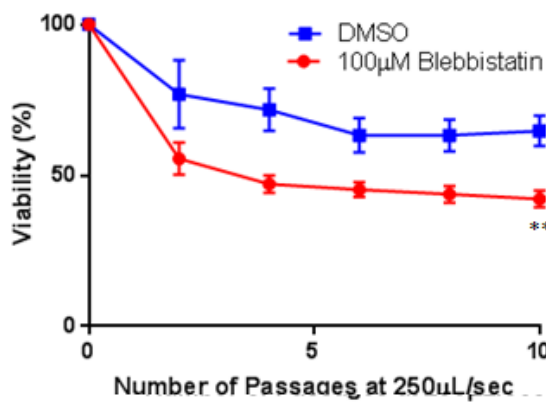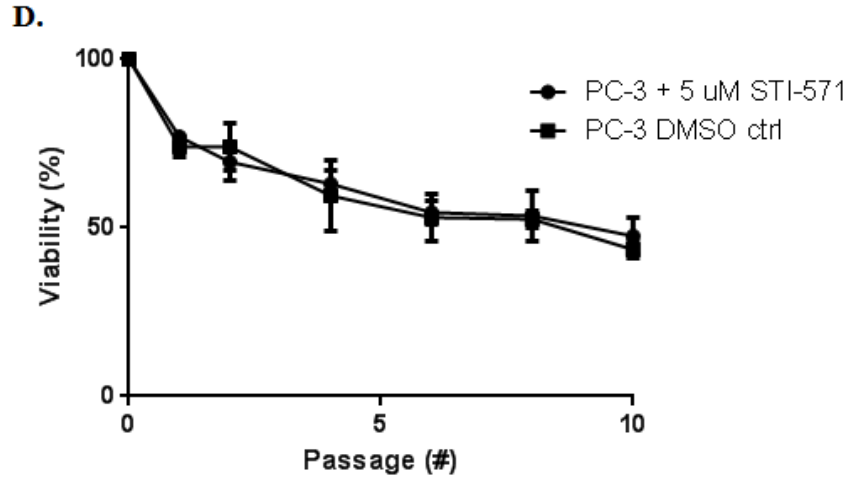
Figure 4.1: Actin cytoskeletal dynamics are required for resistance to fluid shear stress.
All samples are exposed to the fluid shear stress assay at 250 µL/sec in a 30G ½" needle.
A) *i.* RhoA and RhoC knockdown GS689.Li cells (*** RhoA and Scr; n.s. RhoC, Scr.).
ii. Confirmation of knockdown via western blotting. **B)** Inhibition of myosin light chain kinase with ML-7 in PC-3 cells. **C)** Inhibition of myosin II in PC-3 cells with Blebbistatin. DMSO control cells are run in parallel with treated cells. **D)** ells treated with an Abl kinase inhibitor STI-571. Controls cells are run in DMSO containing medium. (**, p<0.01; ***, p<0.001).

A.

B.
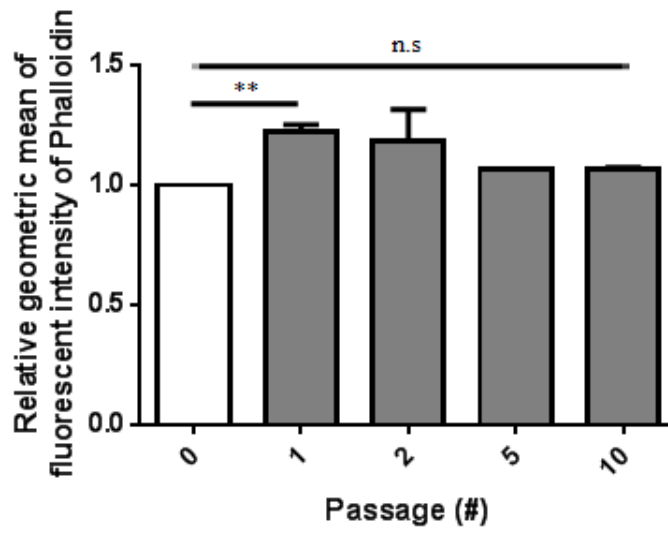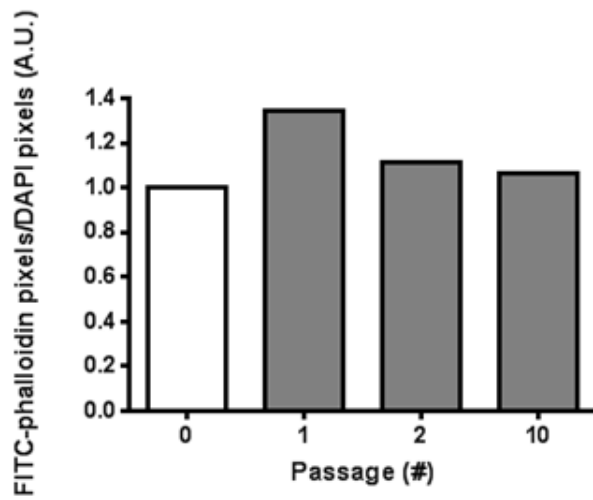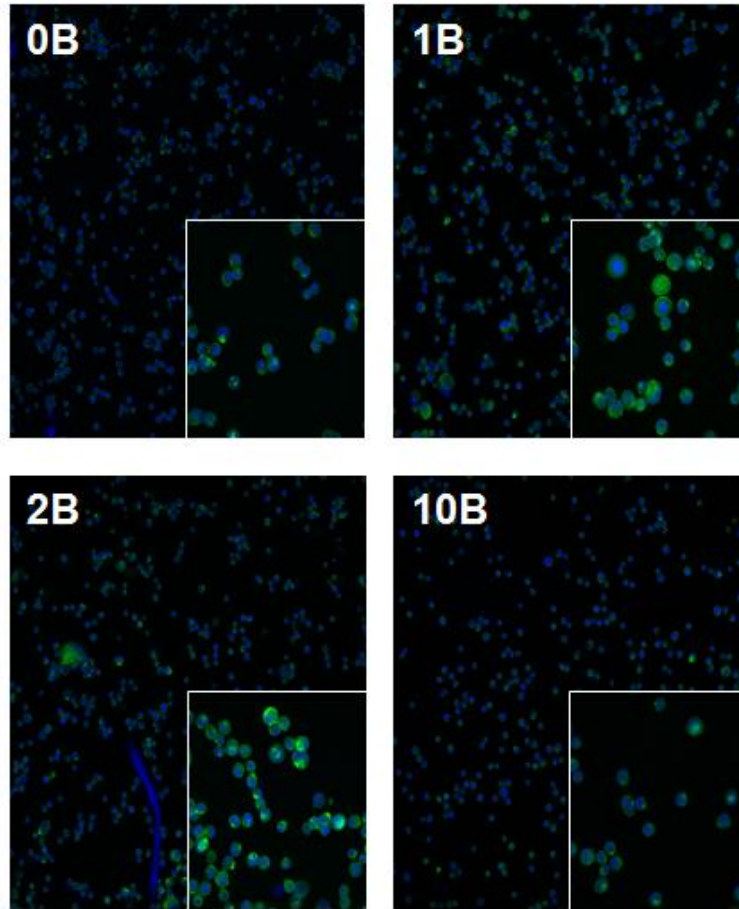
Figure 4.2: Cortical F-actin is altered upon exposure to fluid shear stress.
Staining of F-actin by phalloidin in PC-3 cells after various passages of high levels of fluid shear stress as measured by **A)** flow cytometry and **B)** fluorescent microscopy. Samples normalized to a naïve, unexposed control. (**, $p<0.01$.) **C)** Fluorescent microscopy images at passages 0, 1, 2, and 10.
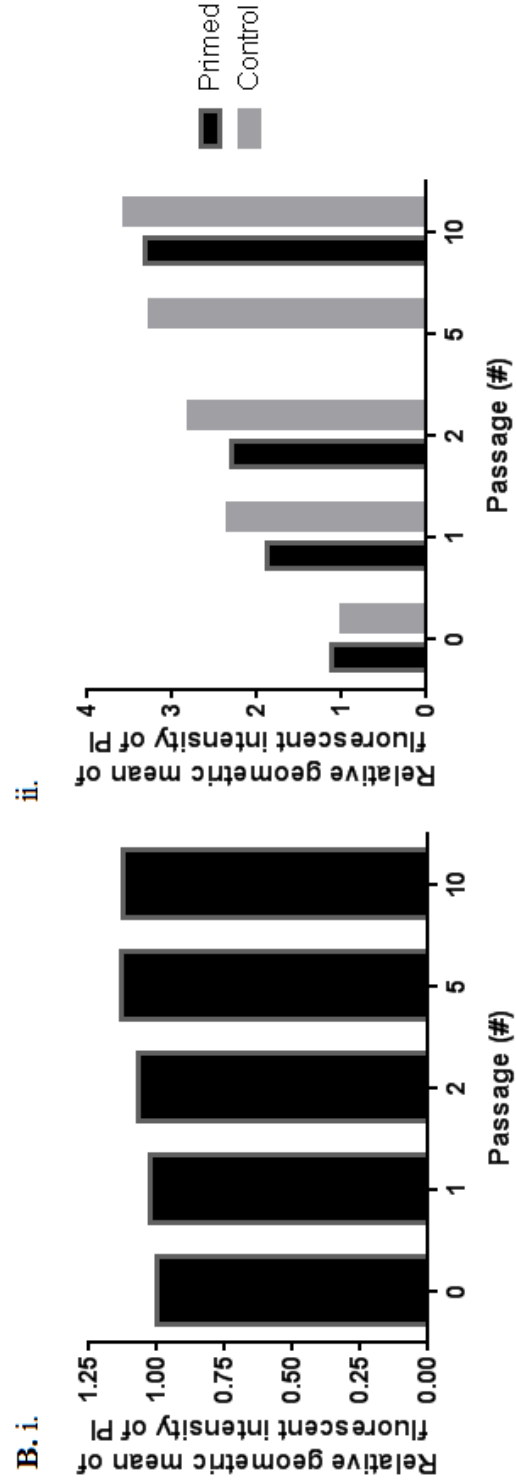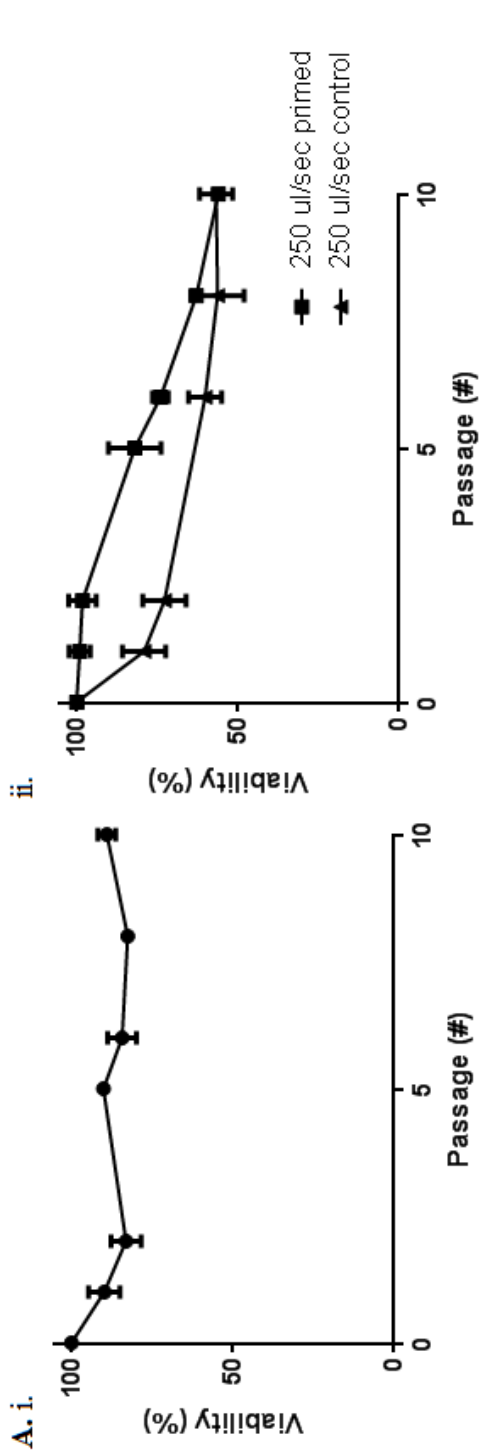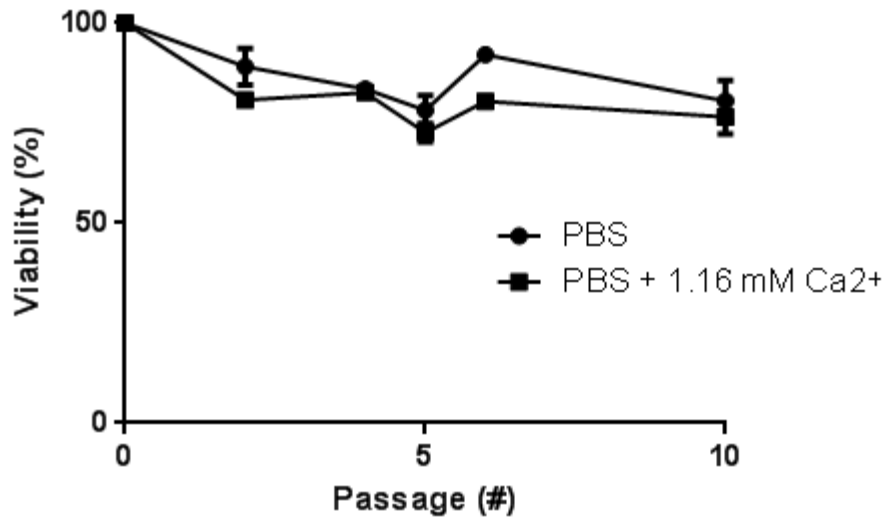
ii.
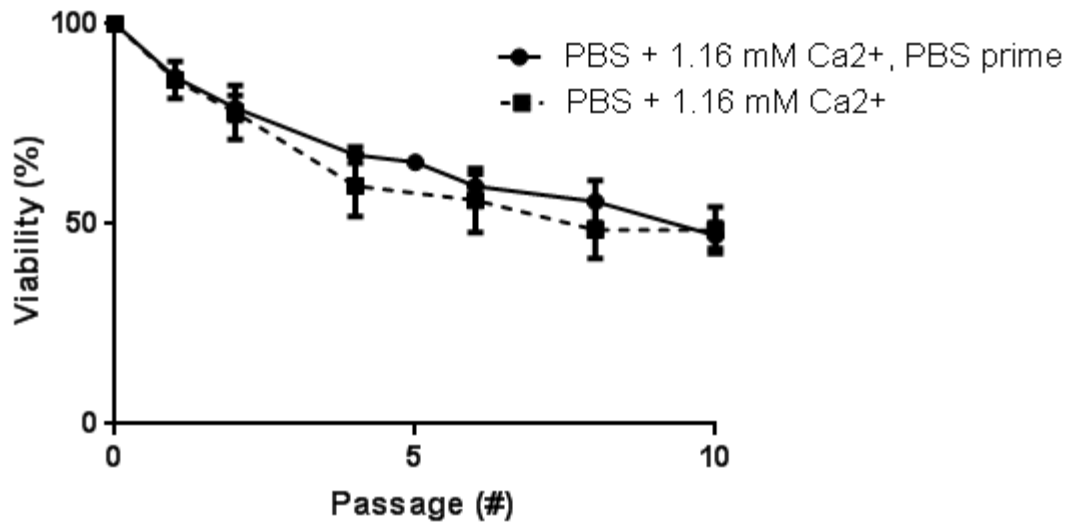
Figure 4.3: Low-shear priming before exposure to high fluid shear stress.
A) *i.* Cells are primed in complete medium at a low flow rate of 35 μL/sec. *ii.* Primed and control cells are exposed to the standard fluid shear stress assay at 250 μL/sec. **B)** Propidium iodide (PI) uptake in viable cells for evidence of membrane injury and repair in both priming (*i.*) and standard exposures (*ii.*). **C)** Cells are primed at 35 μL/sec in the absence or presence of calcium (*i.*) prior to a full 250 μL/sec exposure in calcium-containing medium.

70

A crucial step during tumor invasion and metastasis is reorganization of actin cytoskeleton that allows malignant cells to migrate through diverse tissues. These structural changes are regulated by Rho family small GTPases like Rho and Rac and their effector molecules, such as Rho-associate kinase (Yamazaki, Kurisu *et al.* 2005; Amano, Fukato *et al.* 2000). Rho-kinase (ROCK) regulates phosphorylation of myosin light chain kinase (MLCK) which in turn regulates non-muscle myosin II (NM II) by phosphorylation of the regulatory light chain (Vicente-Manzanares, Ma *et al.* 2009). NM II in turn effects cell adhesion, migration, and cellular structure. Each of these steps of actin cytoskeletal regulation can be targeted to explore the impact on resistance phenotypes to fluid shear forces.

RhoA has been shown to an important factor in actomyosin contractility whereas RhoC plays a larger role in cell locomotion (Wheeler & Ridley 2004). Upregulation of the small GTPases RhoA and RhoC have been implicated with increased metastatic potential (Horiuchi, Imai *et al.* 2003; Kleer, van Golen *et al.* 2002). Knockdown of RhoA influenced resistance to FSS in malignant GS689.Li cells while RhoC did not have a significant effect on viability. RhoA may play a larger role in high stress environments as it controls actin and myosin contraction, effecting force transduction in cells, whereas RhoC effects cellular mechanisms important in navigating solid tissues. RhoA has been shown to regulate the Rho-associated kinase (ROCK).

It was previously shown that inhibition of ROCK with Y-27632 resulted in significantly reduced FSS resistance in PC-3 cells, further signifying the role of these

71

cytoskeletal dynamics in cells ability to respond to FSS. ROCK then regulates the action of myosin light chain kinase (MLCK). Inhibition of MLCK with ML-7 also results in lower resistance to FSS in PC-3 cells. The elevated loss of viability due to FSS after treatment with Y-27632 and ML-7 is similar. However, both treatments results in greater loss when compared to RhoA, suggesting that RhoA knockdown may be able to be compensated by other mechanistic pathways to restore, at least partly, the resistance phenotype in malignant cells. Finally, myosin II can be inhibited with blebbistatin, which binds to myosin and lowers its affinity for actin (McLauchlan, Elliott *et al.* 2003; Limouze, Straight *et al.* 2004). When PC-3 cells are treated with blebbistatin, PC-3 cells are more susceptible to FSS compared to DMSO controls, indicating myosin II is an element that increases resistance to FSS in cells.

In summary, actin cytoskeletal regulation pathways play a critical role in malignant cells resistance to fluid shear stress. When any of the several levels of regulation are inhibited, these resistant tumor cells become sensitized to fluid shear stress and a greater loss of cell viability is measured. RhoA knockdown did not result in as significant FSS sensitization as downstream inhibitors, possibly because other upstream pathways are activated in response to accommodate RhoA loss. ML-7, an inhibitor of MLCK, Y-27632, an inhibitor of ROCK, and blebbistatin, an inhibitor of myosin II, all reduce FSS resistance in malignant PC-3 cells. This decreased resistance is due to loss of a cells ability to respond and adapt to the stressful fluid shear stress environment, possibly due to impaired ability to alter mechanical properties such as stiffness or reduced efficacy of membrane repair.

72

Cortical filamentous (F) actin has been extensively associated with cell adhesion, migration, and division, all of which require regulation of cell shape and force generation (Stricker, Falzone *et al.* 2009). It has also been implicated heavily as the key structure that is able to transmit mechanical stresses (Davies & Tripathi 1993).When endothelial cells are initially exposed to FSS, F-actin turnover increases and after several hours, bundles of F-actin are seen aligned with the flow (Osborn, Rabodzey *et al*. 2006).

A rapid, significant increase in F-actin is seen within seconds of the initial passage of high FSS exposure, as cells are immediately fixed after processing. The F-actin signal also is seen in localized areas of the cellular membrane, possibly assisting in membrane repair in regions of injury. F-actin prevents subcortical lysosomes from fusing to the plasma membrane and needs to be depolymerized initially to allow repair (McNeil, 2002). However, following lysosomal fusion, cortical F-actin must be repolymerized. It is possible this is the step of membrane repair that is being stained with Phalloidin, as the patching process can occur in seconds. The staining is in local areas on the plasma membrane, suggesting that increased F-actin is restricted to only areas of injury. It is interesting to note that F-actin returns to basal levels by passage ten. Reduced membrane injury and repair in later passages, as shown by viability and PI/LAMP-1 curves, may be consistent with this data if the increased F-actin is only transient in nature and dissipates in minutes after repair of the injury site is completed.

Shear stress activates many signaling pathways in various cell types. Most notably, endothelial cells respond to low levels of shear stress. These cells can alter their cellular structures through the formation of stress fibers or by aligning their cytoskeletal elements with the direction of flow (Davies 1995). Phosphorylation of platelet endothelial

cell adhesion molecule-1 is done in response to FSS (Osawa, Masuda *et al.* 1997). Atheroprotective mechanisms are performed by endothelial cells during steady shear stresses (White & Frangos 2007). Thus, it is clear that signal transduction pathways that are dependent on fluid shear stress and mechanical force are important for normal physiological functioning within blood vessels.

Despite evidence of FSS-induced activation of signaling pathways in many cell lines, it does not appear that PC-3 cells are able to sense low levels of FSS and activate pathways that lead to significant FSS-resistance to the high levels of exposure experienced in the standard assay. However, it is clear from the biphasic viability curves that FSS-induced FSS resistance is at play, as cell death is significantly greater in passage one versus later passages at high shear flow rates. Priming cells in 35 μL/sec, corresponding to a ~900 dyn/cm^2 max FSS magnitude, may not be sufficient enough to trigger these responses. Cells may need to sustain some measure of cellular injury before eliciting a FSS-resistance response, as injury at these lower flow rates is marginal. While there appears to be an increased resistance in initial passages in primed cells compared to control samples, it is not consistent with data obtained in calcium dropout control samples that are primed and exposed in calcium-containing medium, where the control closely mirrors expected viability curves. Furthermore, PI uptake is similar in both primed and unprimed cells. Thus, it is difficult to interpret these results to definitively say whether or not an induced resistance is present. Further investigated is required before conclusions can be drawn from these results and the significance of mechanotransduction in the FSS resistance phenotype.

74

APPENDIX A FLUID SHEAR STRESS MODELING

Summary

While the fluid shear stress (FSS) assay is simple in theory, consisting of a straight 30G needle, careful consideration of the fluid mechanics present in the assay is essential in understanding the stresses that cells undergo when exposed. Simple calculations, including determining laminar flow conditions and fluid shear stress profiles, are provided. Further examination of flow behavior is done using computational software. Simulations are run for simple 2D and 3D tubular cases as well as more complicated geometries with the syringe, needle hub, and needle.

Materials and methods

Assay protocol

The experimental protocol used in this section is the same as described in Chapter 1. Various parameters are altered, however, including flow rate, needle diameter, and medium used.

Flow characteristics

As discussed in Chapter 1, fluid shear stress (FSS) is determined using Poiseuille's equation:

$$\tau_{max} = \frac{4Q\mu}{\pi R^3} \tag{1}$$

where τ is the maximum wall shear stress in dyn/cm^2, Q is the flow rate in m^3/s passed through the needle, μ is the dynamic viscosity of the media (dyn*s/cm^2), and R is the radius of the needle. In standard assays, the medium viscosity is treated as water at room temperature of 0.01 dyn*s/cm^2. The standard needle used is a 30G ¾" needle with an internal radius of $7.94 * 10^{-3}$ cm. In several experiments, different needles and flow rates are used.

To assess laminar flow conditions, the Reynold's number, a ratio of inertial to viscous forces, is determined for various flow rates examined. The Reynold's number is calculated using the equation:

$$Re = \frac{\rho v D}{\mu} \tag{2}$$

where ρ is 0.998 g/cm^3 (treated as water at room temperature), v is the average velocity of the flow in cm/s, D is the diameter of the needle in cm, and μ is the dynamic viscosity in dyn*s/cm^2. Values exceeding 2000 indicate a transition to turbulent, chaotic flow and a breakdown of assumptions of Poiseuille flow. At the maximum flow rate of 250 µL/sec, the Reynold's number is 2000, below the threshold for transition to turbulent flow (Table 1) and satisfying the criteria for laminar flow conditions.

In Poiseuille flow, velocity of the fluid is dependent on the radial position of the fluid particles due to the no-slip condition. The no-slip condition states that fluid velocity at the wall of the vessel is zero. This results in a parabolic velocity profile across the

diameter of the circular vessel with zero velocity at the walls and maximum velocity at the axis. The velocity profile can be determined by:

$$v_z = \frac{\Delta P R^2}{4 \mu L} \left[1 - \left(\frac{r}{R} \right)^2 \right] \tag{3}$$

where ΔP is the change in pressure across the needle in dyn/cm^2, L is the length of the needle in cm, the dynamic viscosity is μ in dyn*s/cm^2, r, in cm, is the radial position of interest, and R is the radius of the needle. Thus, cells traveling near the center of the needle will travel at the greatest velocity and have the shortest exposure time and vice versa for cells near the wall.

Average exposure time for cells traveling through the needle is calculated by dividing the flow rate by the internal area of the needle to obtain average velocity and then the length of the needle divided by average velocity. Note that while ½" 30G needles are used, upon closer inspection of the needle hub, the actual length of the needle is ¾", with ¼" embedded within the needle hub and ½" external. On the same note, 1" 30G needles are actually 5/4".

The FSS depends on the gradient of velocity and radial position and is calculated by:

$$\tau(r) = \mu \frac{\partial u}{\partial r} \tag{4}$$

where the dynamic viscosity is μ in dyn*s/cm^2 and $\frac{\partial u}{\partial r}$ is the gradient of velocity in cm/s with respect to the radial position in cm, also known as the strain rate. Due to the parabolic nature of velocity, FSS varies linearly with respect to the radial position with a maximum FSS at the wall and minimum FSS at the axis. The FSS at a given radial position can be calculated:

$$\tau(r) = \tau_{max} * \frac{r}{R} \qquad (5)$$

where r, in cm, is the radial position of interest and R is the radius of the needle. The minimum FSS that a cell will experience can be calculated by setting r equal to the cell radius in Equation (5).

These fluid profiles dictate the magnitude of FSS exposure that a given cell experiences while being passed through the needle. As shown above, higher levels of FSS are paired with longer times of exposure as fluid velocity decreases as it approaches the wall. Thus, cells near the wall of the needle are exposed to elevated levels of FSS for extended periods of time. These cells are then more likely to be destroyed due to mechanical force when compared to cells near the axis. While modeling cell viability loss in the FSS assay, cells are assumed to be uniformly distributed across any given cross section of the needle. However, this assumption may not be valid, especially in cases where cells are close to the wall. A buffering region along the walls of the needle may reduce the likelihood of cells gaining close proximity to the wall. In addition, more deformable particles have been shown to drift towards the axis (Hur, Henderson-MacLennan *et al.* 2011), which would result in lower levels of FSS exposure.

To determine the entrance length of the needles, the following equation is used:

$$L_{h,laminar} = 0.05 \, Re \, D \qquad (6)$$

where Re is the Reynold's number and D is the diameter of the needle. The entrance length is the region of the needle where fluid flow is not yet fully developed. The entrance region is important with regard to fluid shear stress exposure. Within the irrotational flow region that reduces in size across the length of the entrance region, there

is a flat velocity profile that corresponds to minimal FSS. Thus, a large entrance length will reduce the effective FSS that cells are exposed to during passage through the needle.

Computational simulations and modeling

Modeling the syringe, needle hub, and needle is done in FLUENT ANSYS (Ansys, Inc.). Various simulations are performed at different flow rates and configurations. Fluid flow is assumed to be laminar. The fluid properties are a density of 998 kg/m^3 and viscosity of 0.001 kg/(m*s). A syringe and needle are taken apart and measured using a micrometer. The geometry is made in AutoCAD (AutoDESK Inc.). Residuals for continuity and x- and y-velocity are set to $1*10^{-6}$. Results that do not converge are not used for analysis. Momentum is set to second order upwind with standard pressure and least squares cell based for the gradient.

Investigation of turbulent flow effects

To explore turbulent flow effects on PC-3 cells, needle diameter and flow rate are increased, resulting in Reynold's numbers in the transition to turbulence regime. A 30G needle at 250 µL/sec (Re = 2000) has a wall FSS of ~6400 dyn/cm^2. To match the wall FSS in a 27G needle, the flow rate is increased to 582 µL/sec which also increases Re to 3522. Increasing the needle diameter further with a 26G needle requires a flow rate of 1104 µL/sec with a corresponding Re of 5396. All other steps for the FSS assay are the same as the standard protocol. Calculations of FSS in the 26G and 27G cases are not

79

valid in the event of significant turbulence in these flows. Control samples with 30G

needles are run immediately before or after exposure of experimental cells.

Results

Flow characteristics

The parabolic velocity profile within the needle (**Figure A.1A**) and the linear FSS

profile (**Figure A.1B**) are dependent on the flow rate of the FSS assay being performed.

Standard runs are done at 250 µL/sec which results in supra-physiologic FSS magnitudes.

The FSS magnitudes, average exposure times, and Reynold's numbers are shown in

Table A.1 for the various flow rates tested. Brief exposure times in the millisecond to the

sub-millisecond domain are consistent with the physiological conditions where cells

would experience these high magnitudes of FSS.

Fluid behavior within the syringe and needle showed rapid flow development in

the 30G needle with an entrance length of ~400 µm. With a small entrance length, FSS is

nearly constant across the entire length of the needle. Thus, the magnitude of exposure is

independent of axial position. In addition, regions of flow recirculation can be seen in the

syringe-needle hub interface that surrounds the fairly linear flow as it approaches the

needle orifice. These recirculation areas likely facilitate rapid flow development and

reduction in entrance length.

80

Computational simulations in FLUENT ANSYS show fluid velocity, fluid streamlines axial velocities, shear rates, and vorticity at various regions within the FSS assay for the high shear protocol. Fluid at the interface between the needle hub and

Table A.1: Fluid parameters at various flow rates.

Flow rate (μL/sec)	FSS maximum (dyn/cm$^{2)}$)	Mean exposure time (ms)	Re
20	508.7	18.86	160
35	890.3	10.78	177
50	1271.8	7.55	400
100	2543.6	3.77	800
150	3815.4	2.52	1200
250	6359.0	1.51	2000
400	*10174.3**	0.94	3201
582	*6401.2**	1.13	3522
582	*14803.7**	0.65	4657
1104	*6398.1**	0.92	5396

A.

B.
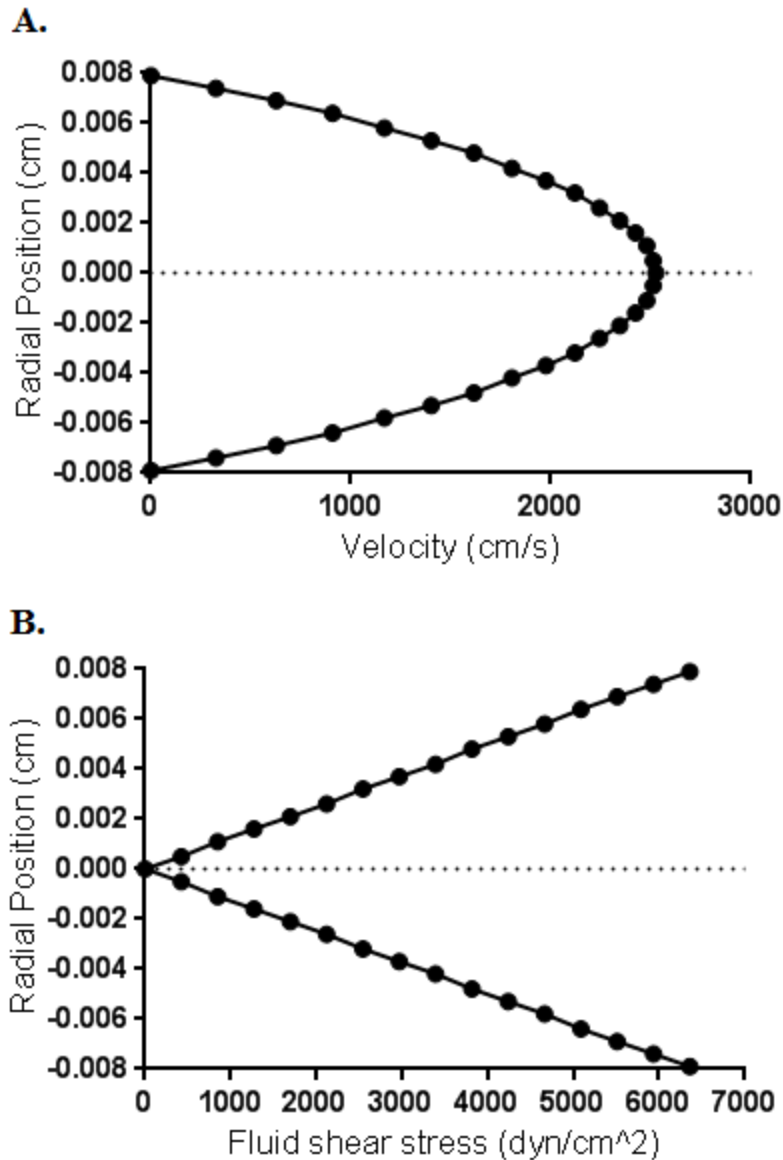
Figure A.1: Velocity and fluid shear stress profiles across diameter of needle.
The velocity and fluid shear stress are dependent on a number of characteristics of the
flow, including the flow rate, Q, viscosity, μ, change in pressure across the needle, ΔP,
and radius of the needle, R. **A)** The parabolic velocity profile where velocity depends on
radial position. **B)** Due to the parabolic nature of velocity, fluid shear stress varies
linearly with respect to the radial position. Values shown are for the flow rate of 250
μL/sec in a 30G needle, radius of $7.94 * 10^{-3}$cm, assuming a viscosity of 0.01
dyn*s/cm^2.

needle entrance is rapidly accelerating as the effective radius decreases suddenly (**Figure A.2A***i*). Focusing on the whole system, velocity streamlines display significant zones of recirculating flow near the walls of the needle hub between the syringe exit and needle entrance (**Figure A.2A***ii*). Convergence of flow on the needle entrance is evident as well.

Axial velocity gradually increases as the cross sectional area reduces as cells exit the syringe and travel towards the needle entrance, where it then rapidly accelerates in the restricted area of the needle (**Figure A.2B**). Shear rate and vorticity are calculated around the needle entrance region (**Figure A.2C**). Similar magnitudes are present, with slightly higher vorticity seen around the constriction and higher shear rate at the corners of the interface.

Transition to turbulent flow results in increased loss of viability with Reynold's numbers higher than 5,000. Below 5,000, matching the maximum FSS in different needle gauges results in similar losses of viability (**Figure A.3**).
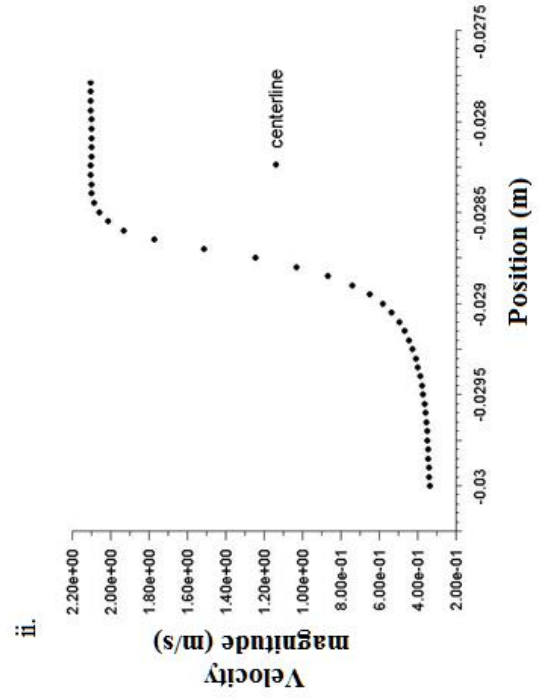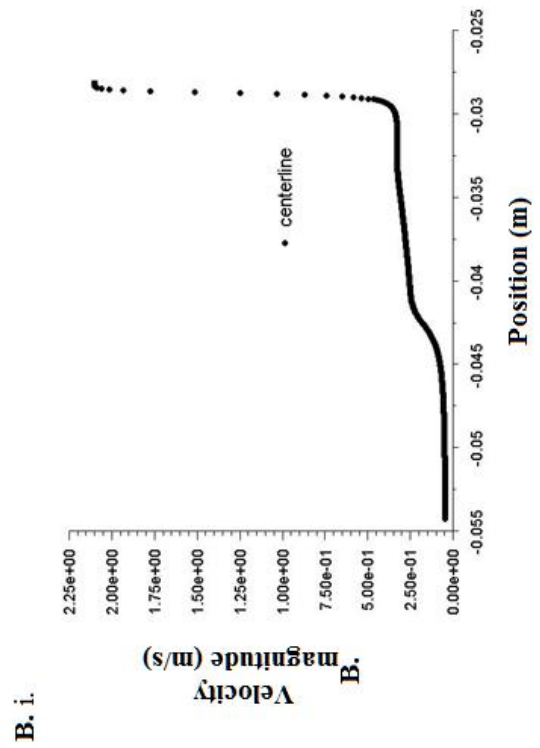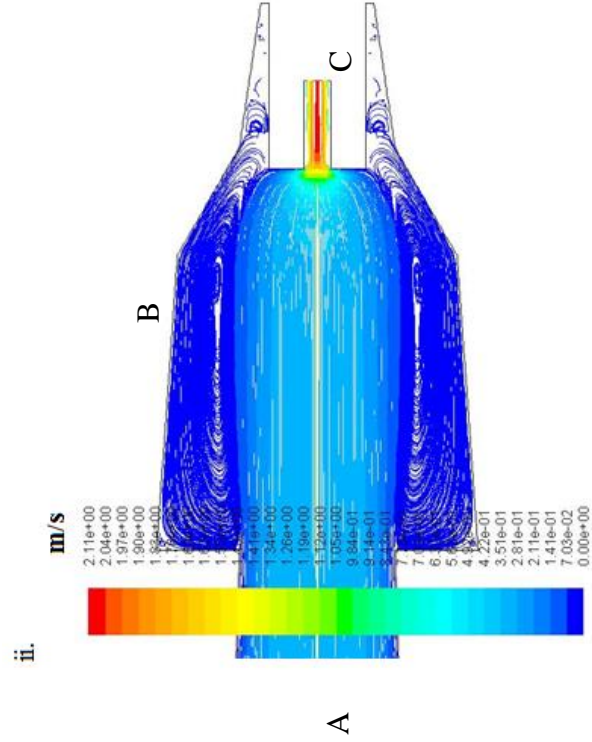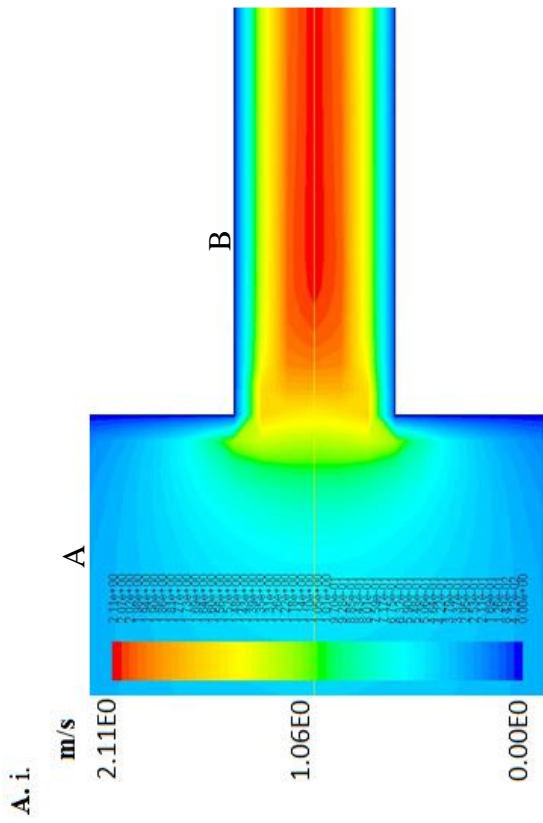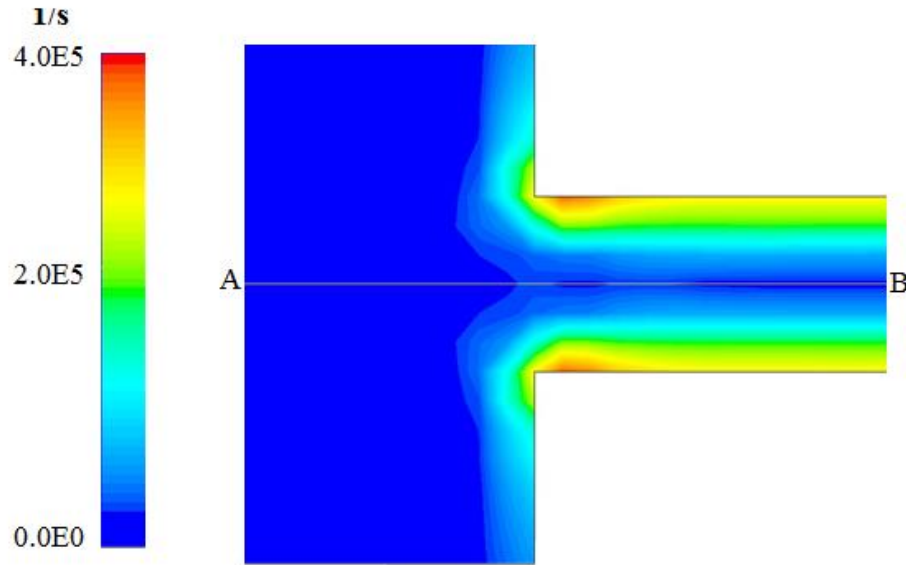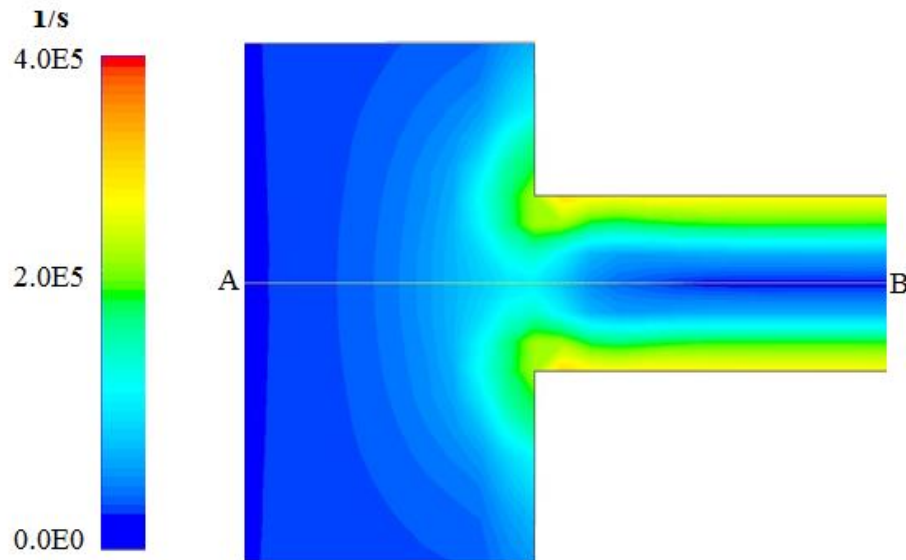
Figure A.2: Standard fluid shear stress assay simulations.
FLUENT simulations of fluid flow through syringe, needle hub, and needle. Flow rate within the 30G needle is 250 μL/sec. **A)** *i.* Velocity contours (m/s) at the interface between the needle (B) and needle hub (A). Rapid acceleration is seen as fluid converges to the needle. *ii.* Velocity streamlines of syringe exit (A, left), needle hub (B, middle), and needle (C, middle right). Recirculation regions are seen in the needle hub near the walls. **B)** *i.* Axial velocity (m/s) of fluid across geometry. *ii.* Axial velocity as fluid converges and accelerates into needle. **C)** Shear rate (1/s), *i.*, and vorticity (1/s), *ii.*, at the interface between needle hub and needle.

86
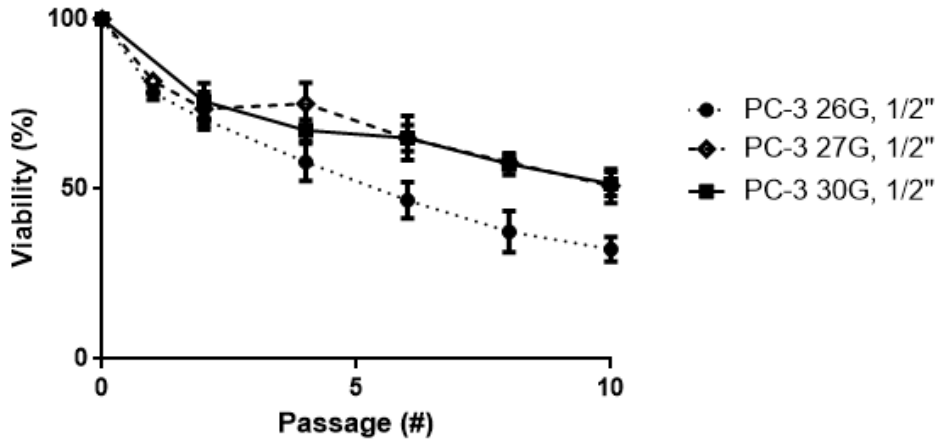
Figure A.3: Turbulent flow reduces cell viability.
Exposing PC-3 cells to the fluid shear stress assay using different gauge needles. The maximum fluid shear stress value is matched by increasing the flow rate. Flow rate increases paired with increased diameter result in Reynold's number that are within the transition to turbulence regime.

<u>Discussion</u>

Supra-physiologic magnitudes of fluid shear stress are present in the FSS assay the high flow rate of 250 µL/sec. With these levels of stress, it is surprising that malignant cells are still 50% viable after ten one-millisecond passages through this stressful environment. The odds of a given cell experiencing a high FSS magnitude near the needle wall, despite the linear dependence of FSS on radial position, are quite high. Thus, these cells likely experience FSS that surpasses maximal FSS in physiological settings at least once during the assay, indicating significant resistance is required in cells that maintain viability after the assay.

In all experimental runs in 30G needles at flow rates of 250 µL/sec or less, flow is laminar. Thus, there is no significant chaotic movement of particles and cells will likely travel along streamlines with little radial migration since axial velocity is high and the channel length is small. Note that all experimental data on the mechanisms involved in FSS resistance are obtained in laminar flow conditions. However, in flow rates above 250 µL/sec, flow theoretically begins to transition to turbulent flow. During transition to turbulent flow ($2{,}000 < Re < 10{,}000$), flow may be either laminar or turbulent, depending on various conditions, such as rapid constriction or expansion of flow. While it is unclear of the extent of turbulent flow at this microscale, where flows are typically laminar due to the small diameter of channels, turbulent flow likely increases viability loss as Reynold's stresses can be quite high. Furthermore, there is significant movement of particles in both axial and radial directions. Finally, in turbulent flow, when the Kolmogorov length scale of turbulence decreases below the diameter of a cell, significantly greater cell death is

witnessed (Croughan, Hamel *et al.*1987; McQueen, Meilhoc *et al.* 1987). When matching theoretical fluid shear stress values using three different gauge needles, an interesting trend is observed. While the Re number is above the laminar values, using a 27G and matching the FSS results in comparable losses of viability to 30G needle control samples, suggesting that no turbulent flow is present and exposure is roughly the same between the two cases. However, a Re above 5,000 in the 26G needle resulted in elevated loss of viability compared to control samples. Turbulent flow may be present in these flows which results in greater loss of viability.

A given magnitude a cell experiences during the fluid shear assay dictates the fate of a cell when exposed to the FSS assay. Thus, understanding how exposure may vary from cell to cell is important in drawing conclusions from some data. Currently, the maximum and minimum fluid shear stress that a given cell experiences differs dramatically based on its radial position. While current assays do not require a uniform exposure from cell to cell within the same sample, it becomes difficult to understand how cells respond to a specific magnitude of fluid shear stress or how viability changes when exposure time halves or doubles. In addition to variable FSS across the radius of the needle, exposure time varies as well. Cells that travel near the wall experience a double dose of high FSS for a long period of time compared to cells traveling for a short period of time in low FSS at the axis. However, fractions of the total flow that pass through the center of the needle and near the walls is small compared to percentage of flow passing through at roughly $0.5R$. Thus, most cells experience an intermediate FSS and exposure time.

Rapid flow development is witnessed in computational simulations. However, calculation of entrance length with a flow rate of 250 µL/sec using standard equations suggested a length of 16 mm before flow is fully developed, only slightly less than the entire length of the 30G needle. This equation assumes plug flow, or a flat constant velocity profile of fluid entering the needle. This is not the case in real assays where fluid is slowly funneled into the needle entrance with gradual accelerations followed by a sharp acceleration as it enters the needle. Funneling of flow reduces entrance length. In addition, recirculation zones around the flow in the needle hub act to further reduce the entrance length. Simulation data calculated an entrance length of approximately 400 µm. Consequently, for the majority of exposure within the needle, cells experience a parabolic velocity profile and linearly dependent FSS and there is no irrotational core where little FSS is present. A rapid flow development is also confirmed with rapid acceleration of the flow as it enters the needle, with a nearly parabolic profile after 0.5 mm.

Computational simulations also suggest an environment where extensional flow is present. Extensional flow often occurs in sudden contractions, where the cross sectional area a fluid is flowing through rapidly decreases. Typically in simple flow the shear rate and vorticity tensors are equal to each other. However, during extensional flow, the shear rate increases beyond vorticity and particles that are suspended in the medium will be stretched axially (Petrie 1995). As the fluid is squeezed into the restricted flow domain, fluid streamlines are compressed with a resultant increase in velocity, causing the elongation of the particle. This elongation then rebounds as flow resumes normal flow within the smaller region. During this second stage, cells that are stretched rebound which, if exceeding critical values, can result in cell death. This process has been

90

suggested to be more effective at causing cell death than FSS (Bentley & Leal 1986). While indicative of extensional flow in the simulations run for the high shear case, it requires further study to confirm its presence. Extensional flow may be an important factor in loss of viability outside of the expected loss in the exposure needle.

91

APPENDIX B DEVELOPMENT OF A MICROFLUIDIC DEVICE

Summary

Despite providing significant advantages in terms of simplicity and cost, the current fluid shear stress (FSS) assay has several drawbacks. Some of these disadvantages include minimal portability, potential for user error, large sample sizes, and reduced parallel processing of multiple samples. In addition, non-uniform exposure to fluid shear stress than can result in exposure being drastically different between cells depending on their axial position is a problem that reduces the potential efficiency of the device and quality of data and interpretations made.

This device has the advantage of being inexpensive, readily producible, and user friendly. Computational results showed a reduction in the maximum cell to cell variability during a given run by 95% compared to the conventional FSS assay. The device functions by pumping a cell suspension through an inlet port and into the microfluidic device containing a high aspect ratio rectangular channel. Cells are forced into the same shear stress profile, resulting in uniform exposure across the sample. A reduction in user interaction while samples are processed reduces user error and the scale of the device reduces sample sizes while also allowing the potential for parallel processing of many samples.

While simulations suggested vastly reduced cell-to-cell FSS exposure and increased user control of parameter optimization for more efficient runs, little cell death is evident, even at fluid shear stress magnitudes that greatly exceed the maximum FSS in

92

the standard 30G needle FSS assay. Fluid mechanics that may explain this discrepancy are examined and discussed, namely lubrication theory.

Materials and methods

Computational Simulations

Prior to device fabrication, simulations are run to confirm the fluid mechanics of the structures. FLUENT ANSYS, a fluid modeling software program, is used to perform these analyses. In these simulations, the fluid is assumed to be water at 20°C with a viscosity of 1 cP and density of 0.998 g/cm^3. Flow under all simulations is laminar as the Reynold's number never exceeded 2000. Both 2D and 3D simulations are run. A minimum of ten elements is used across the smallest dimension of the device which is typically the channel height. This typically corresponded to a mesh size of 10 μm. Residuals are set to $1x10^{-6}$ for continuity, x-velocity, y-velocity, and in 3D cases, z-velocity. Solutions are initialized with the hybrid option and run to convergence. Only solutions that converged are interpreted.

Approximate fluid shear stress values are calculated assuming Poiseuille flow. Other parameters are calculated using equations discussed in Appendix A. Further simulations with single particles suspended in the flow to investigate lubrication effects are run using in-house code. In these 2D simulations, the particle is assumed to have an elastic modulus of 20 Pa, a diameter of 20 μm, and density of 1.05 g/cm^3. The fluid has the same properties as water.

Device fabrication

A common technique that is utilized to develop microfluidic chips is soft lithography. To begin, a master mold is made with positive features for the polymer to be poured onto. A silicon wafer chip is cleaved down to the required size and cleaned with IPA, acetone, DI H_2O, and blown dry with compressed N_2. A positive photoresist, SU-8 10 (MicroChem Corporation), is spun using a photoresist spinner (WS-400-6NPP-LITE Spin Processor, Laurell Technologies) to a desired thickness of 30 μm at 1000 rpm for 30 seconds. The thickness is confirmed using a thin film measurement system. A pre-bake at 65°C for 3 minutes and 95°C for 2 minutes is performed. Transparency films are used as a mask to imprint desired structures. Films are printed at CAD/Art Services, Inc. to a resolution of 5 μm. The film is placed in a mask aligner (Mask Aligner Model 800, OAI) and exposed for eight seconds at 200 mJ/cm^2. The film and wafer are in contact. A post exposure bake is performed at 65°C for 1 minute and 95°C for 3 minutes. The unexposed photoresist is dissolved using SU-8 Developer (MicroChem Corporation) for five minutes. A brief rinse of IPA followed by gentle of N_2 is done to remove debris and dry. Dimensions of the master are confirmed via light microscopy using a micrometer.

Polydimethylsiloxane (PDMS) is used as the polymer for devices (Sigma Aldrich). Upon mixing, the PDMS is degassed using a desiccator (FreezeZone Cascade, Labconco). PDMS is poured into a petri dish to a thickness of approximately 5 mm. The master mold is placed into the dish and allowed to settle to the bottom. The mold is

allowed to cure at 65°C for 24 hours. The PDMS is cut out of the dish using a razor blade and peeled away from the mold. The PDMS is cleaned using IPA, DI H_2O, and N_2 gas.

To bond the PDMS mold to glass and enclose the exposure channels, an oxygen plasma treatment is performed. Prior to treatment, inlet and outlet ports are cut using a 1 mm biopsy punch. Surfaces are cleaned with IPA, acetone, DI H_2O, and finished with compressed N_2 to dry. To ensure surfaces are completely dry, they are put on a hot plate at 95°C for ten minutes. They are then treated using a plasma cleaner (3100 Plasma Cleaner, Branson) for three minutes at 200W on the faces to be bonded. After removal from the plasma cleaner, the PDMS and glass are immediately pressed together firmly on a level surface with pressure applied for one minute. To allow complete dissipation of the hydroxyl groups, they are stored for 24 hours at room temperature. All flow rates tested had required driving pressures that did not exceed the bonding strength between PDMS and glass.

Fluid shear stress assay

Inlet and outlet tubing are connected to blunt 18G needles (#11302, LifeShield) are attached to the respective ports. Needles are attached to syringes and the standard FSS protocol can be followed by placing syringes on a syringe pump and run at desired flow rates. However, cell suspensions are first run through 30 µm nylon meshes (Millipore) to remove particles that could potentially become stuck in the channel. The device is placed under a microscope to assess channel integrity. The syringe pump is angled at 90° so syringes and needles are vertical to reduce error due to cell settling as single passages

take considerably longer than the standard FSS assay. BLI and CTB assays are used to measure viability loss during after exposure.
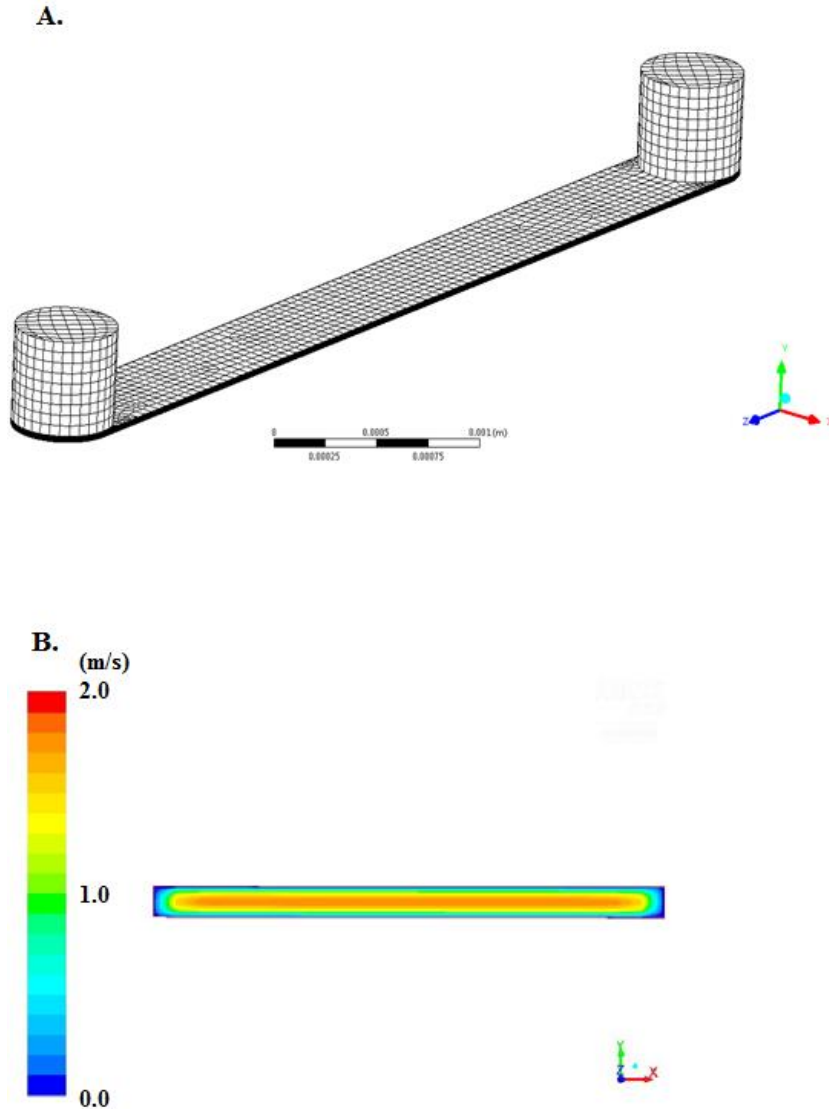
Results

Simulations and fabrication

The simple geometry consisted of two ports, one inlet and one outlet, with a 10 mm rectangular microchannel between (**Figure B.1A**). All samples are within laminar flow conditions. Calculations of average velocity and exposure time, maximum and minimum fluid shear stresses, and Reynold's numbers can be found in **Table B.1**. As is evident from the differences between maximum and minimum fluid shear stress values in the standard FSS assay using a 30G needle (refer to **Table A.1** for values) and the microfluidic device, the percent difference is significantly reduced for this critical experimental parameter in the microfluidic device, leading to a substantially more uniform exposure across all cells experiencing FSS. Velocity contours of a cross section of the channel shows that velocity is independent of a particles position across the width of the channel except near the walls (**Figure B.1B**).

Fabrication of the devices is consistent between the several chips built. The master mold is confirmed to be 500 μm wide with an approximate 30 μm height. The thickness of photoresist, as measured by a thin film measurement system, and thus the height of the mold channel, are shown in **Figure B.2A** for the devices constructed. Multiple measurements are taken at various points of the wafer to confirm uniformity.

Table B.1: Flow parameters at various flow rates.

Flow rate (μL/sec)	Average velocity (m/s)	Mean exposure time (ms)	FSS minimum (dyn/cm²)	FSS maximum (dyn/cm²)	Re
3	0.20	50.0	475	712.0	13
5	0.33	30.0	791	1186.7	21
10	0.67	15.0	1582	2373.3	42
20	1.33	7.5	3164	4746.7	85
30	2.00	5.0	4747	7120.0	127
50	3.33	3.0	7911	11866.7	212

A.

B.

Figure B.1: Geometry and computational modeling.
Computational design and simulation is created and run in FLUENT ANSYS. **A)**
Prototype channel geometry, consisting of two 500 μm diameter ports for inlet and
outlets and a 10 mm exposure channel with a width of 500 μm and height of 30 μm. **B)**
Velocity contours of a cross section of the channel half way between the ports. Inlet flow
rate is set to 5 μL/sec which corresponds to 1200 dyn/cm^2 maximum wall fluid shear
stress.

A.
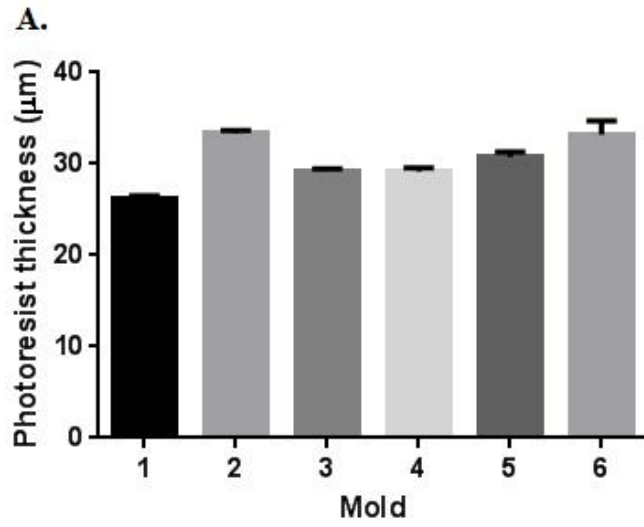
B.

i.
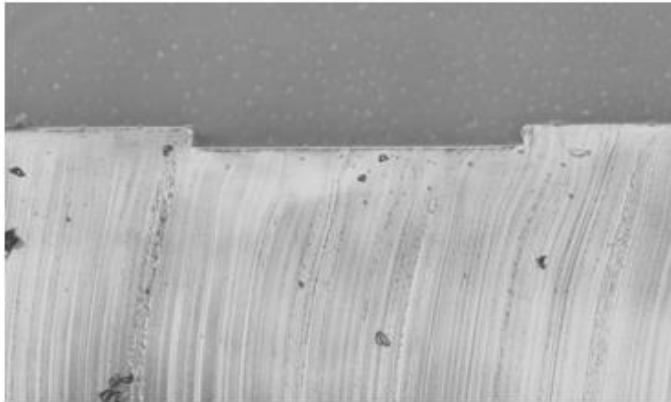
ii.
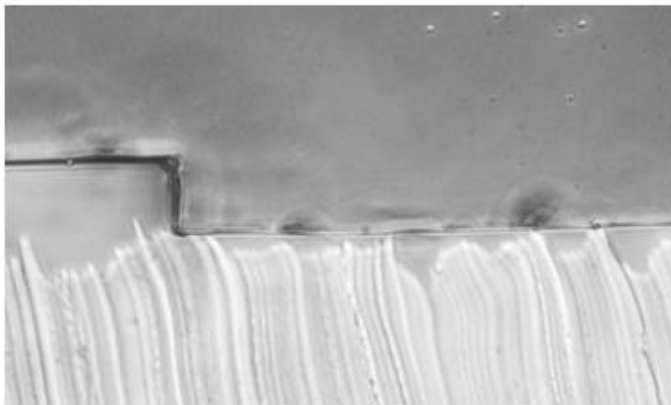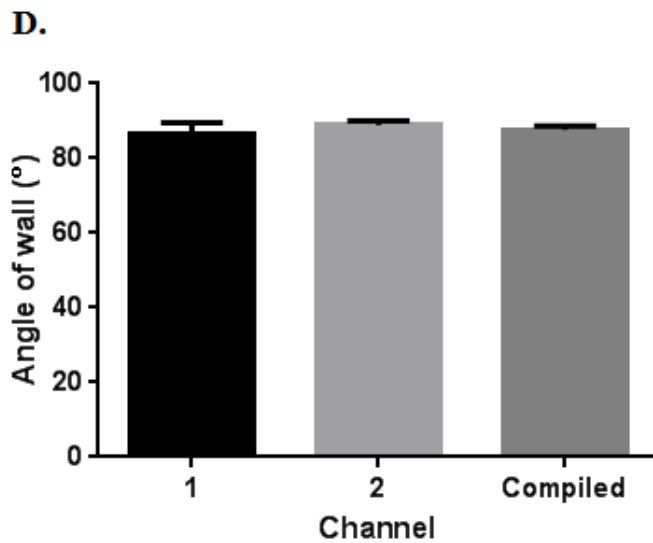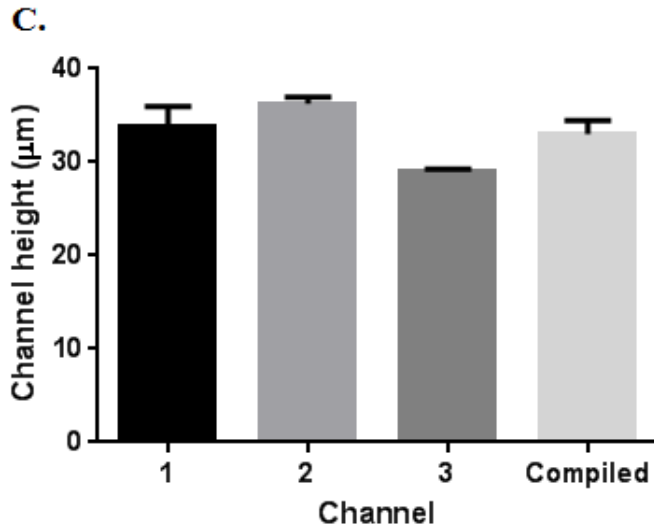
Figure B.2: Dimensions of fabricated masks and microfluidic chips.
A) SU-8 photoresist thickness after spinning as measured by a thin film measurement system. **B)** Cross sections of two different channels. **C)** PDMS channel height from cross sections after curing. Images are taken using an inverted microscope and measured with a micrometer. **D)** Angle of channel wall measured from several cross sections.

Upon device curing, channels are sectioned to assess fidelity of mold (**Figure B.2B**). Height and wall angles are displayed in **Figure B.2C** and **Figure B.2D**, respectively. Minor variations across fabrication cycles are unlikely to affect fluid mechanics significantly.

FSS assay

Significant cell death is not evident in this system. Several flow rates are tested, ranging from 5 µL/sec to 50 µL/sec, for both malignant PC-3 and immortalized wild-type PrEC LH cells (**Figure B.3**). At flow rates exceeding 50 µL/sec, rupture between PDMS and glass is seen. No leaking is present during all other runs. Significant loss of viability is not seen until the flow rate is 50 µL/sec.

Lubrication flow effects

A simulation is performed of a particle flowing through a 2D microchannel with a height of 30 µm. Velocity in both the x (U-velocity) and y (V-velocity) shows how the particle elicits local flow effects (**Figure B.4A-B**). The core region of flow shows high velocity that diminishes as it approaches the wall. Fluid flow is reduced along the edges of the cell and slight tangential velocity of fluid flow can be seen in front and behind the cell as the fluid wraps around it. Dramatically reduced FSS magnitudes are seen along the edges and across the faces of the cell (**Figure B.4C**). FSS is approximately 20 Pa along the top and bottom of the cell near the walls. However, in flow where no particle is

101
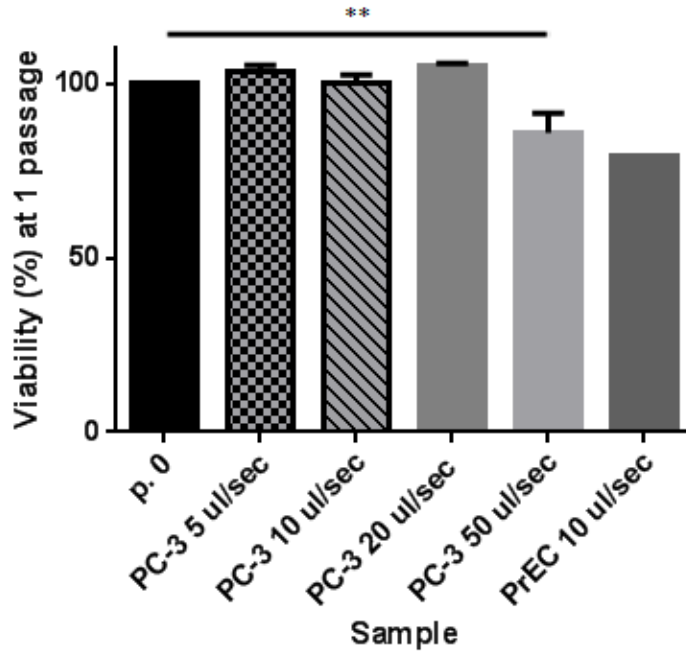
Figure B.3: Viability of cells exposed to fluid shear stress in microfluidic platform.
PC-3 and PrEC LH cells are exposed to increasing flow rates in the microfluidic
prototype. (**, $p < 0.01$).

A.
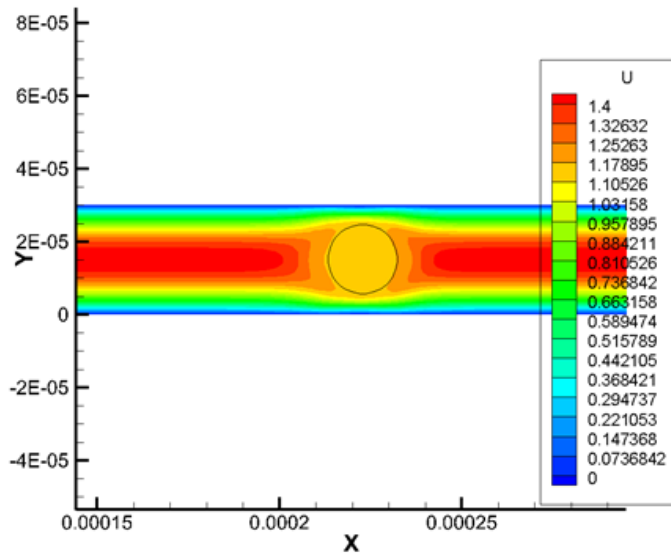
B.
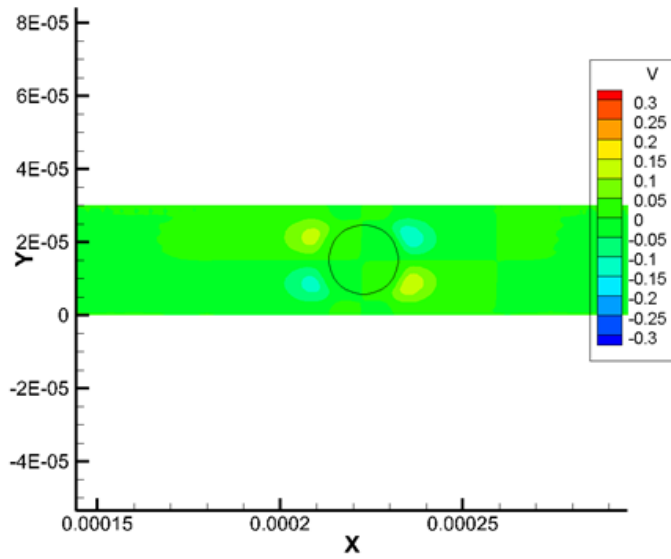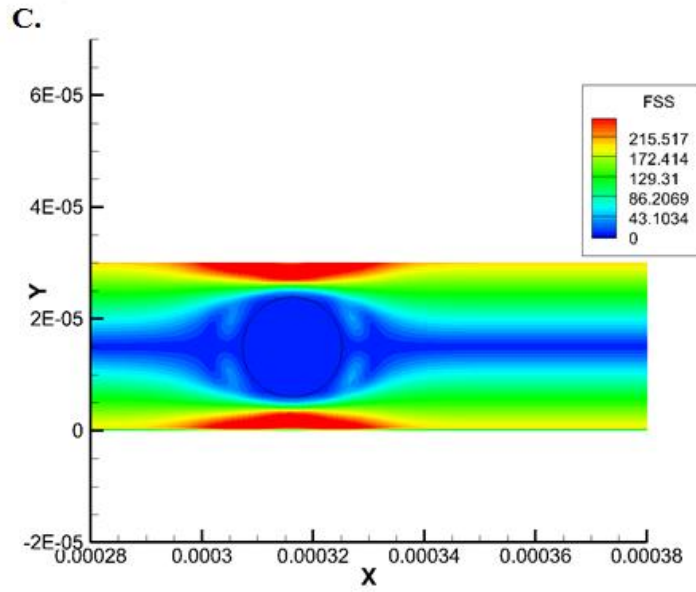
Figure B.4: Lubrication flow effects reduce effective fluid shear stress.
20 µm particles with properties matching cells are suspended in flow within a 2D
microchannel with a height of 30 µm. Localized flow effects around the cell are
observed. **A)** Axial velocity contours. **B)** Tangential velocity contours. **C)** Fluid shear
stress contours displaying reduced magnitudes around the particle suspended in the flow.

104

www.manaraa.com

present, the FSS is roughly 150 Pa. Thus, an almost eight-fold reduction in FSS is experienced by these cells at their outer edges.

Discussion

A device that is capable of isolating circulating tumor cells (CTCs) with high purity and quantity is important in furthering our understanding of metastasis. Isolation of these cells allows researchers and clinicians to discover mechanisms involved in the metastatic process for biomarker detection, disease evolution and progression, and can aid in predicting treatment options and drug responses. The microfluidics industry has been a prime example of expanding interest in fine flow control and manipulation to isolate these rare CTCs. Numerous techniques have been employed, such as antibody binding followed by magnetic capture (Herr, Smith *et al.* 2006), microvortice generation (Scott, Hsu *et al.* 2010), inertial focusing (Ozkumur, Shah *et al.* 2013), and polymer-based methods with conductivity sensors (Adams, Okagbare *et al.* 2008). While the focus of these devices is specifically geared towards CTC isolation, many of these devices have research applications as well.

However, the FSS assay is unique in its ability to be applied broadly to any cells displaying this resistance phenotype label-free. Not only can this phenotype be applied to further sort CTCs from benign cells of similar origin, a frequent case in many of these devices, for example when CTCs are isolated using epithelial biomarkers that can attract benign cells (Nagrath, Sequist *et al.* 2007), it can be used to selectively enrich malignant cells that may be present in other clinical samples, particularly specimens that are fluid

105

based. Yet, despite its significant advantages, the current FSS assay comes with the cost of a fairly non-specific exposure. By reducing cell-to-cell exposure variability, experimental parameters can be better optimized and controlled for higher sample enrichment.

Thus, a microfluidic platform is developed to reduce this exposure variability. By constricting the velocity gradient scale in the z-axis to approach the size of a cell diameter, cells are less likely to be exposed to vastly different FSS based on their vertical position within the channel. Furthermore, by using a high aspect ratio rectangular channel, the device can be approximated as a 2D exposure where FSS magnitude is independent of the cell position across the width of the channel except for very close the walls, further reducing exposure variability.

Flow simulations that confirmed velocity gradients that would result in similar levels of FSS present in the standard FSS assay. However, a preliminary exposure at 5 µL/sec, corresponding to a maximum wall FSS of roughly 1200 dyn/cm^2, resulted in no apparent viability loss in PC-3 cells. Increases in flow rate did not change loss appreciably until 50 µL/sec. At this flow rate, with a maximum FSS of 11900 dyn/cm^2, substantial viability loss is expected. Further increases, to FSS magnitudes over double the maximum experienced in normal physiological functioning, led to only slightly greater cell death. Exposure of PrEC LH cells at 30 µL/sec shows greater loss than PC-3 cells at a greater flow rate of 50 µL/sec, confirming that PrEC LH are more sensitive to FSS. Regardless of sensitivity, minimal loss at these enormous FSS magnitudes is not consistent with the standard assay.

At the microscale, the roles of certain characteristics of the flow, such as surface tension and viscosity, play a much larger role while others, such as inertia, contribute less to the mechanics of flow. Several of these parameters may be reducing the fluid shear stress that exposed cells experience. One microscale phenomenon that is possibly contributing to this behavior is lubrication flow. Data strongly suggests that lubrication flow is profoundly influencing the FSS magnitude that a cell experiences while it is being exposed in this system. dyn/cm^2 is fairly comparable to average FSS in the standard FSS exposure. Lubrication flow effects occur when a particle has a diameter that approaches the height of the channel, resulting in only a small layer of fluid on the order of microns between the particle surface and wall of the channel. This micron(s) thick layer is significantly less than the diameter of the particle. This allows cells to essentially slip along with the flow with significant reductions in shear stress.

To investigate this, using in-house code, advanced simulations are run with a particle that has matching physical properties to cells, including density and stiffness, passing through a 2D cross section of the exposure channel. Close examination of the velocity contours suggests that the velocity gradient is reduced along the edges of the cell, reducing the effective level of FSS. A theoretical eight-fold reduction in maximal FSS a cell experiences explains the significantly reduced loss of viability. At 50 µL/sec, only approximately 15% of PC-3 cells die, matching the loss after one passage in the standard assay at 250 µL/sec. However, at this flow rate, the FSS range is ~8,000-12,000 dyn/cm^2. Thus, nearly all cells are expected to die. An eight-fold reduction to around 1,000-2,000. Potential solutions to this issue, which have yet to be explored, include more extensive investigation of altering channel dimensions, specifically the height, to see if

the lubrication effect can be diminished. Upon completion, a new master can be made

and the FSS assay performed to confirm.

REFERENCES

1. Amano, M., Fukata, Y., & Kaibuchi, K. (2000). Regulation and functions of Rho-associated kinase. *Experimental cell research*, *261*(1), 44-51.

2. Ashworth, T. (1869). A case of cancer in which cells similar to those in the tumours were seen in the blood after death. *Aust Med J*, *14*(3), 146-149.

3. Augenstein, D. C., Sinskey, A. J., & Wang, D. I. C. (1971). Effect of shear on the death of two strains of mammalian tissue cells. *Biotechnology and bioengineering*, *13*(3), 409-418.

4. Aumüller, G., Wilhelm, B., & Seitz, J. (1999). Apocrine secretion—fact or artifact? *Annals of Anatomy-Anatomischer Anzeiger, 181(5)*, 437-446.

5. Bansal, D., & Campbell, K. P. (2004). Dysferlin and the plasma membrane repair in muscular dystrophy. *Trends in cell biology*, *14*(4), 206-213.

6. Bao, G., & Suresh, S. (2003). Cell and molecular mechanics of biological materials. *Nature materials*, *2*(11), 715-725.

7. Barnes, J. M., Nauseef, J. T., & Henry, M. D. (2012). Resistance to fluid shear stress is a conserved biophysical property of malignant cells. *PloS one*, *7*(12), e50973.

8. Bentley, B. J., & Leal, L. G. (1986). An experimental investigation of drop deformation and breakup in steady, two-dimensional linear flows. *Journal of Fluid Mechanics*, *167*, 241-283.

9. Berger R, Febbo PG, Majumder PK, Zhao JJ, & Mukherjee S. (2004) Androgen-induced differentiation and tumorigenicity of human prostate epithelial cells. *Cancer Res 64*: 8867–8875.

10. Brooks DE (1984). The biorheology of tumor cells. Biorheology 21: 85–91

11. Chakrabarti, S., Kobayashi, K. S., Flavell, R. A., Marks, C. B., Miyake, K., Liston, D. R., & Andrews, N. W. (2003). Impaired membrane resealing and autoimmune myositis in synaptotagmin VII–deficient mice. *The Journal of cell biology*, *162*(4), 543-549.

12. Chivukula, V. K., Krog, B. L., Nauseef, J. T., Henry, M. D., & Vigmostad, S. C. (2015). Alterations in cancer cell mechanical properties after fluid shear stress exposure: a micropipette aspiration study. *Cell health and cytoskeleton*, 7, 25.

13. Croughan, M. S., Hamel, J. F., & Wang, D. I. (1987). Hydrodynamic effects on animal cells grown in microcarrier cultures. *Biotechnology and bioengineering*, *29*(1), 130-141.

14. Dao, M., Lim, C. T., & Suresh, S. (2003). Mechanics of the human red blood cell deformed by optical tweezers. *Journal of the Mechanics and Physics of Solids*, *51*(11), 2259-2280.

15. Dasi, L. P., Simon, H. A., Sucosky, P., & Yoganathan, A. P. (2009). Fluid mechanics of artificial heart valves. *Clinical and experimental pharmacology and physiology, 36(2)*, 225-237.

16. Davies, P. F. (1995). Flow-mediated endothelial mechanotransduction. *Physiological reviews*, *75*(3), 519-560.

17. Davies, P. F., & Tripathi, S. C. (1993). Mechanical stress mechanisms and the cell. An endothelial paradigm. *Circulation research*, *72*(2), 239-245.

18. Dewey, C. F., Bussolari, S. R., Gimbrone, M. A., & Davies, P. F. (1981). The dynamic response of vascular endothelial cells to fluid shear stress. *Journal of biomechanical engineering*, *103*(3), 177-185.

19. Di Carlo, D. (2009). Inertial microfluidics. *Lab on a Chip*, *9*(21), 3038-3046.

20. Drake JM, Gabriel CL, Henry MD (2005) Assessing tumor growth and distribution in a model of prostate cancer metastasis using bioluminescence imaging. *Clin Exp Metastasis 22*: 674–684.

21. Egger, G., Burda, A., & Glasner, A. (2001). A simple method for measuring the F-actin content of human polymorphonuclear leukocytes in whole blood. *Virchows Archiv*, *438*(4), 394-397.

22. Fisher, A. B., Chien, S., Barakat, A. I., & Nerem, R. M. (2001). Endothelial cellular response to altered shear stress. *American Journal of Physiology-Lung Cellular and Molecular Physiology, 281(3)*, L529-L533.

23. Gertz, S. D., Uretsky, G., Wajnberg, R. S., Navot, N., & Gotsman, M. S. (1981). Endothelial cell damage and thrombus formation after partial arterial constriction: relevance to the role of coronary artery spasm in the pathogenesis of myocardial infarction. *Circulation, 63(3)*, 476-486.

24. Guck, J., Schinkinger, S., Lincoln, B., Wottawah, F., Ebert, S., Romeyke, M., & Käs, J. (2005). Optical deformability as an inherent cell marker for testing malignant transformation and metastatic competence. *Biophysical journal*, *88*(5), 3689-3698.

25. Han, R., & Campbell, K. P. (2007). Dysferlin and muscle membrane repair. *Current opinion in cell biology, 19(4)*, 409-416.

26. Herr, J. K., Smith, J. E., Medley, C. D., Shangguan, D., & Tan, W. (2006). Aptamer-conjugated nanoparticles for selective collection and detection of cancer cells. *Analytical Chemistry*, *78*(9), 2918-2924.

27. Hochmuth, R. M. (2000). Micropipette aspiration of living cells. *Journal of biomechanics*, *33*(1), 15-22.

28. Horiuchi, A., Imai, T., Wang, C., Ohira, S., Feng, Y., Nikaido, T., & Konishi, I. (2003). Up-regulation of small GTPases, RhoA and RhoC, is associated with tumor progression in ovarian carcinoma. *Laboratory investigation*, *83*(6), 861-870.

29. Hur, S. C., Henderson-MacLennan, N. K., McCabe, E. R., & Di Carlo, D. (2011). Deformability-based cell classification and enrichment using inertial microfluidics. *Lab on a Chip*, *11*(5), 912-920.

30. Idone, V., Tam, C., & Andrews, N. W. (2008). Two-way traffic on the road to plasma membrane repair. *Trends in cell biology*, *18*(11), 552-559.

31. Keefe, D., Shi, L., Feske, S., Massol, R., Navarro, F., Kirchhausen, T., & Lieberman, J. (2005). Perforin triggers a plasma membrane-repair response that facilitates CTL induction of apoptosis. *Immunity, 23(3)*, 249-262.

32. Keshaviah, J. (1970). M.S. Thesis. University of Minnesota, Minneapolis.

33. Kleer, C. G., van Golen, K. L., Zhang, Y., Wu, Z. F., Rubin, M. A., & Merajver, S. D. (2002). Characterization of RhoC expression in benign and malignant breast disease: a potential new marker for small breast carcinomas with metastatic ability. *The American journal of pathology*, *160*(2), 579-584.

34. Kovács, M., Tóth, J., Hetényi, C., Málnási-Csizmadia, A., & Sellers, J. R. (2004). Mechanism of blebbistatin inhibition of myosin II. *Journal of Biological Chemistry*, *279*(34), 35557-35563.

35. Langille, B. L., Reidy, M. A., & Kline, R. L. (1986). Injury and repair of endothelium at sites of flow disturbances near abdominal aortic coarctations in rabbits. *Arteriosclerosis, Thrombosis, and Vascular Biology, 6(2)*, 146-154.

36. Lawler, K., Foran, E., O'Sullivan, G., Long, A., & Kenny, D. (2006). Mobility and invasiveness of metastatic esophageal cancer are potentiated by shear stress in a ROCK-and Ras-dependent manner. *American Journal of Physiology-Cell Physiology*, *291*(4), C668-C677.

37. Lekka, M., Laidler, P., Gil, D., Lekki, J., Stachura, Z., & Hrynkiewicz, A. Z. (1999). Elasticity of normal and cancerous human bladder cells studied by scanning force microscopy. *European Biophysics Journal*, *28*(4), 312-316.

111

38. Leverett, L. B., Hellums, J. D., Alfrey, C. P., & Lynch, E. C. (1972). Red blood cell damage by shear stress. *Biophysical journal*, *12*(3), 257.

39. Lim, C. T., Zhou, E. H., Li, A., Vedula, S. R. K., & Fu, H. X. (2006). Experimental techniques for single cell and single molecule biomechanics.*Materials Science and Engineering: C*, *26*(8), 1278-1288.

40. Limouze, J., Straight, A. F., Mitchison, T., & Sellers, J. R. (2004). Specificity of blebbistatin, an inhibitor of myosin II. *Journal of Muscle Research & Cell Motility*, *25*(4-5), 337-341.

41. Luzzi, K. J., MacDonald, I. C., Schmidt, E. E., Kerkvliet, N., Morris, V. L., Chambers, A. F., & Groom, A. C. (1998). Multistep nature of metastatic inefficiency: dormancy of solitary cells after successful extravasation and limited survival of early micrometastases. *The American journal of pathology*, *153*(3), 865-873.

42. Martinez, I., Chakrabarti, S., Hellevik, T., Morehead, J., Fowler, K., & Andrews, N. W. (2000). Synaptotagmin VII regulates Ca2+-dependent exocytosis of lysosomes in fibroblasts. *The Journal of cell biology*, *148*(6), 1141-1150.

43. McLauchlan, H., Elliott, M., & Cohen, P. (2003). The specificities of protein kinase inhibitors: an update. *Biochemical Journal*, *371*(1), 199-204.

44. McNeil, P. L. (2002). Repairing a torn cell surface: make way, lysosomes to the rescue. *Journal of Cell Science*, *115*(5), 873-879.

45. McNeil, P. L., & Kirchhausen, T. (2005). An emergency response team for membrane repair. *Nature Reviews Molecular Cell Biology*, *6*(6), 499-505.

46. McNeil, P. L., & Steinhardt, R. A. (2003). Plasma membrane disruption: repair, prevention, adaptation. *Annual review of cell and developmental biology*, *19*(1), 697-731.

47. McQueen, A., Meilhoc, E., & Bailey, J. E. (1987). Flow effects on the viability and lysis of suspended mammalian cells. *Biotechnology letters*, *9*(12), 831-836.

48. Mehlen, P., & Puisieux, A. (2006). Metastasis: a question of life or death. *Nature Reviews Cancer*, *6*(6), 449-458.

49. Nagrath, S., Sequist, L. V., Maheswaran, S., Bell, D. W., Irimia, D., Ulkus, L., & Ryan, P. (2007). Isolation of rare circulating tumour cells in cancer patients by microchip technology. *Nature*, *450*(7173), 1235-1239.

50. Noguchi, H., & Gompper, G. (2005). Shape transitions of fluid vesicles and red blood cells in capillary flows. *Proceedings of the National Academy of Sciences of the United States of America*, *102*(40), 14159-14164.

51. Osawa, M., Masuda, M., Harada, N., Lopes, R. B., & Fujiwara, K. (1997). Tyrosine phosphorylation of platelet endothelial cell adhesion molecule-1 (PECAM-1, CD31) in mechanically stimulated vascular endothelial cells. *European journal of cell biology*, *72*(3), 229-237.

52. Osborn, E. A., Rabodzey, A., Dewey, C. F., & Hartwig, J. H. (2006). Endothelial actin cytoskeleton remodeling during mechanostimulation with fluid shear stress. *American Journal of Physiology-Cell Physiology*, *290*(2), C444-C452.

53. Petrie, C. J. (1995). Extensional flow—a mathematical perspective. *Rheologica acta*, *34*(1), 12-26.

54. Reddy, A., Caler, E. V., & Andrews, N. W. (2001). Plasma membrane repair is mediated by Ca 2+-regulated exocytosis of lysosomes. *Cell*, *106*(2), 157-169.

55. Resnick, N., Yahav, H., Shay-Salit, A., Shushy, M., Schubert, S., Zilberman, L. C. M., & Wofovitz, E. (2003). Fluid shear stress and the vascular endothelium: for better and for worse. *Progress in biophysics and molecular biology, 81(3),* 177-199.

56. Rodríguez, A., Webster, P., Ortego, J., & Andrews, N. W. (1997). Lysosomes behave as Ca2+-regulated exocytic vesicles in fibroblasts and epithelial cells. *The Journal of cell biology*, *137*(1), 93-104.

57. Sato, H., Suzuki, M. (1976). Deformability and viability of tumor cells by transcapillary passage, with reference to organ affinity of metastasis in cancer. *Fundamental Aspects of Metastatis*, 311-317.

58. Segre, G., & Silberberg, A. (1962). Behavior of macroscopic rigid spheres in Poiseuille flow. *J. Fluid Mech.*, *14*.

59. Stricker, J., Falzone, T., & Gardel, M. L. (2010). Mechanics of the F-actin cytoskeleton. *Journal of biomechanics*, *43*(1), 9-14.

60. Suresh, S. (2007). Biomechanics and biophysics of cancer cells. *Acta Materialia*, *55*(12), 3989-4014.

61. Tam, C., Idone, V., Devlin, C., Fernandes, M. C., Flannery, A., He, X., & Andrews, N. W. (2010). Exocytosis of acid sphingomyelinase by wounded cells promotes endocytosis and plasma membrane repair. *The Journal of cell biology*, *189*(6), 1027-1038.

62. Theret, D. P., Levesque, M. J., Sato, M., Nerem, R. M., & Wheeler, L. T. (1988). The application of a homogeneous half-space model in the analysis of endothelial cell micropipette measurements. *Journal of biomechanical engineering*, *110*(3), 190-199.

63. Tidball, J. G. (2011). Mechanisms of muscle injury, repair, and regeneration. *Comprehensive Physiology.*

64. van Zijl, F., Krupitza, G., & Mikulits, W. (2011). Initial steps of metastasis: cell invasion and endothelial transmigration. *Mutation Research/Reviews in Mutation Research*, *728*(1), 23-34.

65. Vicente-Manzanares, M., Ma, X., Adelstein, R. S., & Horwitz, A. R. (2009). Non-muscle myosin II takes centre stage in cell adhesion and migration. *Nature reviews Molecular cell biology*, *10*(11), 778-790.

66. Wang, X., Xie, W., Zhang, Y., Lin, P., Han, L., Han, P., & Weisleder, N. (2010). Cardioprotection of ischemia/reperfusion injury by cholesterol-dependent MG53-mediated membrane repair. *Circulation research, 107(1),* 76-83.

67. Ward, K. A., Li, W. I., Zimmer, S., & Davis, T. (1990). Viscoelastic properties of transformed cells: role in tumor cell progression and metastasis formation. *Biorheology*, *28*(3-4), 301-313.

68. Wheeler, A. P., & Ridley, A. J. (2004). Why three Rho proteins? RhoA, RhoB, RhoC, and cell motility. *Experimental cell research*, *301*(1), 43-49.

69. White, C. R., & Frangos, J. A. (2007). The shear stress of it all: the cell membrane and mechanochemical transduction. *Philosophical Transactions of the Royal Society of London B: Biological Sciences*, *362*(1484), 1459-1467.

70. Wirtz, D., Konstantopoulos, K., & Searson, P. C. (2011). The physics of cancer: the role of physical interactions and mechanical forces in metastasis. *Nature Reviews Cancer*, *11*(7), 512-522.

71. Yamazaki, D., Kurisu, S., & Takenawa, T. (2005). Regulation of cancer cell motility through actin reorganization. *Cancer science*, *96*(7), 379-386.

72. Yu, M., Stott, S., Toner, M., Maheswaran, S., & Haber, D. A. (2011). Circulating tumor cells: approaches to isolation and characterization. *The Journal of cell biology, 192(3)*, 373-382.

114